UC Santa Cruz

UC Santa Cruz Electronic Theses and Dissertations

Title

Connecting the causes and consequences of ribosomal stalling

Permalink

https://escholarship.org/uc/item/1tp8t1xz

Author

Monem, Parissa C

Publication Date

2023

Supplemental Material

https://escholarship.org/uc/item/1tp8t1xz#supplemental

Copyright Information

This work is made available under the terms of a Creative Commons Attribution License, availalbe at https://creativecommons.org/licenses/by/4.0/

Peer reviewed|Thesis/dissertation

eScholarship.org Powered by the California Digital Library
University of California

UNIVERSITY OF CALIFORNIA
SANTA CRUZ

CONNECTING THE CAUSES AND CONSEQUENCES OF RIBOSOMAL STALLING

A dissertation submitted in partial satisfaction
of the requirements for the degree of

DOCTOR OF PHILOSOPHY

in

MOLECULAR, CELL, AND DEVELOPMENTAL BIOLOGY

by

PARISSA C. MONEM

June 2023

The Dissertation of Parissa C. Monem
is approved by:

_____
Professor Joshua Arribere, Chair

_____
Professor Manuel Ares

_____
Professor Sarah Loerch

_____
Professor Alan Zahler

_____
Peter Biehl
Vice Provost and Dean of Graduate Studies

TABLE OF CONTENTS

Chapter 1: A ubiquitin language communicates ribosomal distress

Abstract……1

Introduction……1

An array of ubiquitination targets on the ribosome……3

E3 ubiquitin ligases involved in ribosomal ubiquitination……7

Deubiquitinases functioning during translational stress……13

Ubiquitin as a signal for repression……15

Conclusions and future perspectives……16

Chapter 2: Ubiquitination of stalled ribosomes enables mRNA decay via HBS-1 and NONU-1 *in vivo*

Abstract……18

Introduction……18

Results……20

Discussion……38

Methods……43

Chapter 3: Stalled ribosome species evade standard ribosome capture protocols in animals

Abstract……49

Introduction……49

Results……51

Discussion……58

Methods……66

Chapter 4: Conclusions and future directions……70

References……74

LIST OF FIGURES

Figure 1.1: Ribosomal proteins ubiquitinated during translational stress……..4

Figure 1.2: Ribosomal ubiquitination sites localize to the disome interface……..6

Figure 1.3: E3 ubiquitin ligases and their ribosomal protein targets……..…7

Figure 1.4: Distinct stalls generate substrates for different E3 ubiquitin ligases……..8

Figure 1.5: DUBs control the ubiquitination status of 40S subunits and E3 ubiquitin ligases……..……13

Figure 1.6: Translational surveillance effectors recognizing altered ribosomes…….15

Figure 1.7: Ribosomal ubiquitination sites with unclear consequences……..17

Figure 2.1. Genetic screens identify suppressors of No-Go mRNA Decay……21

Figure 2.2: Cell-specific NGD rescue via overexpression of factors……...25

Figure 2.3. ZNF-598 is required for ribosomal ubiquitination in *C. elegans*……...26

Figure 2.4: NGD-deficient ribosomes made via ablation of ubiquitination sites…….28

Figure 2.5. NONU-1 function during NGD requires CUE domains and follows ZNF-598……..……30

Figure 2.6. HBS-1 N-terminus resembles a ubiquitin-binding domain and is dispensable for NGD…….34

Figure 2.7. HBS-1 and PELO-1 are essential for mRNA degradation……36

Figure S2.1. Representative animals demonstrating various overlap scores……40

Figure S2.2. RPS-10 and RPS-20 ubiquitination sites are conserved in *C. elegans*……41

Figure S2.3. *nonu-1* null mutant displays similar NGD suppression as catalytic mutant…….41

Figure S2.4. Known surveillance factor partners exhibit high mutual information…….42

Figure S2.5. Ubiquitin-binding assay shows high level of background binding…….42

Figure S2.6. HBS-1 and PELO-1 exhibit similar phenotypes during NGD in *C. elegans*…….42

Figure 3.1: Poly-proline and poly-arginine ribosomes are differentially captured…….52

Figure 3.2: ZNF-598 controls mRNA levels of and ribosomes on a NGD substrate, but not readthrough levels nor frame maintenance……..54

Figure 3.3: A low abundance of stalled ribosome footprints captured by CHX on a NGD substrate……....56

Figure 3.4: A conspicuous absence of ribosome accumulations within a poly-arginine stall……..57

Figure S3.1: Footprint size and frame distributions in CHX Ribo-seq……62

Figure S3.2: Distribution of nucleotide content in deep sequencing libraries……...62

Figure S3.3: 5’ bias of ribosomes on *unc-54(rareArg)* exceeds that seen on other myosins……..63

Figure S3.4: Post-stall ribosomes remain in frame on a yeast NGD substrate……....63

Figure S3.5: Compromised NGD does not lead to NMD activation on a NGD substrate……64

Figure S3.6: Footprint size and frame distributions in ANS Ribo-seq……...65

Table 1: *C. elegans* strains and oligos

ABSTRACT

CONNECTING THE CAUSES AND CONSEQUENCES OF RIBOSOMAL STALLING

Parissa C. Monem

Ribosomes build and maintain life. It is essential that ribosomes promptly and faithfully decode mRNAs to produce proteins, so as to avoid the development of disease phenotypes such as neurodegeneration.

In the last two decades, major advances have been made in the discovery and characterization of quality control pathways centered around the ribosome. Two of these pathways are No-Go mRNA Decay (NGD) and Nonstop mRNA Decay (NSD). NGD acts on ribosomes at a strong obstacle to elongation, such as a stable secondary structure or a stretch of poly-basic codons. NSD is triggered by ribosomes elongated to the 3'-most edge of an mRNA as a result of premature polyadenylation or mRNA cleavage. Despite their distinct mRNA species, NGD and NSD share a team of cellular machinery specialized to detect the ribosome state, free the ribosome, and destroy the aberrant mRNA. While a number of these players are now identified, the early steps of stall detection and the links that connect factors remained untested. Here, we illustrate mechanisms of mRNA repression prompted by stalled ribosomes.

In Chapter 1, we review the understanding of ubiquitin signals on an array of ribosomal proteins. Some of these ubiquitination events are thought to play a part in NGD and/or NSD, but the vast majority of ribosomal ubiquitination events are uncharacterized. In our review, we put forth a hypothesis that widespread ribosomal ubiquitination participates in a myriad of cellular signaling to swiftly alter translation.

In Chapter 2, we delineate mechanistic links between an E3 ubiquitin ligase (ZNF-598), a ribosome rescue factor (HBS-1), and an endonuclease (NONU-1) that collaborate to carry out NGD. We demonstrate that ubiquitination of two ribosomal proteins

(uS10 and eS10) by ZNF-598 is necessary for NGD, and that inhibition of ubiquitination on these sites produces ribosomes that are immune to NGD. We proceed to characterize a function for these ubiquitination events in NONU-1 recruitment, and we uncover a surprising requirement for HBS-1 in promoting the NONU-1 cleavage reaction. These findings reveal a novel order of events during NGD which will inform future studies, suggesting a model in which ribosome rescue precedes mRNA cleavage.

In Chapter 3, we report a phenomenon present in metazoan ribosome footprint profiling data which is of great importance to the study of NGD. We thoroughly interrogate the dynamics of ribosomes genome-wide and on our genetically validated NGD reporter, revealing an absence of NGD-dependent effects. Key to our studies is the expectation of an effect on our NGD reporter, which was lacking in previous work and limited interpretations. Our findings are consistent with the existence of a fleeting and specialized ribosome state during NGD that evades current ribosome capture protocols. We expect our future work and that of others to enable a greater understanding of these ribosome species.

Overall, this dissertation significantly advances the understanding of the cellular response to ribosomal stalls. In Chapter 4, we reflect on our findings and highlight outstanding questions for future research.

ACKNOWLEDGMENTS

This dissertation includes material from published works: “A ubiquitin language communicates ribosomal distress” (Monem & Arribere, 2023) (Chapter 1) and “Ubiquitination of stalled ribosomes enables mRNA decay via HBS-1 and NONU-1 *in vivo*” (Monem et al., 2023) (Chapter 2). Thank you to those who supported me throughout their preparation, helping me make these publications a reality.

Above all, I am incredibly grateful to have found an advisor as fantastic as Josh. He is in a unique class of mentors that you don’t come across every day and has greatly influenced the scientist and person I’ve become. When I started in his lab, I was relatively new to research and frequently doubted my abilities. I was lucky enough to learn countless skills directly from him, hoping to absorb some of his brilliance through osmosis. However, the skill I was most lucky to have learned from him was to trust myself. He trusted me early on, encouraging my independence and validating my intuitions. He is keenly aware of the prejudices faced by women in science (and in the world) and helped motivate me to proceed without shrinking myself when these biases attempted to hold me back. I’m immensely thankful for the years I’ve had working with him, and I will keep his kind words stored away in a drawer of positivity for years to come.

Before starting my PhD, I found two wonderful mentors. I will be forever grateful to have had Grant Hartzog as my first advisor and for him instilling words of affirmation into my vocabulary. I was also lucky to have taught a year’s worth of intro biology with John Tamkun, navigating the humorous challenges accompanying a class of hundreds of students. The mentorship they both provided played a significant role in my journey.

A huge factor that shaped my experience in grad school was the people I’ve spent countless hours with in the lab. I’ve been around since practically the start of the lab and witnessed lots of turnover, yet it always remained a positive, supportive, and fun environment. I hope to keep many of them as lifelong friends, and I can’t wait to see where they all go from

here. Especially Enisha, who I have had the privilege of collaborating with and mentoring over the years, and who has become one of my dearest friends.

I wouldn't have considered scientific research had it not been for my lovely little oddball group of friends from undergrad. Many of them noticed my strengths and talents before anyone else and encouraged me to go for it. Especially Hannah, who remains my best friend and confidante until this day. I don't know how I would have managed the stressors of grad school without having her as my chosen sister.

I'm thankful for the support I've received from my family, which allowed me to invest the years necessary for my higher education. I grew up without a clear idea of my goals, and they gave me the encouragement and freedom to figure out what I wanted to do.

Lastly, many canine companions worked tirelessly to provide me with support. To Teddy, Sophie, Lila, and Maya: thank you for growing so close to your friend. And to my Goosey Lucy Leucine girl: you changed my life for the better and I adore you.

CHAPTER 1: A UBIQUITIN LANGUAGE COMMUNICATES RIBOSOMAL DISTRESS

ABSTRACT

Cells entrust ribosomes with the critical task of identifying problematic mRNAs and facilitating their degradation. Ribosomes must communicate when they encounter and stall on an aberrant mRNA, lest they expose the cell to toxic and disease-causing proteins, or they jeopardize ribosome homeostasis and cellular translation. In recent years, ribosomal ubiquitination has emerged as a central signaling step in this process, and proteomic studies across labs and experimental systems show a myriad of ubiquitination sites throughout the ribosome. Work from many labs zeroed in on ubiquitination in one region of the small ribosomal subunit as being functionally significant, with the balance and exact ubiquitination sites determined by stall type, E3 ubiquitin ligases, and deubiquitinases. This review discusses the current literature surrounding ribosomal ubiquitination during translational stress and considers its role in committing translational complexes to decay.

INTRODUCTION

Translation is an essential and tightly regulated process, with much of its regulation necessarily hinging on the ribosome. Considering that translation gives rise to all proteins in the cell, it is no surprise that faulty translation contributes to the aggregation of toxic proteins and can elicit disease phenotypes such as neurodegeneration (Bengtson & Joazeiro, 2010; Ishimura et al., 2014). To mitigate this, eukaryotes have evolved translational surveillance mechanisms that ensure ribosomes accurately synthesize proteins from full-length mRNAs in a timely fashion. A key functional intermediate that communicates translation status is a ubiquitinated ribosome, and the precise sites of ubiquitination vary depending on what the ribosome has to “say” about its translation experience.

Ubiquitination is typically considered a hallmark of proteasomal degradation, but ubiquitination also plays a part in non-degradative signaling responses (Clague & Urbé, 2010;

Komander & Rape, 2012). This difference in protein fate lies in the number of ubiquitins and their linkages, the pattern of which creates molecular interfaces that are recognized by effectors (Husnjak & Dikic, 2012; Randles & Walters, 2012). In its non-degradative capacity, ubiquitin functions as a signaling molecule in much the same way that phosphorylation is used in protein signaling cascades throughout biology. Covalent attachment of ubiquitin to substrates is the culmination of a ubiquitin cascade involving ubiquitin-activating (E1), ubiquitin-conjugating (E2), and ubiquitin-ligating (E3) enzymes (Pickart & Eddins, 2004; Deshaies & Joazeiro, 2009). While E1 and E2 enzymes interact with each other and ubiquitin, E3 ubiquitin ligases interact with ubiquitination targets, imparting substrate specificity. To enable this vital precision, organisms encode hundreds of unique E3 ligases (Buetow & Huang, 2016; Zheng & Shabek, 2017). Among the pool of proteins targeted by E3 ligases are ribosomal proteins (Spence et al., 2000; Mayor et al., 2005; Shcherbik & Pestov, 2010; Martínez-Férriz et al., 2021; Koyuncu et al., 2021).

In recent years, there has been a particular focus on cotranslational ribosomal ubiquitination as a mechanism to rapidly alter the outcome of translation. Much of the literature on ribosomal ubiquitination comes from the study of two translational surveillance pathways: No-Go mRNA Decay (NGD) and Nonstop mRNA Decay (NSD) (Sundaramoorthy et al., 2017; Juszkiewicz & Hegde, 2017; Garzia et al., 2017). NGD occurs on mRNAs bearing elongation-inhibiting features, such as secondary structures, rare codons, polybasic amino acid-encoding sequences, or damaged nucleotides (Doma & Parker, 2006). NSD is triggered by mRNAs lacking stop codons, generated by premature polyadenylation or mRNA cleavage (Frischmeyer et al., 2002). While prompted by different mRNA species, NGD and NSD are defined by the recruitment of several of the same effectors, ultimately leading to mRNA decay, ribosome rescue, and nascent peptide degradation. A molecular understanding of the biochemical steps of mRNA repression and ribosome rescue have been reviewed elsewhere and will not be covered here (Shoemaker & Green 2012; Joazeiro, 2017; Inada, 2020; D'Orazio & Green, 2021).

Here, we review the current knowledge of ribosomal ubiquitination during translation and highlight future directions for its study. First, we collect known ribosomal protein sites subject to ubiquitination in the context of surveillance and translational distress. We then discuss structural, genetic, and biochemical data suggesting target specificity mechanisms used by distinct E3 ubiquitin ligases and deubiquitinases. Lastly, we consider downstream consequences of ribosomal ubiquitination, and suggest models in which effectors recognize ubiquitinated aberrant translational complexes and commit such complexes to decay.

AN ARRAY OF UBIQUITINATION TARGETS ON THE RIBOSOME

Similar and distinct ubiquitination sites across organisms

Several studies have exploited mass spectrometry to characterize the ubiquitinated proteome in a process known as ubiquitin remnant profiling (Peng et al., 2003; Kim et al., 2011; Bustos et al., 2012; Yan et al., 2019; Koyuncu et al., 2021). The selective profiling of ubiquitin-modified peptides is made possible due to a unique di-glycine tag left on ubiquitin conjugates following trypsin digestion. This di-glycine tag is the remnant of ubiquitin on its covalently-bound substrate and thus allows for the precise identification of the substrate's participating lysine residue.

Initial studies from several groups suggested that site-specific ubiquitination of ribosomal proteins could influence or be influenced by translation. Yeast RPS7A/eS7A was identified as a target of ribosomal ubiquitination in polysomes (Panasenko & Collart, 2012). The Bennet lab identified 40S small ribosomal subunit proteins (RPS2/uS5, RPS3/uS3, and RPS20/uS10) which were ubiquitinated upon treatment with translation inhibitors such as cycloheximide, anisomycin, and harringtonine (Higgins et al., 2015). Further in support of a link to active translation, later studies revealed a requirement for RPS10/eS10 and RPS20/uS10 ubiquitination in the resolution of ribosomal stalling in human cells (Sundaramoorthy et al., 2017; Juszkiewicz & Hegde, 2017) and *C. elegans* (Monem et al.,

2023), and work in yeast demonstrated a requirement for ubiquitination of RPS20/uS10 (Matsuo et al., 2017) and RPS3/uS3 (Simms et al., 2017).

Work across many groups over the last several years uncovered ubiquitinated 40S proteins and their targeted lysine residue(s) in different organisms (Figure 1.1). Notably, some ubiquitination targets are unique to metazoans or yeast, indicating divergence in ubiquitination targeting mechanisms or ribosomal protein accessibility. Additionally, while most of the literature has focused on monoubiquitination events, work in yeast has demonstrated a requirement for polyubiquitination in translational surveillance (Saito et al. 2015), providing support for K63-linked chains, namely on the yeast-specific RPS7/eS7 as well as RPS3/uS3 (Ikeuchi et al., 2019). Whether polyubiquitination occurs *in vivo* in metazoans is currently unclear.

Ribosomal protein	Organism & lysine residue
RPS2/uS5	*H. sapiens:* K54[*], K58[*,†]
RPS3/uS3	*S. cerevisiae:* K212[*]; *H. sapiens:* K214[*,†], K249[†]
RPS7/eS7	*S. cerevisiae:* K83[*], K84[*]
RPS10/eS10	*H. sapiens:* K138[*,†], K139[*,†], K107[†]; *C. elegans:* K125[*,†]
RPS20/uS10	*S. cerevisiae:* K6[*], K8[*]; *H. sapiens:* K4[*,†], K8[*,†]; *C. elegans:* K6[*,†], K9[*,†]

Figure 1.1: Ribosomal proteins ubiquitinated during translational stress. Table of ribosomal proteins reported to be ubiquitinated upon ribosomal stalling, via treatment with translation drugs and/or expression of stalling reporters. Lysine residues shown are supported by [*]genetic evidence, [†]biochemical evidence, or both in their respective organisms.

Ubiquitination sites reside between collided ribosomes

An important outstanding question in translational surveillance was how cells distinguish problematic stalls from transient pauses in translation. A model emerged to solve this problem: ribosome collisions. Work from several groups supports an important role for ribosome collisions in both ubiquitination and surveillance (Simms et al., 2017; Juszkiewicz et al., 2018; Ikeuchi et al., 2019; Matsuo et al., 2020). As we describe below, ubiquitination sites

coincide with contact sites between collided ribosomes, suggesting a direct relationship between collisions and ubiquitination.

To study discretely stalled ribosomes, the Hegde lab utilized a rabbit reticulocyte lysate translation system supplemented with a mutant release factor, stalling ribosomes at stop codons (Shao et al., 2016; Juszkiewicz et al., 2018). Poly-ribosomes were analyzed by cryo-EM, and the resultant structure revealed the stalled/leading and collided/trailing ribosomes in distinct orientations, producing two 40S inter-ribosomal interfaces (Figure 1.2A). Interface 1 consists of the mRNA exit channel of the stalled ribosome and the mRNA entry channel of the collided ribosome. Notably, this interface lacks ubiquitination sites. Interestingly, interface 2 involves all identified ubiquitination sites on the collided ribosome and RACK1, a ribosomal protein required for stall detection (Figure 1.2B) (Sundaramoorthy et al., 2017).

A trio of structural studies in yeast visualized structures of disomes stalled on an arginine reporter mRNA (Ikeuchi et al., 2019), trisomes stalled on an endogenous stalling mRNA (*SDD1*) (Matsuo et al., 2020), and disomes stalled on endogenous mRNAs (Zhao et al., 2021). While these structures largely agree with one another, there are some key differences (*e.g.*, the relative positioning of RACK1 in (Zhao et al., 2021) compared to (Ikeuchi et al., 2019; Masuo et al., 2020)). It is unclear whether such differences represent distinct ribosome collision types, steps along a ribosome collision pathway, and/or distinct sample preparations.

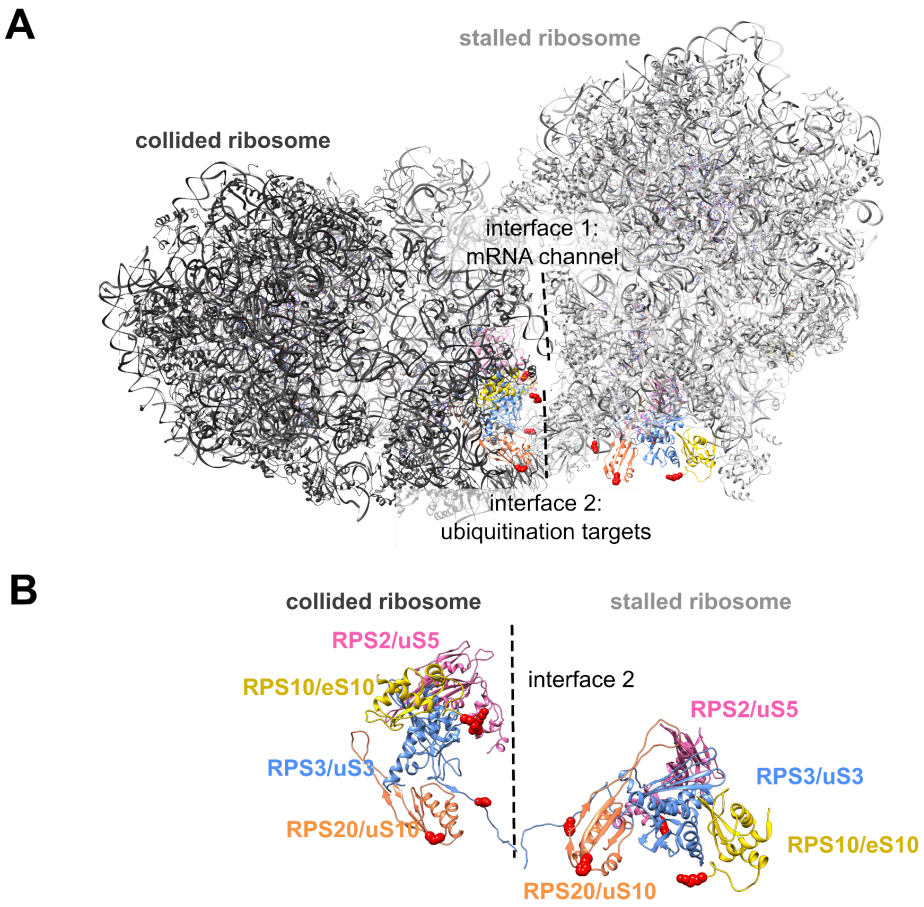

Figure 1.2: Ribosomal ubiquitination sites localize to the disome interface. (A) Cryo-EM structure of rabbit reticulocyte ribosomes from Juszkiewicz et al., 2018 (PDB 6HCQ and 6HCM). The 5'-most, collided/trailing ribosome is shown in dark gray, while the 3'-most, stalled/leading ribosome is shown in light gray. Ribosomal proteins ubiquitinated in metazoans are colored: RPS2/uS5 in pink, RPS3/uS3 in light blue, RPS10/eS10 in yellow, and RPS20/uS10 in orange. Labeled with red spheres are side chains of ubiquitination target lysines of each protein. In cases where the target lysine was not modeled due to its flexibility, the closest visible residue is highlighted. Interfaces 1 and 2 are labeled and defined as regions where the 40S subunits of each ribosome interact. **(B)** Zoom in on the ribosomal proteins indicated in part (A). Identities of ribosomes containing each set of proteins are labeled above.

In addition to revealing the orientations of stalled ribosomes, these structural studies provided information regarding the locations of lysine residues targeted for ubiquitination. These lysines are found on the flexible tails of their respective proteins on the solvent face of the 40S subunit (Figure 1.2A, Figure 1.2B). Due to the flexible nature of these tails, they are often missing from structures, thus preventing visualization of conjugated ubiquitin (if present). Future work optimizing the capture of ubiquitinated ribosomes and visualization of ubiquitin itself on ribosomes will provide important insights into ubiquitination states in

different mutant backgrounds. The potential ubiquitination sites of the trailing/collided ribosomes are much closer to the interface than the same ubiquitination sites on the stalled/leading ribosome. Whether this asymmetry yields a differential outcome with respect to ubiquitination of each ribosome and downstream effects remains unexplored. For more on the emerging understanding of collisions and their effects in the cell, see a recent review (Meydan & Guydosh, 2021).

E3 UBIQUITIN LIGASES INVOLVED IN RIBOSOMAL UBIQUITINATION

Several E3 ubiquitin ligases respond to aberrant translation. While information exists suggesting their ribosomal protein targets (Figure 1.3), the specificity of these ligases for their targets is poorly understood. As every ribosome would be expected to have each of these ribosomal proteins, how each E3 ligase differentiates between ribosomes and sites remains an open question.

E3 ubiquitin ligase	Ribosomal protein target
ZNF598/Hel2	RPS10/eS10; RPS20/uS10; RPS2/uS5; RPS3/uS3; RPS7/eS7
RNF10/Mag2	RPS2/uS5; RPS3/uS3
Not4	RPS7/eS7
MKRN1/2	RPS10/eS10

Figure 1.3: E3 ubiquitin ligases and their ribosomal protein targets. Table of E3 ubiquitin ligases functioning during ribosomal stalling. Ribosomal proteins displaying a change in ubiquitination status in deletions or knockdowns of each E3 ligase are shown.

One E3 ligase (ZNF598) specifically engages ribosomes upon collision, suggesting that ZNF598 recognizes the collision interface (Juszkiewicz et al., 2018). It remains unclear whether this is true of the other E3 ligases; it is possible that different stalls generate different collisions, each with its own distinct interface (Figure 1.4). This model is supported by work suggesting unique E3 ligase dependencies in distinct pathways (Saito et al., 2015; Ikeuchi et al., 2019; Monem et al., 2023; Allen et al., 2021). Additionally, evidence exists supporting a

combinatorial and hierarchical ubiquitination system (Ikeuchi et al., 2019; Garshott et al., 2020; Garzia et al., 2021). Furthermore, there are differences between some disome structures at the ubiquitination sites in the 40S-40S interface (Ikeuchi et al., 2019; Matsuo et al., 2020; Zhao et al., 2021). It is possible that ribosomes stalled in different conformations display targets for an E3 ligase specialized for that collision type. Future work will hopefully tease apart the specificity and ordering of each ribosomal ubiquitination event.

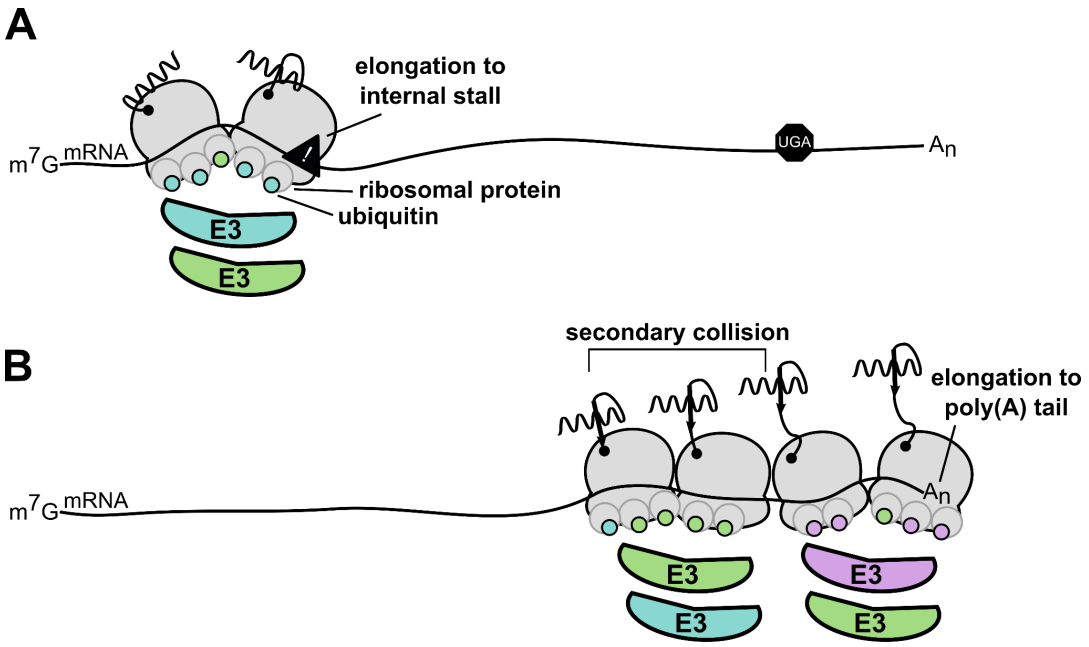

Figure 1.4: Distinct stalls generate substrates for different E3 ubiquitin ligases. (A) Model for E3 ligase targeting during an internal ribosomal stall. Black triangle with an exclamation point represents a stalling feature. Gray circles represent ribosomal proteins experiencing ubiquitination. Colored circles represent ubiquitin, colored according to the E3 ligase responsible for their placement. E3 ligases are shown in their respective colors. **(B)** Model for E3 ubiquitin ligase targeting during a ribosomal stall within the poly(A) tail at the 3' edge of an mRNA. Features shown as in part (A).

Below, we discuss the current understanding of each E3 ligase acting on stalled ribosomes.

ZNF598/Hel2

In yeast, Hel2 was first identified as a RING-domain-containing E3 ubiquitin ligase required for histone regulation (Singh et al., 2012). It is unclear whether this histone

regulatory function for Hel2 is connected to translational control. Hel2 was later found to repress the full-length product of a ribosomal stalling reporter with an internal polybasic stretch (Brandman et al., 2012; Letzring et al., 2013). Knockdown or deletion of ZNF598, the metazoan homolog of Hel2, in humans, worms, and zebrafish generally agrees with the stalling reporter stabilization phenotypes seen in yeast, providing evidence for ZNF598 function during ribosomal stalling in higher organisms (Juszkiewicz & Hegde, 2017; Sundaramoorthy et al., 2017; Garzia et al., 2017; Monem et al., 2023; Mishima et al. 2022).

Multiple groups identified ubiquitination targets of ZNF598 via ubiquitin remnant profiling, uncovering ZNF598-dependent ubiquitination of RPS10/eS10 and RPS20/uS10, and to a lesser extent RPS3/uS3 (Juszkiewicz & Hegde, 2017; Sundaramoorthy et al., 2017; Garzia et al., 2017). Genetic and biochemical studies verified the functional importance of ZNF598-dependent modification of RPS10/eS10, RPS20/uS10, RPS3/uS3, and RPS2/uS5 in metazoans (Garzia et al., 2017; Sundaramoorthy et al., 2017; Juszkiewicz & Hegde, 2017; Garshott et al., 2020; Garshott et al., 2021; Monem et al., 2023; Garzia et al., 2021). Work in yeast revealed Hel2-dependent modification of RPS20/uS10, RPS7A/eS7A, and RPS3/uS3 during ribosome stalling (Simms et al., 2017; Matsuo et al., 2017; Ikeuchi et al., 2019)

Given that ZNF598/Hel2 preferentially ubiquitinated ribosomes upon multi-ribosome collisions (Juszkiewicz et al., 2018) and that multiple ribosomes were required for NGD (Simms et al., 2017), an interest in “disomes” was born. Many studies emerged utilizing ribosome footprint profiling, or Ribo-seq, to map the positions of translating disomes genome-wide (Meydan & Guydosh, 2020; Han et al., 2020; Arpat et al., 2020; Zhao et al. 2021). One such study performed Ribo-seq on yeast disomes in a Hel2 mutant and observed differences in the distributions of disomes genome-wide, thus implicating Hel2 in functioning on the disome unit (Meydan & Guydosh, 2020). Similar disome datasets have yet to be generated in mammalian ZNF598 mutants, nor has robust NGD stalling been observed in metazoan Ribo-seq (Han et al., 2020; Arpat et al., 2020). Future work will help understand

the intricacies of disome Ribo-seq outside of yeast, and will inform endogenous targets of ZNF598.

While ZNF598/Hel2 is widely regarded as a major regulator of stalled ribosomes, evidence exists challenging its prominence in various stall situations, such as NSD (Saito et al. 2015; Ikeuchi et al., 2019; Monem et al., 2023). Much of the field's understanding of ribosomal ubiquitination by ZNF598/Hel2 relies on internally stalling NGD reporters exclusively (Garzia et al., 2017; Juszkiewicz & Hegde, 2017; Sundaramoorthy et al., 2017). Given that NSD and NGD arise on distinct mRNA substrates, a more complete illustration of ribosomal ubiquitination will require a consideration of a variety of stalling substrates. Additionally, work in yeast saw a requirement for Hel2-mediated ubiquitination of RPS3/uS3 at K212 in nonfunctional rRNA decay (NRD) (Sugiyama et al., 2019), but found it dispensable in NGD and ribosome quality control (RQC) of nascent peptides (Ikeuchi et al., 2019, Matsuo et al., 2017). Taken together, these works highlight the distinct functions of ZNF598/Hel2 during a variety of translational stresses.

RNF10/Mag2

Prior work in human cells found ZNF598-enhanced ubiquitination of RPS2/uS5 and RPS3/uS3; however, much of these ubiquitinated species persisted in ZNF598 knockouts (Juszkiewicz et al., 2018; Meyer et al., 2020). This finding prompted a consideration of different E3 ubiquitin ligases acting during NGD, leading to work focused on RNF10/Mag2 (Garzia et al., 2021; Garshott et al., 2021).

Known as RNF10 in humans and Mag2 in yeast, RNF10/Mag2 is a RING-domain-containing E3 ubiquitin ligase initially linked to translational surveillance during 18S NRD in yeast (Sugiyama et al., 2019). In this work from the Inada lab, Mag2 was found to be required for ubiquitination of RPS3/uS3 on non-functional 80S ribosomes to enable their dissociation and to facilitate 18S rRNA degradation.

Additional groups observed a requirement for human RNF10 to ubiquitinate RPS2/uS5 and RPS3/uS3 in the context of treatment with elongation and initiation inhibitors (Garzia et al., 2021; Garshott et al., 2021). These results support a function for RNF10 in ubiquitinating RPS2/uS5 and RPS3/uS3 (Garzia et al., 2021). It is also possible that E3 ligases collaborate to bring about repression, as is supported by data showing ZNF598 affecting ubiquitination of RPS2/uS5 and RPS3/uS3 during elongation stalls (Juszkiewicz et al., 2018; Meyer et al., 2020; Garzia et al., 2021). It thus remains a possibility that ZNF598 and RNF10 work together to ubiquitinate ribosomes at RPS2/uS5 and RPS3/uS3. NRD data in yeast are consistent with an E3-collaboration model, suggesting that Mag2 initially monoubiquitinates RPS3/uS3, followed by K63-polyubiquitination by Hel2 and an additional E3 ligase Rsp5 (Sugiyama et al., 2019).

Not4

The conserved Ccr4-Not complex is critical for RNA metabolism, regulating various steps from transcription to decay (Panasenko, 2014; Collart, 2016). Ccr4-Not is key to initiating mRNA decay via deadenylation and promotion of decapping (Tucker et al, 2001; Sandler et al., 2011). One component of the Ccr4-Not complex is the RING finger E3 ubiquitin ligase Not4. While Not4 is conserved in humans as CNOT4, it is only a stable subunit of the Ccr4-Not complex in yeast (Collart, 2016) and has only been characterized in translational surveillance in yeast and flies (Wu et al., 2018).

Multiple groups have found Not4 to be required for a variety of translational roles in yeast, including the polysome association of Not4 during stalling with cycloheximide (Panasenko & Collart, 2012; Preissler et al., 2015), the degradation of NGD stalling peptides (Dimitrova et al, 2009; Matsuda et al, 2014; Allen et al., 2021), and cotranslational decay of stalling reporter mRNAs and mRNAs with suboptimal codons (Allen et al., 2021; Buschauer et al., 2020). Notably, Not4 is also required for the ubiquitination of RPS7/eS7, a

yeast-specific ribosomal ubiquitination target (Panasenko & Collart, 2012; Ikeuchi et al., 2019; Allen et al., 2021).

Recent works point toward potential downstream consequences of Not4-mediated ribosomal ubiquitination in yeast. One study found that Not4 is required for mRNA cleavages upstream of a stall site, possibly acting through RPS7/eS7 monoubiquitination at K84 (Ikeuchi et al., 2019). While this model illustrates a downstream function for Not4, effectors which directly recognize Not4-mediated ubiquitination remain poorly understood. Another recent study teased apart the functions of Otu2 and Ubp3 as two deubiquitinases (DUBs) potentially working with Not4 to modulate ribosomal ubiquitination events on RPS7/eS7 at K83 (Takehara et al., 2021). Specifically, knockout of Otu2 or Ubp3 resulted in increased RPS7/eS7 ubiquitination on 40S subunits or 80S ribosomes and polysomes, respectively. This study saw reduced protein synthesis as a consequence of perturbing the deubiquitination cycle of RPS7/eS7, consistent with prior work showing decreased polysomes in a Not4 knockout (Panasenko & Collart, 2012). Together these works link Not4 with a pair of DUBs controlling translation efficiency. Further work is needed to understand the biological contexts in which ribosomes are affected by RPS7/eS7 ubiquitination, as well as the direct function of these ubiquitin marks.

MKRN1/2

MKRN1 and MKRN2 are two paralogs of a conserved RNA-binding RING finger E3 ubiquitin ligase. Previously implicated in a variety of roles such as regulating telomere length and interacting with poly(A)-binding protein (PABPC1) (Kim et al., 2005; Cassar et al., 2015), MKRN1/2 was more recently linked to translational surveillance.

Given its history with PABPC1, a recent study validated the interaction between MKRN1/2 and PABPC1, and proposed a model for MKRN1/2 mRNA binding and function during translation of poly(A) sequences (Hildebrandt et al., 2019). Upon MKRN1/2 knockdown, this work observed increased full-length translation of an internal poly(A)-stalling

reporter. Notably, ubiquitin remnant profiling of untreated cells uncovered MKRN1/2-dependent ubiquitination of RPS10/eS10 at K107, which is a distinct site from the commonly-studied ZNF598-dependent RPS10/eS10 ubiquitination at K138 and K139 (Hildebrandt et al., 2019). The function of ubiquitinating RPS10/eS10 at these various sites remains a question to be addressed in future studies.

DEUBIQUITINASES FUNCTIONING DURING TRANSLATIONAL STRESS

Deubiquitinases (DUBs) are enzymes responsible for removing ubiquitin peptides from substrates (Clague et al., 2019). Here, we discuss DUBs that function alongside E3 ubiquitin ligases as an additional avenue to affect translation (Figure 1.5).

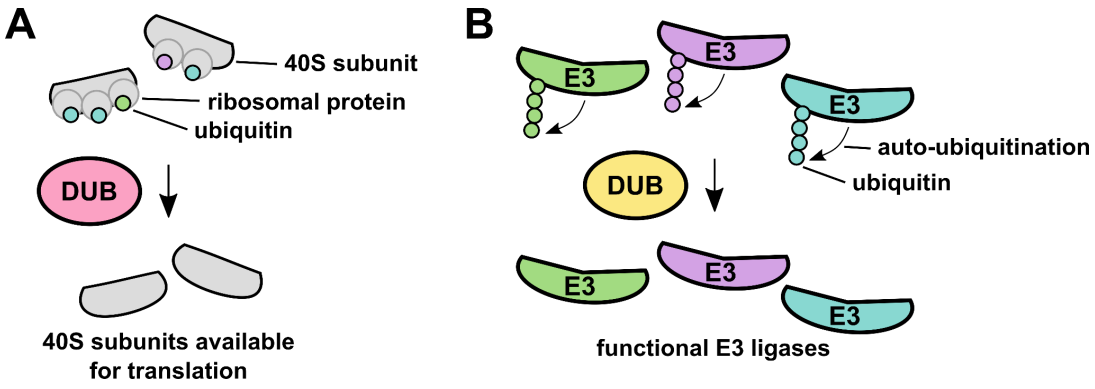

Figure 1.5: DUBs control the ubiquitination status of 40S subunits and E3 ubiquitin ligases. (A) Model for deubiquitinase (DUB) function during ribosomal ubiquitination. Gray ovals represent 40S subunits, with gray circles as ribosomal proteins experiencing ubiquitination. Ubiquitins are indicated with colored circles. DUB acting on 40S subunits is shown in pink. **(B)** Model for DUB function during E3 ubiquitin ligase auto-ubiquitination. Poly-ubiquitin chains are shown as strings of colored circles. E3 ligases are shown in their respective colors. DUB acting on E3 ligases is shown in yellow.

40S subunit homeostasis: OTUD3, USP21, and USP10

The DUBs OTUD3 and USP21 were recently linked to translational surveillance via an overexpression screen selecting for readthrough of NGD poly(A) stalls (Garshott et al., 2020). This work uncovered roles for OTUD3 and USP21 in deubiquitinating 40S proteins (Figure 3A) targeted by ZNF598 (namely RPS20/uS10 and RPS10/eS10), as well as a role

for USP21 in deubiquitinating RPS3/uS3 and RPS2/uS5. Both of these functions were enhanced upon UV-induced RQC, suggesting a role for DUBs in maintaining the 40S pool during cellular stresses.

Interestingly, ZNF598 protein was previously found to be in vast excess compared to OTUD3 and USP21 in human cells (Itzhak et al., 2016), suggesting a model in which cells entrust ZNF598 with the power to ubiquitinate 40S proteins which are slowly deubiquitinated. Subsequent work supports this model, revealing that 40 to 100-fold overexpression of OTUD3 and USP2 is required to suppress ZNF598 function (Garshott et al., 2020). Taken together, these works point toward a necessity for ZNF598 (and other E3 ligases) to accurately target aberrant ribosomes to maintain 40S subunit levels.

Additionally, the DUB USP10 was also identified in the same overexpression screen selecting for readthrough of NGD poly(A) stalls (Garshott et al., 2020). Further work observed increased RPS3/uS3 and RPS2/uS5 ubiquitination in USP10 knockout cells, and ultimately 40S subunit degradation upon constitutive, drug-induced ubiquitination of these sites by the E3 ligase RNF10 (Meyer et al., 2020; Garshott et al., 2021; Garzia et al., 2021).

E3 ubiquitin ligase abundance: USP9X

A recent proteomic study linked the DUB USP9X and translational surveillance, identifying USP9X as a ZNF598-interacting protein (Garzia et al., 2017). USP9X has since been shown to regulate protein abundance of both MKRN1/2 and ZNF598 (Figure 3B), with work observing lower levels of these E3 ligases and reduced NGD function upon USP9X knockdown (Clancy et al., 2021). These data support a model where MKRN1/2 and ZNF598 auto-ubiquitinate, as is common for RING E3 ligases, and thus require USP9X for stability. Further work focused on E3 ligase regulation, at the DUB level and beyond, will prove useful in understanding how cells keep ubiquitination of ribosomes under tight control.

UBIQUITIN AS A SIGNAL FOR REPRESSION

While ubiquitination is required for NGD and NSD, it remains unclear how ubiquitin commits translational complexes to decay and recycling. That is, ubiquitin in and of itself does not elicit mRNA repression nor ribosome rescue. A hint comes from the observation that key repressive effectors required for NGD and NSD contain ubiquitin-binding domains (Table 3). It thus is plausible that ubiquitin serves to localize effectors to problematic mRNAs, which use their effector domain(s) to alter translational complexes. Distinct ubiquitination sites, in combination with nearby ribosomal proteins and rRNA, could feasibly provide unique contact sites, allowing for accurate differentiation between aberrant stalls and innocuous pauses.

Effector	Effector domain	Recruitment domain
CUE2/NONU-1	Smr nuclease	CUE[*,†]
HBS-1	eEF1A-like GTPase	Uba-like triple-helix bundle[^]
CUE3/ASCC	RecA-like helicase	CUE[*,†]

Figure 1.6: Translational surveillance effectors recognizing altered ribosomes. Table of known translational surveillance effectors suspected to act downstream of and dependent on ribosomal ubiquitination. Effector domains shown are defined by the established function in translational surveillance pathways. Recruitment domain is supported by [*]genetic evidence demonstrating its requirement in surveillance, [†]biochemical evidence displaying its ubiquitin-binding ability, or [^]structural homology with other ubiquitin-binding domains.

For example, recruitment of CUE2/NONU-1 (D'Orazio et al., 2019; Glover et al., 2020) via CUE domains was recently discovered to link ribosomal ubiquitination with mRNA decay (Tomomatsu et al., 2022; Monem et al., 2023). Additionally, recruitment of HBS-1 and CUE3/ASCC could link ribosomal ubiquitination with ribosome rescue, therefore allowing for subunit recycling and downstream nascent chain degradation (Matsuo et al., 2020; Juszkiewicz et al., 2020; Monem et al., 2023).

A major challenge is the identification of ubiquitin-binding domains. Some effectors (*e.g.*, CUE2/NONU-1, CUE3/ASCC) have ubiquitin-binding domains recognizable at the primary sequence level. However, among the many known ubiquitin-interacting domains in

biology, there is little sequence conservation even among homologs in different organisms, which is a hallmark of the nature of the often hydrophobic interaction between a protein and ubiquitin (Husnjak & Dikic, 2012; Randles & Walters, 2012). As ubiquitin-binding motifs can be encoded by as little as a few alpha helices or beta sheets, our ability to identify them from sequence alone is expected to remain poor. While prediction of ubiquitin-binding domains from sequence may improve, until then we expect that ubiquitin-binding assays will remain critical to learn whether a downstream effector is recruited via ubiquitin or by some other means. Given the relatively poor identification of ubiquitin-binding domains from sequence alone, we expect that many more effectors are ubiquitin-dependent than is currently appreciated.

CONCLUSIONS AND FUTURE PERSPECTIVES

The work discussed above highlights the major focus placed on regulatory ribosomal ubiquitination in recent years. Reports of ubiquitination on many 40S subunit proteins have since been linked to a group of E3 ubiquitin ligases responsible for their modification, with deubiquitinases regulating levels of 40S subunits and E3s themselves. These studies have laid a groundwork of molecular interactions to help understand NGD and NSD.

Taken together, ribosomal ubiquitination can function to recruit a group of effectors which carry out commitment steps toward repression. However, it remains unclear how ubiquitin-binding effectors actually bind ubiquitin, especially considering that some effectors contain multiple ubiquitin-binding domains and that they are presented with a constellation of potential ubiquitin sites to bind. We anticipate future studies will reveal direct functions of individual ubiquitination sites, characterize the ubiquitin-binding domains within effectors, and identify novel ubiquitin-binding effectors.

Lastly, much of the study of ribosomal ubiquitination comes from situations in which a large number of ribosomes experience the same stress. Whether subsets of endogenous mRNAs have their ribosomes ubiquitinated is poorly understood, in part because only a small

number of ribosomes would be on such an mRNA at once, thus complicating a clear measure of their ubiquitination status. In this way, we are currently only “listening” to the ubiquitin language of the “loudest” ribosomes communicating an assault on translation. Considering that the cell is essentially a crowded room of ribosomes, each with their own ubiquitin story to tell, we are currently missing what the “quieter” ribosomes are saying. This gap in knowledge is exemplified by the finding of ~60 metazoan ribosomal proteins ubiquitinated at a total of ~268 residues, while we only have hints at function for ~10 residues on the small subunit (Figure 1.7) (Higgins et al., 2015; Koyuncu et al., 2021). There is little understanding of the biological significance and/or functional consequences of ribosomal ubiquitination outside of these handful of sites. We look forward to works delving into the meaning of these largely uncharacterized ubiquitination events and expect these contributions to amplify the voices of translation.

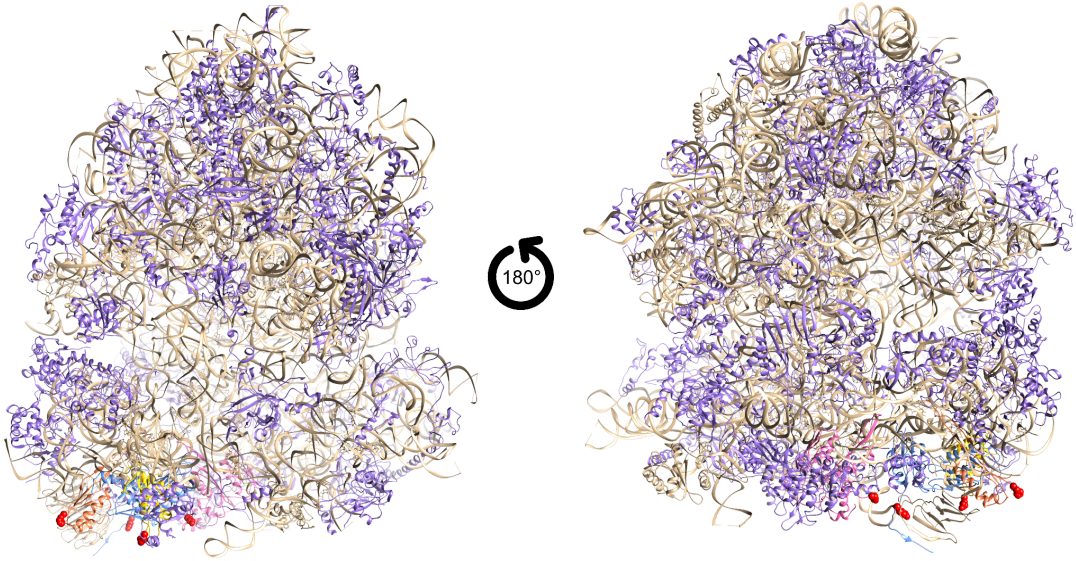

Figure 1.7: Ribosomal ubiquitination sites with unclear consequences. Cryo-EM structure collided/trailing ribosome from Juszkiewicz et al., 2018 (PDB 6HCQ). Characterized ribosomal ubiquitination protein targets and lysine residues (Table 1) are colored as in Figure 1. Uncharacterized ribosomal ubiquitination protein targets from Higgins et al., 2015 and Koyuncu et al., 2021 are colored in lavender. Other ribosomal proteins and rRNA are colored in beige.

CHAPTER 2: UBIQUITINATION OF STALLED RIBOSOMES ENABLES mRNA DECAY VIA HBS-1 AND NONU-1 *IN VIVO*

ABSTRACT

As ribosomes translate the genetic code, they can encounter a variety of obstacles that hinder their progress. If ribosomes stall for prolonged times, cells suffer due to the loss of translating ribosomes and the accumulation of aberrant protein products. Thus to protect cells, stalled ribosomes experience a series of reactions to relieve the stall and degrade the offending mRNA, a process known as No-Go mRNA Decay (NGD). While much of the machinery for NGD is known, the precise ordering of events and factors along this pathway has not been tested. Here, we deploy *C. elegans* to unravel the coordinated events comprising NGD. Utilizing a novel reporter and forward and reverse genetics, we identify the machinery required for NGD. Our subsequent molecular analyses define a functional requirement for ubiquitination on at least two ribosomal proteins (eS10 and uS10), and we show that ribosomes lacking ubiquitination sites on eS10 and uS10 fail to perform NGD *in vivo*. We show that the nuclease NONU-1 acts after the ubiquitin ligase ZNF-598, and discover a novel requirement for the ribosome rescue factors HBS-1/PELO-1 in mRNA decay via NONU-1. Taken together, our work demonstrates mechanisms by which ribosomes signal to effectors of mRNA repression, and we delineate links between repressive factors working toward a well-defined NGD pathway.

INTRODUCTION

An organism's growth, function, and response to environmental changes rely on ribosomes accurately producing proteins. Subtle errors in mRNAs are often elusive, requiring active translation to detect and trigger downstream repression. If left unchecked, defective mRNAs have the potential to produce toxic proteins resulting in disease phenotypes, such as neurodegeneration (Ishimura et al., 2014; Bengtson & Joazeiro, 2010).

Ribosomes that translate problematic mRNAs can elicit various repressive mechanisms. Two such mechanisms are Nonstop mRNA Decay (NSD) and No-Go mRNA Decay (NGD). NSD is triggered by mRNAs lacking stop codons, which can arise from polyadenylation or from mRNA cleavage (Frischmeyer et al., 2002). NGD occurs on mRNAs containing a variety of elongation-inhibiting features, such as stable secondary structures, stretches of rare codons, polybasic amino acid-encoding sequences, or damaged nucleotides (Doma and Parker, 2006). While triggered by different mRNA species, both of these pathways result in mRNA decay, ribosome rescue, and nascent peptide degradation through the coordinated recruitment of several effectors.

One key event in NGD is the generation of a stalled, collided ribosome species at a problematic site on the mRNA. This species is thought to be unique to NGD and could conceivably recruit downstream effectors (Simms et al., 2017; Juszkiewicz et al., 2018; Ikeuchi et al., 2019). The interface between collided ribosomes is the site of ubiquitination events on multiple ribosomal proteins near the mRNA's path (Juszkiewicz et al., 2018; Ikeuchi et al., 2019). The conserved E3 ubiquitin ligase ZNF-598 is thought to deposit ubiquitin marks on at least two ribosomal proteins, including RPS-10 (eS10) and RPS-20 (uS10) (Juszkiewicz & Hegde, 2017; Sundaramoorthy et al., 2017). Prior work overexpressing ubiquitination-deficient point mutations of eS10 suggests that ribosomal protein ubiquitination is important for NGD (Juszkiewicz & Hegde, 2017), though whether additional, ubiquitination-independent mechanisms contribute remains unclear. Our limited understanding of ribosomal ubiquitination is in part due to the difficulty in recovering viable mutants of the target ribosomal proteins, which has thus far complicated a straightforward analysis of individual ubiquitination sites and their relationship to repression via ZNF-598. Harnessing a system to study the functional contributions of ribosomal ubiquitination would clarify its importance.

Early NGD work pointed towards *Saccharomyces cerevisiae* Dom34 and Hbs1 (Pelota and HBS1 in higher eukaryotes) as being important for mRNA cleavage (Doma &

Parker 2006). Despite an early study claiming nuclease activity of Dom34, it is now thought that this requirement is indirect (Passos et al., 2009) with subsequent work on Dom34/Hbs1 showing a biochemical role in ribosome rescue (Shoemaker et al., 2010; Becker et al., 2011; Saito et al., 2013; Hilal et al., 2016). Later work in both *Caenorhabditis elegans* and *S. cerevisiae* identified NONU-1/Cue2/YPL199C as endonucleases responsible for cleaving targets of NSD and NGD in the vicinity of stalled ribosomes (Glover et al., 2020; D'Orazio et al., 2019). While NONU-1 is required for efficient NSD and NGD, it remains unclear how and when the factor is targeted to stall-inducing mRNAs. However, clues to its recruitment mechanism exist: NONU-1 and its homologs contain at least two conserved ubiquitin-binding CUE domains (Glover et al., 2020).

Much of what is known about NGD comes from studying the effect of individual factors and events, and it is unclear how these steps relate to one another to bring about target mRNA repression. Here, we deployed *C. elegans* to unravel the series of events during NGD. We show that mutation of ribosomal ubiquitination sites on RPS-10 (eS10) and RPS-20 (uS10) phenocopies knock out of ZNF-598. We present data in support of a model in which ZNF-598 first ubiquitinates ribosomes at stall sites, followed by mRNA degradation via NONU-1. Interestingly, we also recovered a role for HBS-1 and PELO-1 in mRNA decay via NONU-1 cleavage, consistent with early northern data in *S. cerevisiae*, suggesting that ribosome rescue may be an important step that precedes mRNA cleavage.

RESULTS

A novel ribosome stalling screen identifies core NGD machinery

To establish *C. elegans* as a system to study NGD, we built a ribosome stalling reporter using CRISPR/Cas9 at the *unc-54* locus. UNC-54 encodes a major muscle myosin required for animal movement, but dispensable for life (Moerman et al., 1982; Anderson & Brenner, 1984; Bejsovec & Anderson, 1988). UNC-54 has also been the starting point for a number of genetic screens, and its expression is relatively well-characterized. To build a NGD

reporter, we added a T2A ‘stop-and-go’ peptide, a FLAG tag, twelve rare arginine codons, and GFP to the C-terminus of UNC-54 via CRISPR/Cas9, and we call the resultant allele *unc-54(rareArg)* (Fig 2.1A). We selected rare arginine codons for two reasons: (1) arginine is a positively charged amino acid and prior work (Lu and Deutsch, 2008; Chandrasekaran et al., 2019) suggests this may induce ribosome stalling via interactions with the peptide exit tunnel, and (2) the Arg-tRNAs decoding two of the rarest codons (CGG, AGG) in *C. elegans* are very lowly expressed under normal growth conditions (Aidan Manning, Todd Lowe, personal communication, June 2021), providing a second avenue by which stalling may occur.

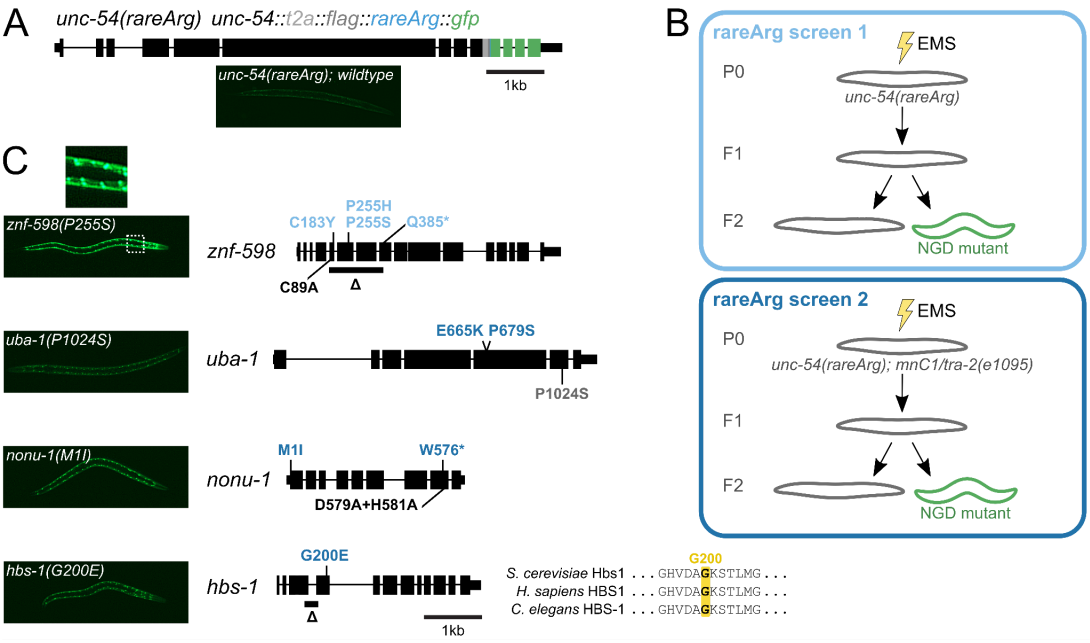

Figure 2.1. Genetic screens identify suppressors of No-Go mRNA Decay. (A) Gene diagram showing annotated exons (black rectangles) of *unc-54(rareArg)*. Colored rectangles represent CRISPR/Cas9 insertions at the endogenous *unc-54* locus: T2A sequence (gray), FLAG (dark gray), 12 rare arginine codons (blue), and GFP (green). **(B)** Schematics of rareArg genetic screens. **(C)** *znf-598, uba-1, nonu-1,* and *hbs-1* alleles with representative image of one allele per gene on the left. Black rectangles represent exons, thicker rectangles are CDS, and thin lines are introns. Mutations made via EMS in the rareArg screen 1 (light blue) or rareArg screen 2 (dark blue), and via CRISPR/Cas9 (black) or CGC (gray) are shown. For HBS-1, multiple sequence alignment shows conserved glycine (G200) in GTPase domain.

Strains with the *unc-54(rareArg)* construct showed an uncoordinated (Unc) phenotype consistent with reduction of UNC-54 protein. As other C-terminal tags of UNC-54

are functional (Arribere et al., 2016), the loss of UNC-54 protein suggests that mRNAs produced from the *unc-54(rareArg)* locus are repressed. *unc-54(rareArg)* animals also exhibited very low levels of GFP, suggesting that few ribosomes make it to the 3'end of *unc-54(rareArg)* due to reduced mRNA levels and/or high amounts of stalling during translation elongation.

To initially validate the *unc-54(rareArg)* reporter as a target of NGD, we crossed it with alleles of two factors known to be required for NGD in *C. elegans* (*nonu-1(AxA)*) and other systems (*znf-598(Δ)*) (Brandman et al., 2012; Juszkiewicz & Hegde, 2017; Sundaramoorthy et al., 2017; Glover et al., 2020). In each case we observed de-repression of the reporter, manifest as increased fluorescence and an improvement in animal movement and egg laying (UNC-54 is required in the vulva muscles for egg laying). The *nonu-1* result is consistent with our prior work showing that this stretch of twelve rare arginine codons confers *nonu-1*-dependent mRNA decay (Glover et al., 2020). Notably, the phenotypic effects seen upon *nonu-1* knockout differ from that seen in *S. cerevisiae:* knockout of the homologous *CUE2* in *S. cerevisiae* only confers effects upon simultaneous knockout of additional factors (D'Orazio et al., 2019). Given that most of our mechanistic understanding of NGD comes from work in *S. cerevisiae* (Doma and Parker, 2006; Simms et al., 2017; D'Orazio et al., 2019), and that genetic screens in human K562 cells failed to identify the NONU-1 homolog (Hickey et al., 2020), we reasoned that a genetic screen in *C. elegans* would prove insightful and augment information gained from other systems.

Using *unc-54(rareArg),* we performed two genetic screens (Methods) (Fig 2.1B). In the first of these screens, we EMS-treated *unc-54(rareArg)* animals, harvested eggs, and screened ~90,000 F1 genomes. Among these, we found six mutants across six plates with increased movement (indicative of de-repression of *unc-54(rareArg)*) and increased GFP (indicative of translation to the end of the *unc-54(rareArg)* transcript). Evidence of stall readthrough was visible by the nuclear localization of GFP upon its de-repression (Fig 2.1C). This observation revealed our serendipitous construction of an N-terminal motif (a run of

arginines) matching the sequence requirements for a nuclear localization signal (Lu et al., 2021). We genetically mapped and identified variants, and found that four alleles mapped to *znf-598* (Fig 2.1C).

Reasoning that there was more to NGD than *znf-598*, we repeated the screen using a chromosomal balancer covering the *znf-598* locus to preclude recovery of recessive *znf-598* mutations. We screened an additional ~105,000 F1 genomes, among which we found an additional 14 mutants across 14 plates. The increase of movement and GFP in these animals were less pronounced than the *znf-598* mutants from the first screen. Nevertheless, the phenotypes were robust enough to allow us to genetically map and identify causative loci. Here we report a total of nine alleles in four genes from both screens (Fig 2.1C). Five alleles in one additional gene were identified (*catp-6*, Table 1); mapping and characterization of the remaining six mutants is ongoing.

Seven alleles were split amongst three readily-identifiable NGD components: *nonu-1, znf-598*, and *hbs-1*. We found two mutations in *nonu-1*, as would be expected based on the *unc-54(rareArg)* reporter validation. We isolated four mutations in *znf-598* (all from the first genetic screen), three of which were missense mutations. One mutation (C183Y) was within a region that matches the consensus for a C2H2 zinc finger in *C. elegans* and *Homo sapiens,* but is not conserved in *S. cerevisiae.* Two alleles at P255 (P255S, P255H) mutated a highly conserved proline at the start of a C2H2 zinc finger. One allele was found in the *C. elegans*' homolog of HBS1 (*k07a12.4*, hereafter *hbs-1*). This allele was in a conserved GTP-binding and active site residue (G200E) (Fig 2.1C), consistent with a functional requirement for GTP binding and hydrolysis by HBS-1 in NGD.

Two additional mutations mapped in *uba-1*, the sole E1 ubiquitin-activating enzyme in *C. elegans*. Both *uba-1* mutations (E665K, P679S) exhibited poor viability, as would be expected as complete loss of *uba-1* is thought to be lethal (Kulkarni & Smith, 2008). We confirmed the *uba-1* result by crossing in a known temperature-sensitive loss-of-function allele of this gene (*it129*; *P1024S*), and observed temperature-dependent de-repression of

GFP. As ZNF-598 is known to function in other systems as a ubiquitin ligase (Juszkiewicz & Hegde, 2017; Sundaramoorthy et al., 2017), we expect that *uba-1* loss-of-function compromised the ubiquitin-conjugation cascade, giving rise to *unc-54(rareArg)* de-repression.

Cell-specific NGD rescue via overexpression of factors

We also developed a system to analyze the effects of overexpression of particular NGD pathway components using extrachromosomal arrays. Overexpression is a useful means to generate hyperactive alleles of factors to test their relative order in a pathway. Injection of foreign DNA into the germline of *C. elegans* results in fusion of the DNA sequences into an extrachromosomal array (Stinchcomb et al., 1985; Mello et al., 1991). The resultant array can be both meiotically and mitotically inherited, albeit with reduced efficiencies compared to endogenous chromosomes. We created a plasmid vector to overexpress a gene of interest on a transgenic array with the following components: (1) a *myo-3* promoter, to drive expression in the body wall muscle where *unc-54* is also expressed, (2) a fluorescent mCherry protein, to monitor inheritance and expression of the array, (3) a 'stop-and-go' T2A sequence, to separate mCherry from the gene-of-interest, and (4) a site to insert a gene-of-interest. We constructed plasmids encoding fluorescent proteins linked to *C. elegans*' *znf-598* and *nonu-1*.

To check the functionality of factors expressed from an array, we made overexpression arrays in each of the cognate mutant backgrounds. Overexpression of the wild-type ZNF-598 and NONU-1 protein restored repression of *unc-54(rareArg)* and rescued the loss-of-function phenotype of *znf-598* (Fig 2.2A) and *nonu-1* (Fig 2.2B), respectively. Thus the overexpressed factors were functional. Arrays can be stochastically lost or silenced in cell lineages of the animal, allowing us to examine rescue on a cell-by-cell level. For each of *znf-598* and *nonu-1*, we observed an inverse relationship between factor expression (monitored via mCherry) and *unc-54(rareArg)* (monitored via GFP). Thus the rescue was

cell-autonomous, as would be expected under current models of ZNF-598 and NONU-1 acting directly on ribosomes and mRNAs.

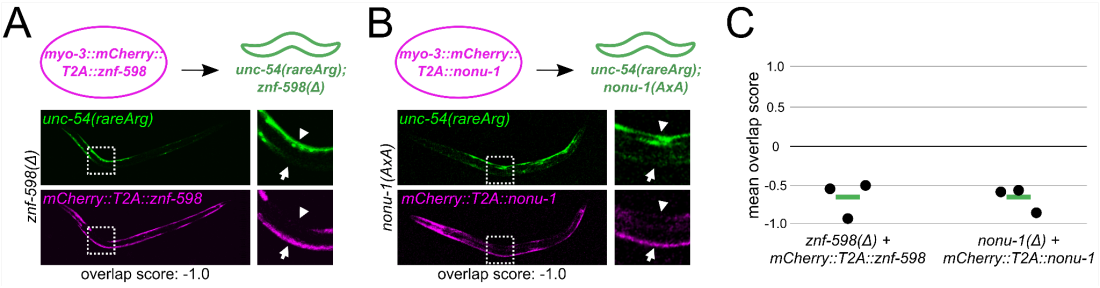

Figure 2.2: Cell-specific NGD rescue via overexpression of factors. (A) Schematic of *znf-598* construct plasmid and *znf-598* strain subject to germline microinjection. Below are GFP and mCherry images of a representative animal expressing the above construct, with a zoom in of an area demonstrating the effect of mCherry-marked factor expression on NGD (GFP). **(B)** As in (A) for *nonu-1* construct in *nonu-1* strain. **(C)** Mean overlap score of strains in (A, B). Each black dot represents the mean of one independent isolate (n≥4 animals/isolate), with the mean of all isolates shown as a green bar.

To quantify the inverse relationship of factor overexpression (mCherry) to NGD (GFP), we calculated an overlap score, based on the brightest red and green pixels across multiple, independent animals (Methods) (Fig S2.1). If mCherry and GFP are non-overlapping (as would be expected from rescue), the overlap score would be negative. If mCherry and GFP overlap (as would be expected without rescue), the overlap score would be positive. For *znf-598* and *nonu-1*, we observed values close to -1 (Fig 2.2C), demonstrating the generality of rescue across animals.

With a functional readout of NGD (*unc-54(rareArg)*), mutants in factors (*znf-598*, *nonu-1*, *hbs-1*, and *pelo-1*), and the overexpression/rescue system, we set out to characterize the molecular mechanisms by which factors relate and repress gene expression in response to ribosomal stalling.

ZNF-598 is required for ribosomal ubiquitination in *C. elegans*

In the NGD screen, we recovered several alleles of *znf-598*. ZNF-598 homologs are thought to recognize ribosomal collisions and ubiquitinate sites on the small subunit, including RPS-10 (eS10) and RPS-20 (uS10) (Juszkiewicz & Hegde, 2017; Sundaramoorthy et al.,

2017). By multiple sequence alignment, we identified a highly conserved cysteine (C89) (Fig 2.3A) (Sundaramoorthy et al., 2017) known to be required for ubiquitin conjugation by Hel2/ZNF598, and we generated a point mutation (C89A) via CRISPR/Cas9 at the endogenous locus. The *znf-598(C89A)* mutant displayed *unc-54(rareArg)* de-repression indistinguishable from the phenotype of *znf-598(Δ)* (Fig 2.3B), supporting a role for ubiquitination in repression of stall-inducing mRNAs in *C. elegans*, as in other systems.

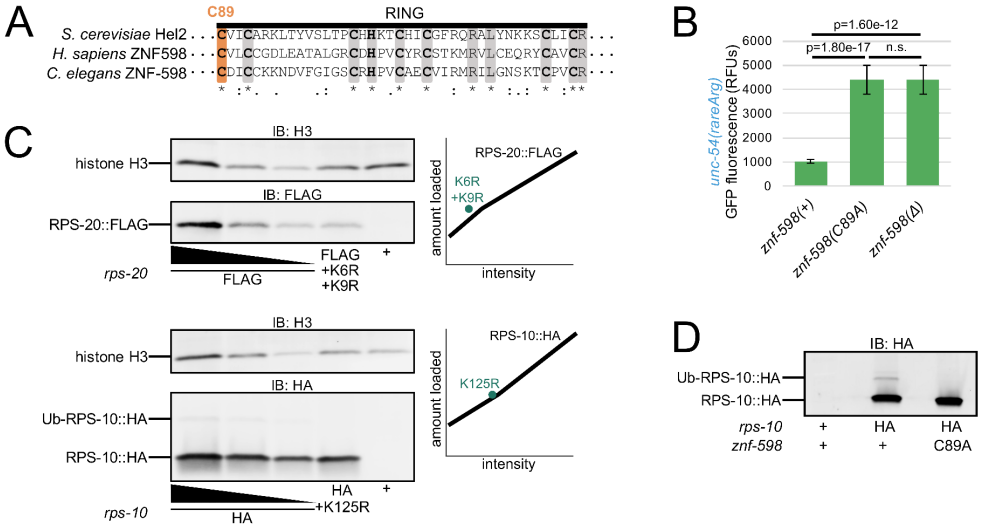

Figure 2.3. ZNF-598 is required for ribosomal ubiquitination in *C. elegans*. (A) Multiple sequence alignment of *S. cerevisiae* Hel2, *H. sapiens* ZNF598, and *C. elegans* ZNF-598 RING finger domains. Conserved residues (gray) and C89 (orange) are highlighted. Conservation below alignment is as follows: asterisks indicate identity, colons indicate amino acids with strongly similar properties, periods indicate amino acids with weakly similar properties. **(B)** Mean RFUs (relative fluorescence units) of indicated strains (n≥15 animals/strain) in the *unc-54(rareArg)* background. One standard deviation shown as error bars. p values from Welch's t-test. **(C)** Western blot of indicated strains to monitor RPS-20 and RPS-10 expression. Dilutions of wild type tagged proteins were loaded as indicated, with two-fold more and two-fold less than other two samples, to generate a standard curve shown as a black line in plots on the right. Lysine mutants of tagged proteins were quantified and plotted as teal points in the plots on the right. **(D)** Western blot of indicated strains to monitor ubiquitination of HA-tagged RPS-10.

To investigate the ribosomal protein targets of ZNF-598, we tagged both RPS-10 (eS10) and RPS-20 (uS10) at the endogenous locus via CRISPR/Cas9. By immunoblot we observed robust expression of the cognate ribosomal protein in each strain (Fig 2.3C). We also mutated conserved lysines in RPS-10 and RPS-20 known to be sites of ubiquitination in other systems (Fig S2.2A, Fig S2.2B) (Juszkiewicz & Hegde, 2017; Sundaramoorthy et al.,

2017). The K>R substitutions did not adversely impact RPS-10 and RPS-20 expression (Fig 2.3C) nor animal viability. In the case of RPS-10, we also observed a band corresponding to the expected size of Ub-RPS-10. This band was absent in *rps-10(K125R)* (Fig 2.3C) and *znf-598(C89A)* mutants (Fig 2.3D). These results show that *znf-598* is required for ubiquitination of RPS-10 on K125.

NGD-deficient ribosomes made via ablation of ubiquitination sites

Prior work underscored the importance of ribosomal ubiquitination events in NGD (Sundaramoorthy et al., 2017; Juszkiewicz & Hegde, 2017). However, the precise functional contributions of individual ubiquitination sites has remained unclear, in part due to the difficulty in obtaining viable mutants in the relevant ribosomal proteins. In prior work, overexpression of RPS-10 with K>R substitutions at ubiquitination sites conferred de-repression of a stalling reporter in between that observed in wild-type and ZNF598 knockout human cells (Juszkiewicz & Hegde, 2017). Interpretation of this experiment is complicated by a number of factors, including residual expression of wild-type RPS-10. Would complete removal of RPS-10 ubiquitination sites mimic loss of ZNF598? Does ZNF598 contribute to functional repression outside of its role in ribosomal ubiquitination? Our work thus far supported a NGD mechanism similar to that of human cells, and therefore our system seemed a useful model to explore these questions. In particular, the viability of ribosomal point substitutions at endogenous loci as well as the ease of making double mutants and overexpression constructs provided us with the means to test models of the functional importance of ribosomal ubiquitination and its relationship to ZNF-598.

To initially test for a functional role of ribosomal ubiquitination in NGD, we crossed *rps-10(K125R)* and *rps-20(K6R+K9R)* into *unc-54(rareArg)*. In each case we observed a defect in NGD, manifest as an increase in GFP produced by *unc-54(rareArg)* (Fig 2.4A). The double mutant (*rps-10(K125R)*; *rps-20(K6R+K9R)*) exhibited an even stronger defect in NGD, comparable to that observed in *znf-598* mutants. We interpret these data to indicate that

ribosomal ubiquitination is required for NGD, and that ablation of these two sites alone is sufficient to prevent functional NGD. Interestingly, these experiments demonstrate that it is possible to make a version of the ribosome deficient in NGD via mutation of a few lysines, highlighting the central role of the ribosome and ubiquitination in NGD.

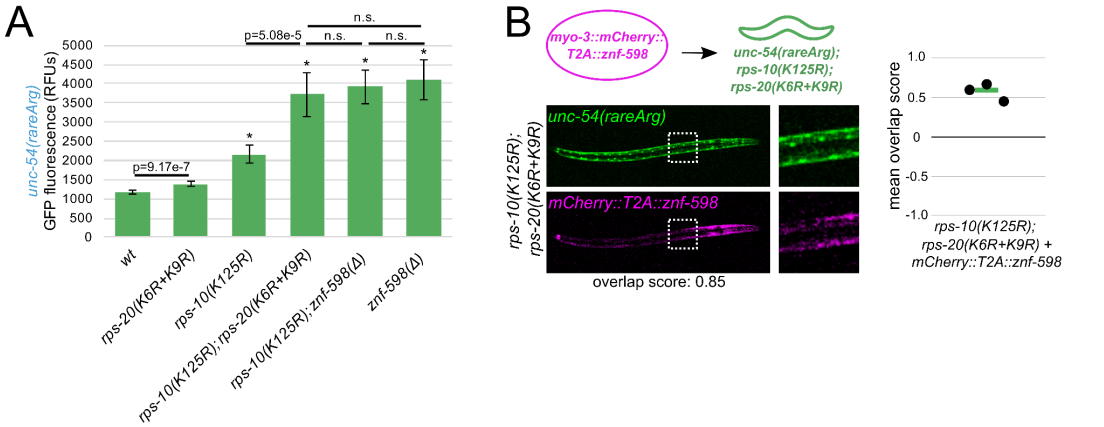

Figure 2.4: NGD-deficient ribosomes made via ablation of ubiquitination sites. (A) Mean RFUs (relative fluorescence units) of indicated strains (n≥15 animals/strain) in the *unc-54(rareArg)* background. One standard deviation shown as error bars. p values from Welch's t-test, with asterisks indicating p<0.01 for all comparisons with wild type. **(B)** As in Fig 2, with *znf-598* construct in *rps-10; rps-20* strain.

We also performed additional experiments to clarify the function of ribosomal ubiquitination in relation to *znf-598*. First, we performed a double mutant analysis. In a model where ribosomal ubiquitination is functionally independent of *znf-598*, we would expect that a *rps-10(K125R)*; *znf-598(Δ)* mutant would exhibit a stronger NGD phenotype (more GFP) than either single mutant alone. However, if ZNF-598 and Ub-RPS-10 lie on the same pathway, we would expect the *rps-10(K125R)*; *znf-598(Δ)* phenotype to resemble one of the single mutants. The *rps-10(K125R)*; *znf-598(Δ)* phenotype was indistinguishable from the *znf-598(Δ)* single mutant (Fig 2.4A), consistent with the latter model. Second, we used our overexpression system. In a model where *rps-10(K125R)* and *rps-20(K6R+K9R)* are on a partially redundant pathway to *znf-598* (*i.e.*, that *znf-598* contains additional repressive functions outside of ubiquitination at these two sites), we would expect that overexpression of ZNF-598 would provide restoration of NGD in the *rps-10(K125R)*; *rps-20(K6R+K9R)* mutant.

However, if ZNF-598 acts through RPS-10 and RPS-20, overexpression of ZNF-598 in a *rps-10(K125R)*; *rps-20(K6R+K9R)* mutant would yield the same phenotype as *rps-10(K125R)*; *rps-20(K6R+K9R)*. We observed the latter (Fig 2.4B), again suggesting that ZNF-598 works through ubiquitination of RPS-10 and RPS-20.

Taken together, our experiments suggest that ZNF-598 is a ubiquitin ligase required for ubiquitination of at least RPS-10 and RPS-20, and that these ubiquitination events are essential to NGD. The fact that loss of *znf-598* can be mimicked by mutation of ribosomal proteins provides compelling evidence that the primary function of ZNF-598 during NGD is to deposit ubiquitins on ribosomes.

NONU-1 function during NGD requires CUE domains and follows ZNF-598

Having established a requirement for ubiquitination by ZNF-598 in this system, we decided to investigate the relationship of ubiquitination to mRNA decay. A key effector of NGD is NONU-1, which was identified in our screen (Fig 2.1C) and also in our prior NSD screen (Glover et al., 2020). In our prior work, we noted that NONU-1 and its homologs contain CUE domains (Fig 2.5A), which are known to bind ubiquitin, suggesting a mechanism of recruitment for NONU-1 to sites of ribosome stalling. To test a requirement for the CUE domains in *nonu-1* function, we deleted the CUE domains and observed a phenotype indistinguishable from other *nonu-1* mutants (Fig 2.5B). This result is consistent with CUE domains being essential to NONU-1 function. We also attempted to examine expression of NONU-1 by tagging the N-terminus (Table 1), but tagged alleles were non-functional. We did not tag the C-terminus of NONU-1 as it is conserved. We look forward to future work where we can determine whether the requirement of CUE domains in NONU-1 is merely for NONU-1 expression or for its biochemical functions.

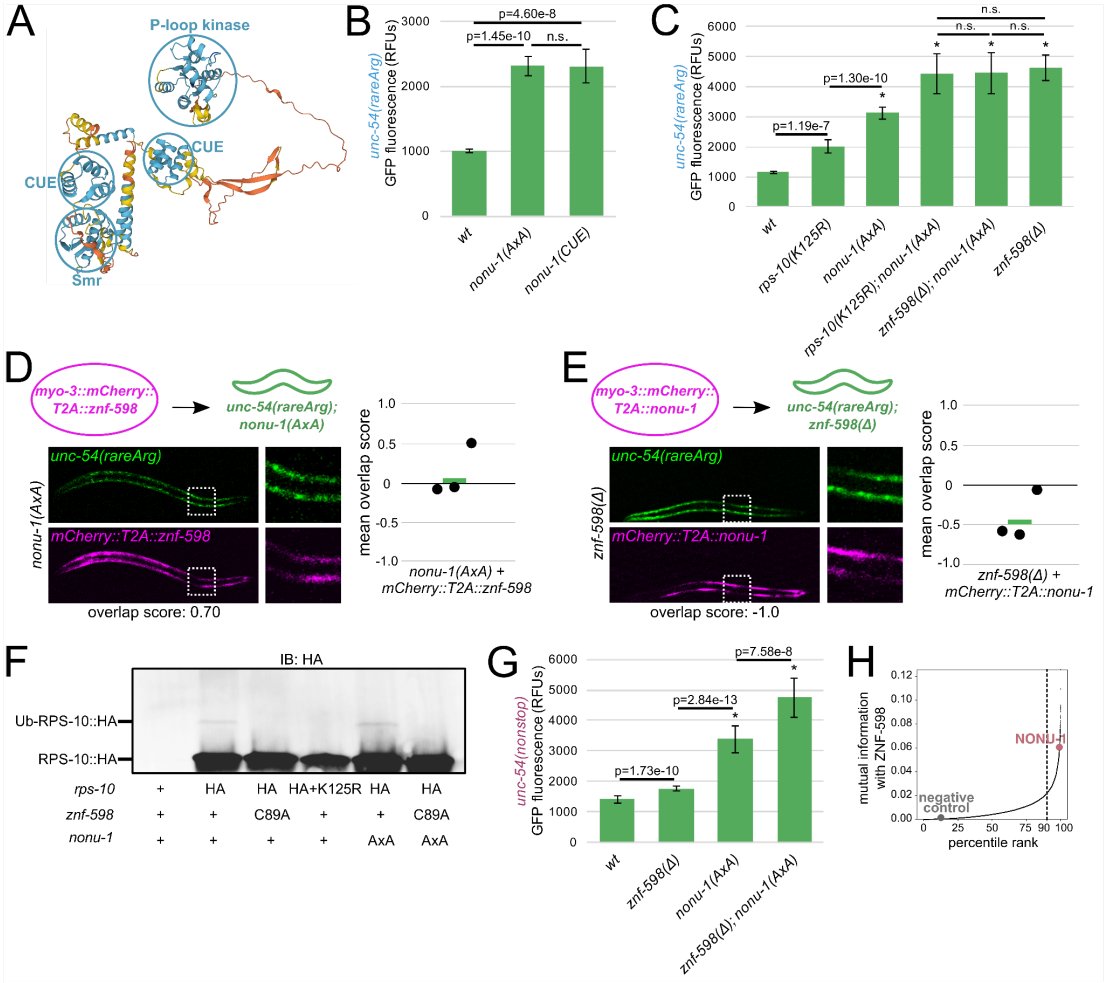

Figure 2.5. NONU-1 function during NGD requires CUE domains and follows ZNF-598. (A) *C. elegans* NONU-1 protein structure as predicted by AlphaFold (Jumper et al., 2021). Prediction confidence is as follows: blue regions are confident, yellow regions are low confidence, orange regions are very low confidence. Confident domains are circled in blue and labeled. **(B, C)** Mean RFUs (relative fluorescence units) of indicated strains (n≥15 animals/strain) in the *unc-54(rareArg)* background. One standard deviation shown as error bars. p values from Welch's t-test, with asterisks indicating p<0.01 for all comparisons with wild type. **(D)** As in Fig 2, with *znf-598* construct in *nonu-1* strain. **(E)** As in Fig 2, with *nonu-1* construct in *znf-598* strain. **(F)** Western blot of indicated strains to monitor ubiquitination of HA-tagged RPS-10. **(G)** Mean RFUs (relative fluorescence units) of indicated strains (n≥15 animals/strain) in the *unc-54(nonstop)* background. One standard deviation shown as error bars. p values from Welch's t-test, with asterisks indicating p<0.01 for all comparisons with wild type. **(H)** ZNF-598 mutual information plot. 90% percentile cutoff is shown as a dashed line, NONU-1 is highlighted in pink, and a negative control protein is highlighted in gray.

To determine whether NONU-1 acts in the same pathway as ZNF-598, we performed a double mutant analysis. If the two factors function in different pathways, we would expect additive phenotypes on the *unc-54(rareArg)* reporter in a double mutant. However, if NONU-1 and ZNF-598 work in the same pathway of repression, we would expect the double mutant to

resemble one of the single mutants. We combined mutations in *znf-598* and ribosomal ubiquitination sites with *nonu-1(AxA)*, a catalytic mutation of *nonu-1* that is indistinguishable from a deletion of *nonu-1* (Fig S2.3) (Glover et al., 2020). The *nonu-1*; *znf-598* double mutant mimicked the *znf-598* single mutant (Fig 2.5C), consistent with the two factors functioning in the same pathway in NGD.

We next investigated the ordering of ZNF-598 and NONU-1 relative to one another in NGD. In a first pair of experiments, we overexpressed ZNF-598 in a *nonu-1* mutant, and also overexpressed NONU-1 in a *znf-598* mutant. According to classical logic when ordering genes in functional pathways, we expect that overexpression of an upstream factor will not compensate for loss of a downstream factor, but that overexpression of a downstream factor will compensate for loss of an upstream factor (Smith & Mitchell, 1989; Dolan & Fields, 1990; Han et al., 1990; Shaham & Horvitz, 1996). We observed little effect of the *nonu-1* phenotype by ZNF-598 overexpression (Fig 2.5D), and we saw rescue of the *znf-598* phenotype by NONU-1 overexpression (Fig 2.5E). These results support a model where NONU-1 acts downstream of ZNF-598. In a second set of experiments, we examined RPS-10 ubiquitination by immunoblot in *nonu-1(AxA)* and observed it to be unchanged (Fig 2.5F). We interpret this result to indicate that the defect in a *nonu-1* mutant is after ribosomal ubiquitination, *i.e.*, in the commitment of ubiquitinated ribosomes to mRNA decay.

We were curious to determine whether *nonu-1* and *znf-598* function together in NSD as well. Thus, we quantified mutants' effects on the *unc-54(nonstop)* reporter, an allele of *unc-54* tagged with a C-terminal GFP and lacking all stop codons (Arribere and Fire, 2018; Glover et al., 2020). In contrast to its strong effect on the *unc-54(rareArg)* reporter, the *znf-598* mutant showed mild *unc-54(nonstop)* de-repression (Fig 2.5G). This result is consistent with a more modest role for *znf-598* in NSD than that observed at *unc-54(rareArg)*, and explains why prior NSD screens failed to identify *znf-598* (Arribere and Fire, 2018; Glover et al., 2020). A *nonu-1* mutant exhibited a greater de-repression of *unc-54(nonstop)* than *znf-598*, and the double mutant expressed higher levels of GFP than either single mutant.

The fact that *nonu-1* and *znf-598* together exhibit additive effects suggests that NONU-1 is recruited via an E3 ubiquitin ligase other than ZNF-598 during NSD. For more on this, see Discussion.

Taken together, our results with the *unc-54(rareArg)* reporter support a model in which ZNF-598 and NONU-1 function together in NGD. Based on our genetic and molecular analyses, we favor a model in which ribosomal ubiquitination recruits NONU-1 to mRNAs for cleavage.

A conserved role for ZNF-598 and NONU-1 throughout eukaryotes

To determine if the relationship between ZNF-598 and NONU-1 is a broadly conserved phenomenon throughout eukaryotes, we performed phylogenetic profiling (reviewed in Dey & Meyer 2015). Briefly, phylogenetic profiling scores pairs of proteins using mutual information, which can be interpreted as the tendency of the protein pair to function together, either redundantly or sequentially. High mutual information can be achieved when two proteins are inherited together or lost together, or when two proteins are genetically redundant and at least one protein is maintained.

We carried out phylogenetic profiling by searching 111,921 profile HMMs (Mi et al., 2021) on genomic and transcriptomic sequences from 473 protists as these represent diverse eukaryotic lifestyles (Methods). To validate this approach, we calculated mutual information between pairs of factors known to function together in a complex, such as PELO-1/HBS-1 (Fig S4A) and LTN-1/RQC-2 (Fig S4B) (Kostova et al., 2017; Shoemaker et al., 2010; Becker et al., 2011; Hilal et al., 2016). PELO-1/HBS-1 and LTN-1/RQC-2 exhibited high mutual information, scoring in each others' top 99.88% (PELO-1 ranked 19th of 15,909 interactions with HBS-1) and 98.86% (RQC-2 ranked 181th of 15,909 interactions with LTN-1), respectively. Similarly, we observed that ZNF-598 and NONU-1 ranked in each others' top 99.38% (NONU-1 ranked 99th of 15,909 interactions with ZNF-598) (Fig 5H). Thus ZNF-598 and NONU-1 are a broadly conserved functional pair across diverse eukaryotes, with our

work in *C. elegans* suggesting that this pair functions in NGD to degrade mRNAs that stall ribosomes.

HBS-1 N-terminus resembles a ubiquitin-binding domain and is dispensable for NGD

Several of our NGD suppressor mutants (*znf-598*, *nonu-1*, *uba-1*) encoded factors involved in ubiquitin-dependent processes, so we were initially surprised that this screen also identified the ribosome rescue factor *hbs-1*. We therefore examined HBS-1 to determine whether it could conceivably function in a ubiquitin-dependent manner.

The HBS-1 protein consists of an N-terminal domain, a disordered linker region, a GTPase domain, and two beta-barrel domains (Becker et al., 2011; Hilal et al., 2016) (Fig 2.6A). In two published structures, we noticed that the N-terminal domain of HBS-1 is found near known ubiquitination sites on the ribosome (uS10 and uS3) and adopts a distinct triple helix bundle (Becker et al., 2011; Hilal et al., 2016). The fold is classified by Pfam as a member of the ubiquitin-binding Uba clan (Fig 2.6B). Notable members of the Uba clan include the Uba and CUE domains, found in *S. cerevisiae* Rad23 and *C. elegans* NONU-1, respectively. We also noticed that plant HBS-1 N-term homologs contain a conserved C4-type zinc finger (ZnF) homologous to a known ubiquitin-binding C4 ZnF domain present in the rat Npl4 (Fig 2.6C) (Alam et al., 2004). These observations show that HBS-1 N-termini from diverse organisms lack sequence or structural homology with each other, and yet many N-termini instead share homology with domains that bind ubiquitin. Given this homology to ubiquitin-binding domains, we hypothesized that the N-terminal domain of HBS-1 may bind ubiquitin during NGD.

To determine whether the N-terminus of HBS-1 is required for its functions in NGD, we generated an N-terminal deletion mutant of *hbs-1* by deleting the region spanning the triple helix bundle and much of the linker region, yielding an HBS-1 consisting of only the first few amino acids, a short linker, and the GTPase domain. Surprisingly, when measuring *unc-54(rareArg)* GFP levels, deleting the N-terminus of HBS-1 had no discernible phenotype,

indicating that the N-terminal domain of HBS-1 is dispensable for NGD in *C. elegans* (Fig 2.6D).

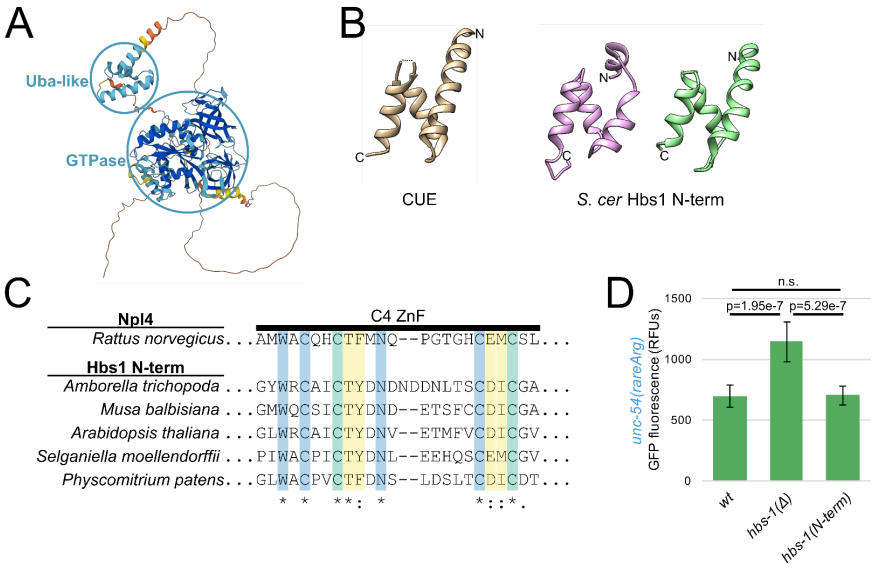

Figure 2.6. HBS-1 N-terminus resembles a ubiquitin-binding domain and is dispensable for NGD. **(A)** *H. sapiens* Hbs1 protein structure as predicted by AlphaFold (Jumper et al., 2021). Prediction confidence is as in Fig 5A, with dark blue showing regions of high confidence. Confident domains are circled in blue and labeled. **(B)** Structural homology between Hbs1 N-terminal domain and ubiquitin-binding domains. At left is a structure representative of the UBA clan: CUE from (Prag et al., 2003) (tan, *S. cerevisiae* Vps9p, 1P3Q). At right are two structures of the Hbs1 N-terminus from (Becker et al., 2011) (pink, *S. cerevisiae,* 3IZQ) and (Hilal et al., 2016) (green, *S. cerevisiae,* 5M1J). Amino and carboxy termini indicated with N and C, respectively. Note overall similarity in topology and fold across structures. **(C)** The N-terminal zinc finger (ZnF) of plant Hbs1 is homologous to the Ub-binding ZnF of rat Npl4. Multiple sequence alignment of the ZnF of Hbs1 from phylogenetically diverse plants. Residues that are highly conserved among Npl4 homologs are in blue, residues that contact Ub are in yellow, and residues that are both conserved and contact Ub are in green. Coloring and annotation of Npl4 residues from (Alam et al., 2004). **(D)** Mean RFUs (relative fluorescence units) of indicated strains (n≥15 animals/strain) in the *unc-54(rareArg)* background. One standard deviation shown as error bars. p values from Welch's t-test.

While our genetic analyses supported a role for HBS-1 in NGD independent of the N-terminal domain, it did not rule out a ubiquitin-binding role for the domain outside of NGD. To test this possibility, we performed an *in vitro* ubiquitin-binding assay (Shih et al., 2002). However, we failed to observe ubiquitin-binding above background (Fig S2.5). We speculate that the success of *in vitro* binding assays may be hindered by a requirement for a ribosome surface to promote HBS-1 binding, as the N-terminus binds to ribosomes in structural studies

(Becker et al., 2011; Hilal et al., 2016). We look forward to future work to explore the function of the HBS-1 N-terminus on the ribosome.

HBS-1 and PELO-1 are essential for mRNA degradation

HBS-1 functions with PELO-1 in other contexts, and so we decided to test a functional role of *pelo-1* in NGD. We crossed a *pelo-1* mutant (*cc2849*, bearing a large deletion) (Arribere & Fire, 2018) into the *unc-54(rareArg)* reporter. The *pelo-1* mutant exhibited a de-repression of *unc-54(rareArg)* comparable to that observed in the *hbs-1* mutant (Fig S2.6). Furthermore, the *hbs-1*; *pelo-1* double mutant exhibited a phenotype similar to the single mutants (Fig S2.6), suggesting that the two factors function together in NGD as is known in other systems.

HBS-1 and PELO-1 are predominantly known for their role in ribosome rescue, and we were initially surprised by their requirement for repression of the *unc-54(rareArg)* reporter. Despite a well-characterized biochemical role in ribosome rescue (Shoemaker et al., 2010; Becker et al., 2011; Pisareva et al., 2011; Saito et al., 2013; Hilal et al., 2016), there is also a known but poorly understood requirement for HBS-1/PELO-1 in mRNA degradation in NGD in other systems (Doma & Parker, 2006) as well as in NSD in *C. elegans* (Arribere & Fire, 2018). We hypothesized that HBS-1/PELO-1 may facilitate mRNA decay during NGD in *C. elegans*. To test this hypothesis, we performed RNA-seq on *znf-598*, *nonu-1*, and *hbs-1* mutants bearing the *unc-54(rareArg)* reporter (Fig 2.7A). We observed an increase in *unc-54(rareArg)* mRNA levels comparable to the level of GFP de-repression observed in each strain, with *znf-598* conferring the highest levels and *nonu-1* and *hbs-1* exhibiting a lesser and similar increase in mRNA levels. Therefore, we conclude that HBS-1 is required for mRNA degradation during NGD in *C. elegans*.

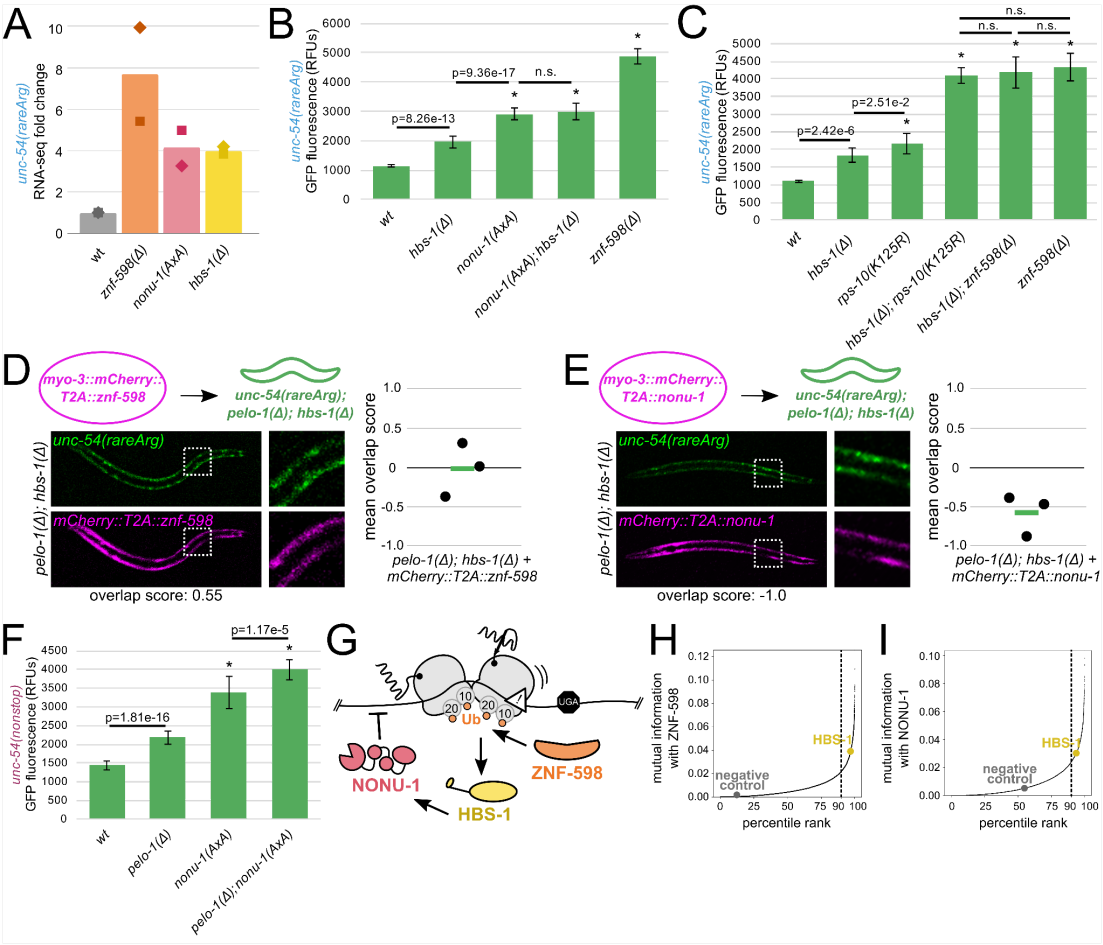

Figure 2.7. HBS-1 and PELO-1 are essential for mRNA degradation. (A) RNA-seq mean fold change of *unc-54(rareArg)* in the indicated strains from two biological replicates (shown as diamonds and squares). **(B, C)** Mean RFUs (relative fluorescence units) of indicated strains (n≥15 animals/strain) in the *unc-54(rareArg)* background. One standard deviation shown as error bars. p values from Welch's t-test, with asterisks indicating p<0.01 for all comparisons with wild type. **(D)** As in Fig 2, with *znf-598* construct in *pelo-1; hbs-1* strain. **(E)** As in Fig 2, with *nonu-1* construct in *pelo-1; hbs-1* strain. **(F)** Mean RFUs (relative fluorescence units) of indicated strains (n≥15 animals/strain) in the *unc-54(nonstop)* background. One standard deviation shown as error bars. p values from Welch's t-test, with asterisks indicating p<0.01 for all comparisons with wild type. **(G)** Model for NGD via ZNF-598, HBS-1, and NONU-1. **(H)** ZNF-598 mutual information plot. 90% percentile cutoff is shown as a dashed line, HBS-1 is highlighted in yellow, and a negative control protein is highlighted in gray. **(I)** As in (H), showing NONU-1 mutual information with HBS-1.

Studies in *S. cerevisiae* identified homologs of *hbs-1* and *pelo-1* (*HBS1* and *DOM34*) as being required for endonucleolytic cleavages during NGD (Doma & Parker, 2006; Passos et al., 2009; van den Elzen et al., 2010), though at the time of that work, the identity of the nuclease was unknown. Based on this literature and our RNA-seq analysis, we hypothesized

that HBS-1/PELO-1 may act in the same pathway as NONU-1. To test this hypothesis, we performed double mutant analysis with *hbs-1* and *nonu-1*. The *nonu-1*; *hbs-1* double mutant was indistinguishable from a *nonu-1* single mutant, suggesting that HBS-1 acts in the same pathway as NONU-1 (Fig 2.7B). We also found HBS-1 to act in the same pathway as ZNF-598 (Fig 2.7C).

To place HBS-1 relative to ZNF-598 and NONU-1 in NGD, we tested whether excess ZNF-598 or NONU-1 could compensate for the loss of *pelo-1* and *hbs-1*. Overexpression of ZNF-598 resulted in little change to the NGD phenotype (Fig 7D), consistent with a model where HBS-1/PELO-1 act downstream of ZNF-598. In contrast, overexpression of NONU-1 rescued NGD in *pelo-1*; *hbs-1* animals (Fig 7E). This result suggests that NONU-1 acts downstream of HBS-1/PELO-1. Interestingly, analyses using the NSD reporter indicate separate capabilities for NONU-1 and HBS-1/PELO-1 in NSD: a double mutant analysis of *pelo-1* and *nonu-1* in NSD displayed an additive effect (Fig 7F).

Taken together, our analyses place HBS-1 and PELO-1 on a pathway with ZNF-598 and NONU-1 during NGD, and suggests a model where HBS-1 acts downstream of ZNF-598 to promote mRNA decay by NONU-1 (Fig 7G).

HBS-1 is broadly conserved with NONU-1 and ZNF-598

In light of our genetic analyses, we were curious to measure the conservation of the relationships between HBS-1 and both NONU-1 and ZNF-598. To this end, we carried out phylogenetic profiling of HBS-1 with ZNF-598 homologs, and observed a relatively high level of mutual information falling in each others' 96.9%/98.3% (Fig 7H), suggesting that HBS-1 and ZNF-598 function together throughout eukarya. NONU-1 and HBS-1 fell in each others' 93.7% and 96.7%, still exhibiting some conservation, but less so than either factor with ZNF-598 (Fig 7I). Taken together, our conservation analyses support a conserved relationship between ZNF-598 and HBS-1, with a less conserved relationship between HBS-1 and NONU-1.

DISCUSSION

Here, we investigated the functions of and interplay between several factors required for NGD. Overall, our work supports a model where ubiquitination of RPS-10 and RPS-20 by ZNF-598 recruits NONU-1 via ubiquitin-binding to elicit mRNA decay, and HBS-1 acts downstream of ZNF-598 to enable mRNA cleavage by NONU-1.

Our data are consistent with a model in which ZNF-598 directly ubiquitinates RPS-10 and RPS-20. We note that our data could also be explained by a model in which ZNF-598 indirectly affects RPS-10 and RPS-20 ubiquitination, *e.g.*, through an intermediary E3 ligase. While we did not identify other E3 ligases in our screen, it is possible that loss of such E3 ligases would be inviable, precluding their recovery. Additional work will be required to distinguish between these models.

Regardless of whether ZNF-598 acts directly or indirectly on RPS-10 and RPS-20, our data suggest these proteins act in a single pathway to bring about mRNA repression. There may also be additional ubiquitination sites functioning on the ribosome during NGD, as has been suggested in other systems (Garshott et al., 2020; Garzia et al., 2021). It is notable that we can efficiently block mRNA degradation via ablation of RPS-10 and RPS-20 sites alone. Our analysis of NONU-1's relationship to ribosomal ubiquitination sites suggests a model that is more complicated than a simple one-ubiquitination-site-one-effector model. This may be expected given NONU-1's multiple ubiquitin-binding domains. Further genetic work will be required to elucidate the network of ubiquitination sites functioning in NGD, and given the combinatorial possibilities of sites on collided ribosomes, we expect structural studies to be insightful.

While our *unc-54(rareArg)* reporter indicated that NONU-1 and ZNF-598 largely function in the same pathway during NGD, our NSD data are consistent with flexibility in NONU-1's recruitment. Given the minor effect of ZNF-598 in NSD, and the absence of *znf-598* alleles in NSD screens (Arribere & Fire, 2018; Glover et al., 2020), we hypothesize that a factor other than ZNF-598 is used to recognize ribosomes stalled at the 3'end of an

mRNA. Other E3 ligases have been implicated in surveillance, and future work will hopefully clarify the recruitment mechanisms of each (Ikeuchi et al., 2019; Hildebrandt et al., 2019; Garzia et al., 2021). These data could also be explained by differences in the stalling mechanism and/or reporter readout on *unc-54(nonstop)* vs. *unc-54(rareArg).* Regardless, the mild NSD de-repression seen in *znf-598* indicates that ZNF-598 does act on some ribosomes during NSD. We hypothesize that collisions targeted by ZNF-598 are worsened in a *nonu-1* mutant, explaining the greater effect of *znf-598* on NSD in a *nonu-1* mutant (Fig 5G). These ideas are consistent with other models suggesting multiple types of collisions, with the relative amount of each depending on the genetic background (Ikeuchi et al., 2019).

Here, we discovered that the N-terminal domain of HBS-1 is dispensable for NGD, despite sharing structural homology to ubiquitin-binding domains. Our sequence analyses revealed that HBS-1 N-termini encode domains homologous to ubiquitin-binding domains despite little primary sequence conservation. While this suggests that HBS-1 binds ubiquitin, we failed to observe ubiquitin binding above background, suggesting that additional factors may be required for an interaction. It is also possible that the HBS-1 N-terminus interferes in the ubiquitination reaction. Given that current structures of ribosome-bound HBS-1 lack density for ubiquitin, we expect structural studies with ubiquitinated ribosomes will prove insightful.

Given prior work in *S. cerevisiae* revealing a role for Hbs1 in NGD cleavage (Doma & Parker, 2006; Passos et al., 2009; van den Elzen et al., 2010), and in light of our data here, we favor a model where HBS-1 activity greatly enhances mRNA cleavage by NONU-1. We note that we recovered an HBS-1 GTPase mutant in our screen, suggesting that GTP hydrolysis is required for HBS-1 function in mRNA decay. We therefore hypothesize that, in the process of rescuing ribosomes, HBS-1/PELO-1 generate a substrate for NONU-1 or otherwise enable NONU-1 action. In this model it is unclear which ribosomes are rescued, but prior work supports HBS-1/PELO-1 function on internally-stalled ribosomes (Pisareva et al., 2011), consistent with a rescue-first-cleavage-second NGD model. These mechanistic ties

between HBS-1 and NONU-1 will enable discovery of the molecular mechanisms underlying the known but poorly understood link between ribosome rescue and mRNA decay.

Overall, our work augments information gained from other systems by demonstrating the conservation of NGD factors in a metazoan, and ordering the sequence of events carried out by ZNF-598, HBS-1/PELO-1, and NONU-1 to bring about mRNA repression in response to ribosomal stalls.

SUPPLEMENTAL FIGURES

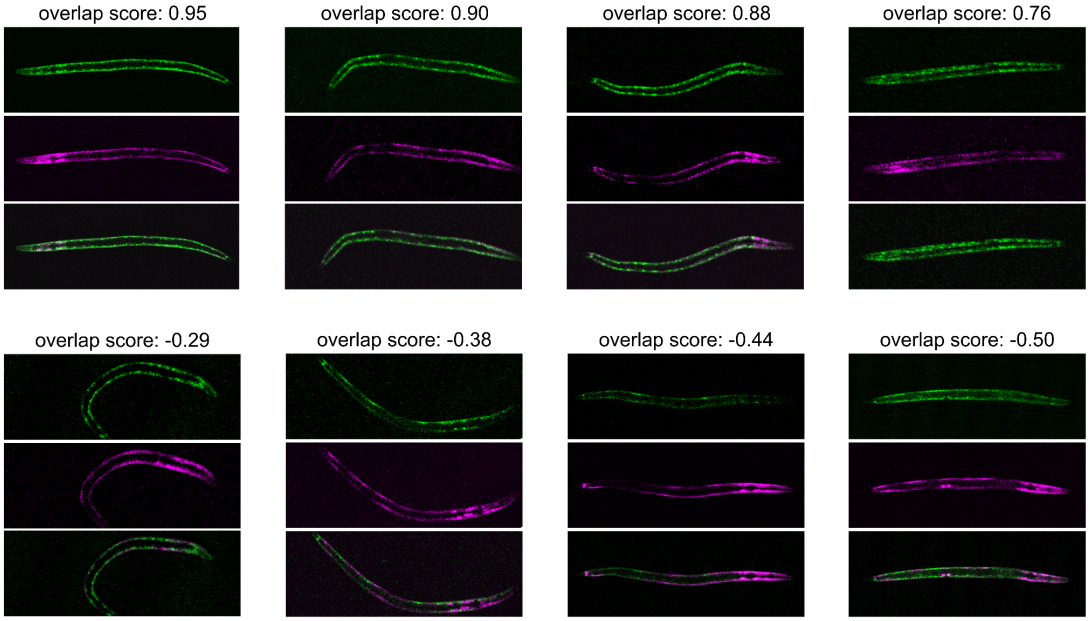

Figure S2.1. Representative animals demonstrating various overlap scores. GFP and mCherry images of representative animals expressing *unc-54(rareArg)* and an mCherry-tagged array. Above is the calculated overlap score.

Figure S2.2. RPS-10 and RPS-20 ubiquitination sites are conserved in *C. elegans*. (A) Pairwise sequence alignment of *H. sapiens* eS10 and *C. elegans* RPS-10. K125 is highlighted in green. Conservation is as shown in Fig 3A. **(B)** As in (A), showing *H. sapiens* uS10 and *C. elegans* RPS-20 with K6 and K9 highlighted in green.

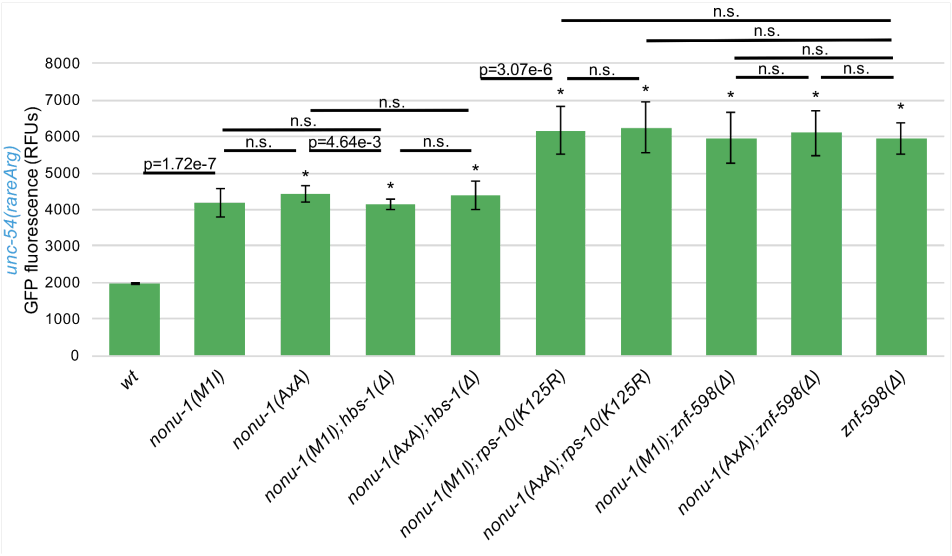

Figure S2.3. *nonu-1* null mutant displays similar NGD suppression as catalytic mutant. Mean RFUs (relative fluorescence units) of indicated strains (n≥15 animals/strain) in the *unc-54(rareArg)* background. One standard deviation shown as error bars. p values from Welch's t-test, with asterisks indicating p<0.01 for all comparisons with wild type.

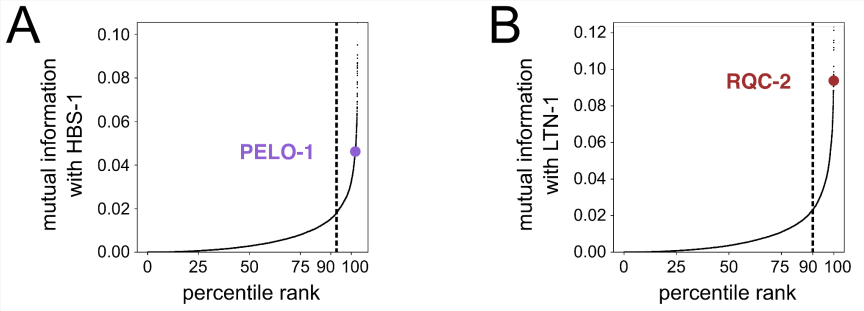

Figure S2.4. Known surveillance factor partners exhibit high mutual information. (A) HBS-1 mutual information plot. 90% percentile cutoff is shown as a dashed line and PELO-1 is highlighted in purple. **(B)** As in (A), showing LTN-1 mutual information with RQC-2 in red.

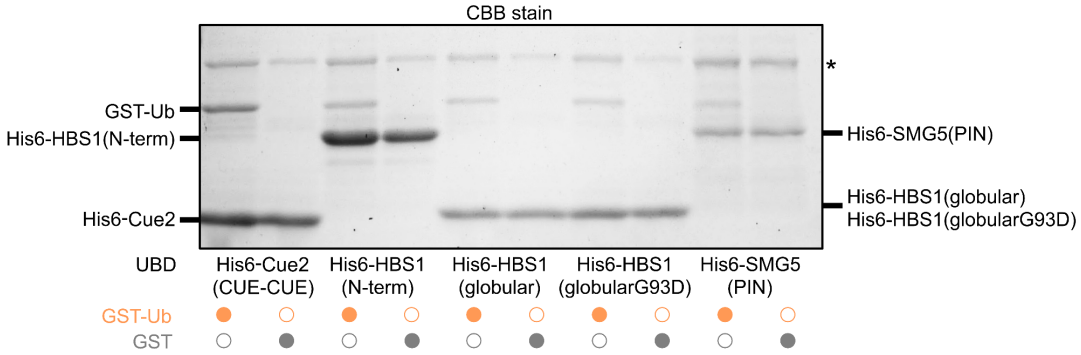

Figure S2.5. Ubiquitin-binding assay shows high level of background binding. His6-tagged constructs of *S. cerevisiae* Cue2 CUE domains, *H. sapiens* HBS1 N-term domain, *H. sapiens* HBS1 N-term globular (triple helix) domain, *H. sapiens* HBS1 N-term globular (triple helix) domain with G93D mutation (Gly in predicted binding site found from [55]), and *H. sapiens* SMG5 PIN domain. His6 constructs were immobilized on cobalt metal affinity resin and incubated with *E. coli* lysates expressing GST-Ub or GST. Proteins boiled from resin are shown on Coomassie stained gel, with proteins indicated. Asterisk indicates nonspecific peptide present on resin.

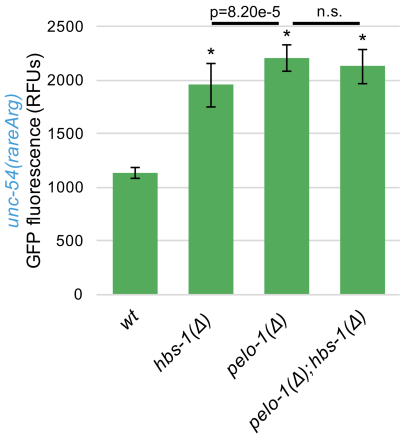

Figure S2.6. HBS-1 and PELO-1 exhibit similar phenotypes during NGD in *C. elegans*. Mean RFUs (relative fluorescence units) of indicated strains (n≥15 animals/strain) in the *unc-54(rareArg)* background. One standard deviation shown as error bars. p values from Welch's t-test, with asterisks indicating p<0.01 for all comparisons with wild type.

METHODS

C. elegans strain construction and propagation

C. elegans strains were derived from the VC2010 strain (N2) (Thompson et al., 2013), and the CB4856 (Hawaiian) strain was used for suppressor mutant mapping. Animals were grown at 16C or 20C on NGM plates seeded with OP50 as a food source (Brenner, 1974). Some strains were obtained from the Caenorhabditis Genetic Center (CGC), which is funded by NIH Office of Research Infrastructure Programs (P40 OD010440). CRISPR/Cas9 was performed to introduce genomic edits as previously described (Arribere et al., 2014). Multiple independent isolates of each mutation were recovered and observed to have identical phenotypes. Mutant combinations were generated by crossing. A full list of strains, sequences of mutant alleles, PCR primers, and sources is available in Table S1.

EMS mutagenesis and suppressor mutant screens

EMS mutagenesis was performed essentially as described (Arribere and Fire, 2018). Briefly, a large population of each strain was washed with M9 to a final volume of 4mL. EMS was added to a final concentration of ~1mM and animals were incubated at room temperature for 4 hr with nutation. Animals were washed and left overnight at room temperature on NGM plates seeded with OP50. The next day, animals were washed and eggs were collected by hypochlorite treatment. 100-200 eggs were placed on single small NGM+OP50 plates and allowed to propagate. Plates were screened for F2/F3 animals with increased GFP fluorescence and increased movement. Only a single isolate was kept per NGM plate to ensure independence of mutations.

The first rareArg screen was saturated with hits at *znf-598*, occluding our ability to recover additional alleles at other loci. To address this, we constructed a double-balanced strain covering the region of chromosome II harboring *znf-598*, similarly to an approach used in an NMD suppressor screen (Cali et al., 1999). This strain (WJA 1040) was homozygous on chromosome I for *unc-54(srf1004)* and heterozygous on chromosome II for

mnC1[dpy-10(e128) unc-52(e444) nls190 let-?] (AG226) and *tra-2(e1095)* (CB2754). Animals homozygous for *mnC1* or homozygous for *tra-2(e1095)* were inviable or Tra/sterile, respectively, allowing us to eliminate recovery of recessive suppressor mutants within the balanced region. This strain was subjected to EMS mutagenesis as described above. Only isolates maintaining the *mnC1/tra-2* heterozygous balancer were kept, as seen by *myo-2::GFP* (marking *mnC1*)*, a* nonTra phenotype, and subsequent viability.

Suppressor mutant mapping and identification

Following recovery of mutants from EMS screens, we employed a Hawaiian SNP mapping approach as described (Doitsidou et al., 2010). We crossed each isolated suppressor mutant to Hawaiian (CB4856) *unc-54(cc4112)* males (expressing an UNC-54::mCherry fusion engineered by CRISPR/Cas9). Cross progeny were isolated and allowed to self-fertilize. The F2 GFP+ progeny were then backcrossed to the *unc-54(cc4112)* males at least 2 times.

After rounds of backcrossing, several phenotypically suppressed animals (~20-30) for a given mutant were pooled together onto a single plate and propagated until starvation. Upon starvation, animals were washed off the plate with 1mL EN50, and further washed with EN50 to remove residual *E. coli*. Genomic DNA was extracted after proteinase K treatment and resuspended in 50uL TE pH7.4. 50ng genomic DNA was used as an input for Nextera (Tn5) sequencing library preparation. Libraries were sequenced at Novogene Corporation Inc. UC Davis Sequencing Center on a NovaSeq 6000.

Reads were mapped to the *C. elegans* genome using bowtie2 (version 2.3.4.1). Reads were assigned to haplotypes using GATK (McKenna et al., 2010) and a previously published dataset of Hawaiian SNPs (Thompson et al., 2013). The fraction of reads that were assignable to Hawaiian or N2 animals was calculated across the genome, and linkage was identified by portions of the genome with 0% Hawaiian. Regions of linkage were then manually inspected to identify candidate lesions and loci.

Fluorescence microscopy and image analysis

All animals were maintained at 20C. L4 animals were selected and anesthetized in 3uL EN50 with 1mM levamisole in a microscope well slide with a 0.15mm coverslip.

A Zeiss AxioZoom microscope was used with a 1.0x objective to acquire images for GFP quantification experiments. The following parameters were used for all images: exposure time of 250ms., shift of 50%, and zoom of 80%. 15-25 representative animals were imaged for each strain. All comparisons shown are between images obtained during the same imaging session. We used FIJI to define the area of the animal, subtract the background, and determine mean pixel intensity for the area of each animal.

A Leica SP5 confocal microscope was used with a 10.0x objective to simultaneously acquire images of mCherry and GFP in overexpression experiments. The following parameters were used for all images: pinhole size set to 106.2 µm; bidirectional scan at 400 Hz with a line average of 2; 488 laser to capture GFP and 594 laser to capture mCherry, both at 50% power with a gain of 700 and offset of -0.2%. 4-10 animals were analyzed from a total of 3 independent isolates for each overexpression experiment. A custom python script was used to define the area of the animal, then parse out locations and intensities of green and red pixels. We considered the brightest 1,000 green and brightest 1,000 red pixels and calculated the Jaccard index. The theoretical maximum of the Jaccard index is 1, indicating no overlap of green and red pixels. The observed minimum of the Jaccard index among our strains was ~0.75, higher than the theoretical lower bound of zero, which is the result of expression of mCherry and GFP being driven in the same tissue. To display the image quantification more intuitively, we transformed the Jaccard index into an overlap score. This was done by performing a simple linear transformation of 0.75 (more overlap) to 1.0 (less overlap) in Jaccard space into an overlap score of -1.0 (less overlap) to 1.0 (more overlap). See Fig S2.1 for images of animals representing various overlap scores.

Immunoblotting

Animals were propagated on NGM plates with OP50 until freshly starved, then washed twice with 1ml M9 and flash frozen in liquid nitrogen. Animal pellets were boiled for 10 min at 99C in 1x SDS loading buffer (0.1M Tris-HCl, 20% glycerol, 4% SDS, 0.1M DTT, 0.05% bromophenol blue). Samples were vortexed and spun to pellet animals and supernatants were collected. Protein was quantified by Qubit and 15ug protein was run on a 4-20% Mini-PROTEAN(R) TGX Stain-Free Protein gel (Bio-Rad). Protein was transferred to a low background fluorescence PVDF membrane (Millipore Sigma) and the membrane was blocked in 5% nonfat milk in 1x TBST. Anti-HA antibody (Enzo Life Sciences 16B12) was used at a 1:2000 dilution to detect HA-tagged RPS-10 protein. Anti-FLAG antibody (Millipore Sigma F1804) was used at a 1:1000 dilution to detect FLAG-tagged RPS-20 protein. Anti-H3 antibody (Millipore Sigma SAB4500352) was used at a 1:2000 dilution to detect the histone H3 protein. Secondary antibody staining was performed with 1:15000 LI-COR goat anti-mouse or LI-COR goat anti-rabbit (LI-COR). Imaging was done using a LI-COR Odyssey Imaging System (LI-COR), with quantification done in ImageStudio.

Mutual information calculation

Phylogenetic profiling was performed using the PANTHER HMM library Version 16.0 on Ensembl Protists Genome (release 51) combined with MMETSP (Keeling et al., 2014). To identify homologs of proteins from the PANTHER Subfamily HMMs, we used HMMER's hmmsearch function using the following parameters --noali --notextw --cpu 2. We then parsed each output file from HMMER and determined the presence (1) or absence (0) of a homolog in each organism for a sub-family HMM.

Briefly, if multiple subfamily HMMs matched a given protein in a species, the protein was assigned to the subfamily with the highest bit score, and lesser-scoring subfamilies were ignored. Subfamilies with homologs in <5% or >95% of species were discarded; such subfamilies exhibit too little variation for accurate mutual information calculations. Similarly,

species with hits for <10% of subfamilies were discarded; such species may represent poor transcriptome coverage and/or assemblies. We also computed the pairwise hamming distance between all species and discarded species until the pairwise hamming distance between all species was at least 0.1, so as to ensure biodiversity. Mutual information for discrete variables was then calculated as: sum(i=0,1); sum(j=0,1) [-log_2(p_ij/(p_i*p_j))].

Negative controls for mutual information calculations were generated as follows. For a given pair of factors A and B, we randomized the binary vector of presence (1) and absence (0) of B in organisms to create a new negative control factor. Mutual information for discrete variables was then calculated between factor A and the newly created negative control.

RNA-seq and analysis

Animals were synchronized by hypochlorite treatment, propagated on NGM plates with OP50 at 16C, and harvested at the L4/young adult stage. Animals were washed off with N50, passed through a 5% sucrose cushion in N50 to remove *E. coli,* and snap frozen in liquid nitrogen. Animals were lysed by grinding in a mortar and pestle cooled in liquid nitrogen in the presence of frozen PLB (20mM Tris pH8.0, 140mM KCl, 1.5mM MgCl2, 1% Triton) and 100ug/mL cycloheximide. Ground animals were stored as frozen powder at -70C. Total RNA was extracted with trizol, resuspended in TE pH7.4, and quantified by Qubit. Ribosomal RNA was depleted using custom *C. elegans*-specific rRNA hybridization oligos, similar to a planarian protocol as described (Kim et al., 2019). Oligos for this protocol are included in Table S1. Libraries were prepared using an NEBNext Ultra II Directional RNA Library Prep Kit for Illumina sequencing. Libraries were sequenced at Novogene Corporation Inc. UC Davis Sequencing Center on a NovaSeq 6000.

We generated a custom *C. elegans* genome (Ensembl, WBCel235) containing *unc-54(rareArg)* as a separate chromosome and a masked endogenous *unc-54* locus. Reads were mapped to this genome including annotated splice junctions using STAR v2.5.4b (Dobin

and Gingeras, 2015) allowing for zero mismatches. All downstream analyses were restricted to uniquely mapping reads.

In vitro ubiquitin-binding

Ubiquitin-binding assay was performed essentially as described in (Shih et al., 2002). Briefly, recombinant proteins were induced in *E. coli* with 1 mM IPTG at 37C for 4 hours. Cells were harvested and suspended in 1x PBS (137mM NaCl, 2.7mM KCl, 10mM Na2HPO4, and 1.8mM KH2PO4), followed by lysis in xTractor buffer (Takara) per the manufacturer's protocol. Lysates were cleared by centrifugation and immobilized on TALON metal affinity resin (Takara) per the manufacturer's protocol. Immobilized proteins were washed with 1x PBS and incubated overnight at 4C with clarified lysates containing various GST-fusion constructs. Bound proteins were washed four times with 1x PBS with 5mM imidazole and eluted by heating to 99C for 5 min in 1x SDS loading buffer. Eluted protein was run on a 4-20% Mini-PROTEAN(R) TGX Stain-Free Protein gel (Bio-Rad) and stained with Coomassie brilliant blue.

CHAPTER 3: STALLED RIBOSOME SPECIES EVADE STANDARD RIBOSOME CAPTURE PROTOCOLS IN ANIMALS

ABSTRACT

Some mRNAs possess unusual features which halt translating ribosomes. While it is known that ribosomal stalls can trigger the decay of the aberrant mRNAs, endogenous mRNAs that experience stall-induced decay remain few and far between. Here, we investigate the dynamics of ribosomal stalling in *C. elegans*. Using a genetically validated stalling reporter, we demonstrate that, despite its strong effect on mRNA stability, the E3 ubiquitin ligase ZNF-598 has little effect on ribosome density, stall readthrough, and post-stall frame maintenance. Surprisingly, by standard ribosome footprint profiling, we reveal the absence of a ribosome species of significant relevance to the study of ribosomal stalling. We expect that future modifications to ribosome capture will illuminate the molecular dynamics of ribosomal stalling and reveal endogenous stalling targets.

INTRODUCTION

It is crucial that organisms carry out gene expression in a timely and faithful manner. A key step in this process is the translation of mRNAs into proteins by ribosomes. During the task of protein synthesis, a ribosome can stall on an mRNA. If left unresolved, strong stalls in translation can cause organisms to suffer due to a reduction of the pool of available ribosomes. Additionally, the defective and often truncated peptides from stall-encoding mRNAs can be toxic and can contribute to disease phenotypes such as neurodegeneration (Ishimura et al., 2014; Bengtson & Joazeiro, 2010; Radwan et al., 2020; Kriachkov et al., 2023). Recent studies have also reported an accumulation of stalled ribosomes during aging (Stein et al., 2022).

To combat stall-inducing mRNAs, eukaryotes have a specialized series of reactions known as No-Go mRNA Decay (NGD). NGD machinery targets mRNAs containing various

translation-inhibitory features, including polybasic amino acid-encoding sequences, rare codons, stable secondary structures, or damaged nucleotides (Doma and Parker, 2006). Several studies have identified factors required for NGD, and we recently delineated the sequence of events leading to mRNA decay upon ribosome stalling (Monem et al., 2023). Interestingly, NGD factors must differentiate between ribosomal stalls which require decay and ribosomal pauses which resolve themselves. Common instances of ribosomal pausing include the translation of poly-proline motifs and cotranslational translocation. To maintain tight control of decay, NGD machinery detects unique features of stalled ribosomes.

Recent advances have been made towards characterizing the early detection steps of NGD. One key upstream event is the generation of a stalled, collided ribosome species at a problematic site on the mRNA. This species is thought to be unique to NGD (Simms et al., 2017; Juszkiewicz et al., 2018; Ikeuchi et al., 2019). The interface between collided ribosomes is the site of ubiquitination events on multiple ribosomal proteins near the mRNA's path (Juszkiewicz et al., 2018; Ikeuchi et al., 2019). The conserved E3 ubiquitin ligase ZNF-598 is thought to deposit ubiquitin marks on at least two ribosomal proteins (Juszkiewicz & Hegde, 2017; Sundaramoorthy et al., 2017; Monem et al., 2023). Our recent work has demonstrated the importance of ZNF-598 in destabilizing No-Go mRNAs via ribosomal ubiquitination (Monem et al., 2023).

While studies revealed multiple collided ribosome structures, the relationship of these collided ribosomes to *in vivo* stalls on mRNAs remains poorly understood. Recent work has mapped the locations of ribosome species thought to represent collisions, known as disomes or di-ribosomes (Meydan et al., 2020; Han et al., 2020; Arpat et al., 2020; Zhao et al., 2021). However, the application of these data to NGD is lacking, in part due to the absence of work containing validated reporters and the lack of bonafide endogenous NGD targets.

Here, we interrogate various stalled ribosome species in the context of NGD *in vivo*. We utilize our established NGD genetic system in *C. elegans* to demonstrate a requirement for ZNF-598 in the control of the mRNA levels and ribosome abundance on a NGD substrate.

We observe that a low (~20%) proportion of ribosomes complete elongation through a stall, and that ribosomes largely remain in-frame during and after the stall. Interestingly, while we recovered ribosomes at slowly-decoding sequences (*e.g.*, PPG), we did not recover ribosomes at a NGD-inducing stall. While surprising, our results are in agreement with several animal studies. We find that the inability to capture ribosomes at and around stalls persists with the use of different ribosome-stabilizing drugs and upon the collection of higher-order ribosome species of unusual footprint sizes. Our findings thus reveal a missing ribosome species in animal ribosome footprint profiling data of significant relevance to the study of NGD.

RESULTS

Poly-proline and poly-arginine ribosomes are differentially captured

To provide novel insight into ribosomal stalling, we aimed to understand the variety of ribosome species underlying NGD. Key to this undertaking was a knockout of the NGD E3 ubiquitin ligase ZNF-598 (Fig 3.1A). We selected *znf-598* because our prior work showed knockout of this factor blocked the NGD pathway (Monem et al., 2023). We therefore reasoned that ZNF-598-dependent changes in ribosome distributions would reveal NGD-dependent changes. To this end, we performed 28-30nt monosome and 50-62nt disome Ribo-seq with and without *znf-598* deletion using the translocation inhibitor cycloheximide (CHX) (Meydan et al., 2020; Han et al., 2020; Arpat et al., 2020; Zhao et al., 2021) (Fig S3.1).

As expected, we captured a robust signal of ribosomes paused at poly-proline stretches, specifically the Pro-Pro-Gly motif, and saw no dependence on ZNF-598/NGD (Fig 3.1B). This result is consistent with several metazoan disome Ribo-seq studies where proline stalls were most abundant (Han et al., 2020; Arpat et al., 2020). The mechanism of proline pausing is strikingly different from that which is expected during NGD. During proline pausing, peptidyl transfer between proline and glycine proceeds more slowly than at other codons

(Gutierrez et al., 2013; Schmidt et al., 2016; Schuller et al., 2017). Thus, our monosome and disome libraries recovered slower-decoding ribosomes.

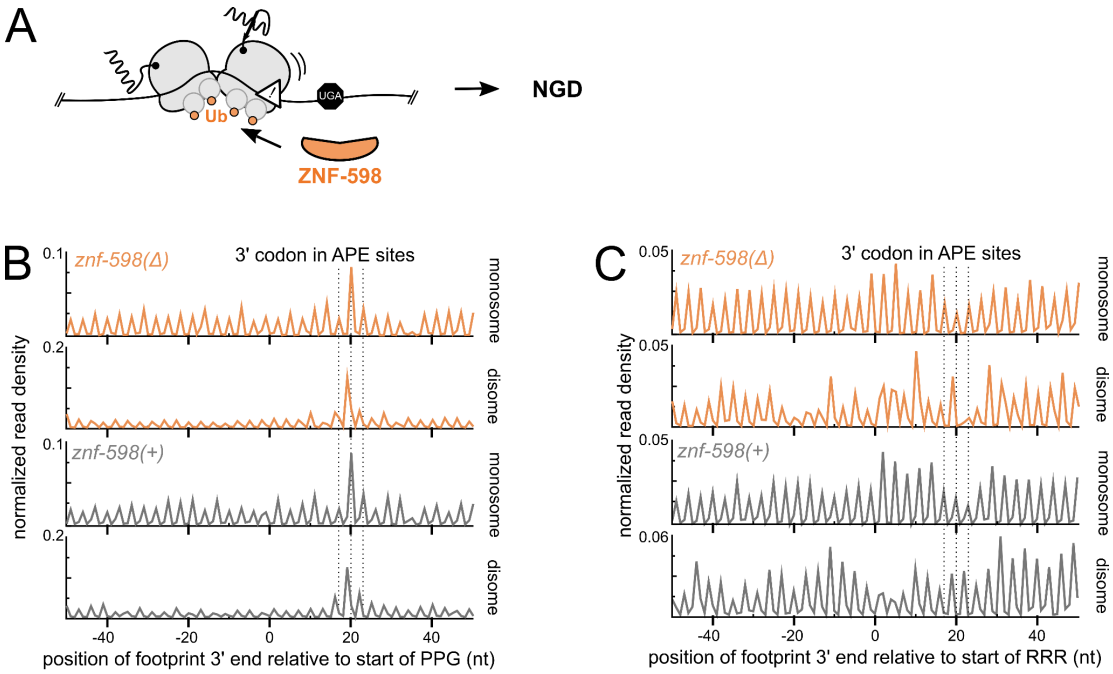

Figure 3.1: Poly-proline and poly-arginine ribosomes are differentially captured. (A) Schematic of ZNF-598 function in NGD. **(B)** Normalized read density of 29nt CHX monosome and 58nt CHX disome Ribo-seq genome-wide at PPG amino acid motifs in the indicated backgrounds. Reads are aligned by their 3' ends. Dotted lines indicate footprint 3' end position when the 3' codon of each motif is in each ribosomal site. PPG is expected to slow elongation during peptidyl transfer of an incoming glycine. This stall is seen by the peak of ribosomes with the 3' glycine codon in the P-site. **(C)** As in (B), at RRR amino acid motifs.

We next sought to measure ribosome density at poly-arginine sites genome-wide. Prior work has reported slower translocation within stretches of poly-basic codons due to interactions between the negatively-charged ribosome peptide exit tunnel and the positively-charged nascent peptide (Lu and Deutsch, 2008; Chandrasekaran et al., 2019). We thus expected an accumulation of ribosomes decoding arginine codons. Surprisingly, we instead observed a depletion of ribosomes at poly-arginine sites genome-wide (Fig 3.1C), independent of nucleotide-capture bias (Fig S3.2). We reanalyzed and similarly observed a slight reduction in arginine-decoding ribosomes across multiple *C. elegans* datasets (Stadler and Fire, 2011; Glover et al., 2020), as well as human (Han et al., 2020), zebrafish (Han et

al., 2020), and mouse data (Arpat et al., 2020). The comparative lack of arginine-decoding ribosomes stands in contrast to datasets made from *S. cerevisiae* which exhibit robust arginine-dependent ribosome accumulations (Meydan et al., 2020; D'Orazio et al., 2019; Zhao et al. 2021). Taken together, we conclude that the ribosomal states including PPG-stalled ribosomes are distinct from those states stalled on arginine stretches.

ZNF-598-dependent effects on a validated NGD substrate

Given the lack of a strong stall signal at poly-arginine motifs genome-wide, we were curious to analyze ribosome footprints on our previously characterized NGD reporter, *unc-54(rareArg)* (Fig 3.2A). This reporter utilizes a stretch of twelve rare arginine codons to stall ribosomes, followed by GFP. We reasoned that it would display stalled ribosomes based on its prior genetic characterization as a NGD target (Monem et al., 2023).

Consistent with the stabilization of *unc-54(rareArg)* previously seen by RNA-seq, we observed an increase in both monosome and disome footprints throughout the *unc-54(rareArg)* reporter in a *znf-598* mutant background (Fig 3.2B). We sought to determine whether the increase in footprints in *znf-598* was simply the result of increased mRNA levels or whether there were additional *znf-598*-dependent effects. We observed quantitative agreement between the change in ribosome footprints and the changes in mRNA levels for the *unc-54(rareArg)* reporter (Fig 3.2C). We also observed similar agreement between mRNA levels and disome density in wildtype and *znf-598*. These data indicate that the increase in ribosomes on *unc-54(rareArg)* in *znf-598* is largely explained by the increase in mRNA levels.

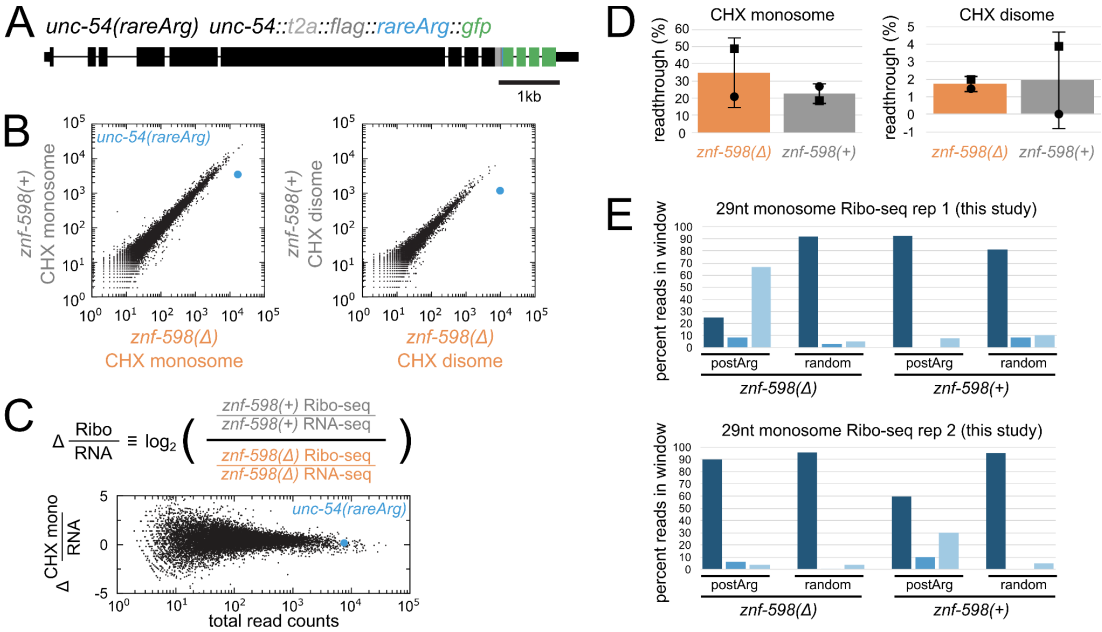

Figure 3.2: ZNF-598 controls mRNA levels of and ribosomes on a NGD substrate, but not readthrough levels nor frame maintenance. (A) Gene diagram showing *unc-54(rareArg)* as seen in (Monem et al., 2023). **(B)** Read count plots of CHX monosome and disome Ribo-seq reads per million (RPM). All genes are shown as black dots and *unc-54(rareArg)* is highlighted in blue. **(C)** Top: Equation used to calculate the change in ribosome footprints per mRNA reads. Log change score is determined by dividing Ribo-seq read counts by RNA-seq read counts in each background, then dividing values for *znf-598(+)* by values for *znf-598(Δ)*. Bottom: Scatter plot showing the change in ribosome footprints per mRNA reads between *znf-598(+)* and *znf-598(Δ)* CHX monosome libraries. Y-axis position is the change score as calculated by the equation at top. A more positive score indicates fewer monosome Ribo-seq read counts normalized to RNA-seq in *znf-598(Δ)*; a more negative score indicates fewer monosome Ribo-seq read counts normalized to RNA-seq in *znf-598(+)*. X-axis position is the total number of read counts in all libraries. All genes are shown as black dots and *unc-54(rareArg)* is highlighted in blue. **(D)** Percentage of readthrough CHX monosome (28-30nt) footprints (left) and CHX disome (50-62nt) footprints (right) on *unc-54(rareArg)* in indicated backgrounds from two biological replicates. Data points from replicate one are shown as black circles and replicate two are shown as black squares. One standard deviation shown as error bars. See Methods. **(E)** Percent of 29nt CHX monosome Ribo-seq reads (from two biological replicates) in each frame post-rareArg and in 100 windows of equal size pre-rareArg on *unc-54(rareArg)*. Frame 0 is shown in dark blue, frame 1 in medium blue, and frame 2 in light blue. The post-rareArg window begins at the 5' end of a ribosome with the first Arg in its P-site and ends at the 5' end of a ribosome with the first out-of-frame stop (in the +2 frame) in its A-site.

Readthrough and frame maintenance during ribosome stalling

We next focused on the distribution of ribosomes along *unc-54(rareArg)*. As seen in our prior work, GFP production from this reporter relies on translation through the stall. We thus hypothesized that some population of ribosomes must escape the stall and evade clearance, but that many ribosomes would not. Indeed, we observed that monosome density downstream of the stall was 18-49% the level seen prior to the stall, with at most a mild effect

by *znf-598* on this metric (Fig 3.2D). The reduction in footprints downstream of the stall persisted in disomes (Fig 3.2D). We conclude that ZNF-598 does not dramatically alter the relative number of ribosomes upstream versus downstream of the stall. Interestingly, we note that monosome footprints in wildtype and *znf-598* were enriched in the 5' end of the mRNA (Fig S3.3). This result could emerge from increased ribosome loading on No-Go mRNAs, ribosome drop-off during elongation, technical artifacts in the capture of large mRNAs such as *unc-54*, or some combination of these effects.

Prior work in *S. cerevisiae* observed frameshifting on some NGD substrates (Wang et al., 2018; Simms et al., 2019). We considered frameshifting as a mechanism by which ribosomes may pass through the arginine stall on *unc-54(rareArg)*. Within and downstream of the stall, we detected no significant change in frame in ribosome footprints in either wildtype or in *znf-598* animals (Fig 3.2E). We observed a similar maintenance of frame through re-analysis of data on a yeast stalling reporter (Fig S3.4) (D'Orazio et al., 2019).

As a second way of assessing the contributions of frameshifting to expression of *unc-54(rareArg)*, we examined expression in a *smg-1* mutant which has a nonfunctional Nonsense-mediated mRNA Decay (NMD) pathway. Ribosomes that frameshift would be expected to terminate at an out-of-frame stop codon just past the arginine stall and trigger NMD. We observed no increase in reporter expression in a *smg-1* mutant (Fig S3.5).

Taken together, these results argue against frameshifting as a substantial contributor to expression of *unc-54(rareArg)*. We note these results are perhaps not surprising given that Mbf1 was intact in our experiments; Mbf1 is known to enhance frame maintenance at stalls (Wang et al., 2018). We thus conclude that, while Mbf1 is important for reading frame maintenance in certain contexts, reading frame loss does not substantially contribute to the expression of NGD targets.

A conspicuous absence of ribosome accumulations within a poly-arginine stall

We proceeded to investigate the positioning of ribosomes on *unc-54(rareArg)* at the stall site. Despite the requirement of poly-arginine synthesis to produce GFP, we observed few ribosomes decoding the rareArg stretch (Fig 3.3A, Fig 3.3B). The low abundance of footprints in this region was notably independent of mapping error; the arginine codons we selected were arranged in a non-random order to enable unique read-mapping. While surprising, this result was in agreement with our genome-wide analysis of poly-arginine motifs and suggests a failure of cycloheximide-based ribosome footprint profiling to capture arginine-decoding ribosomes.

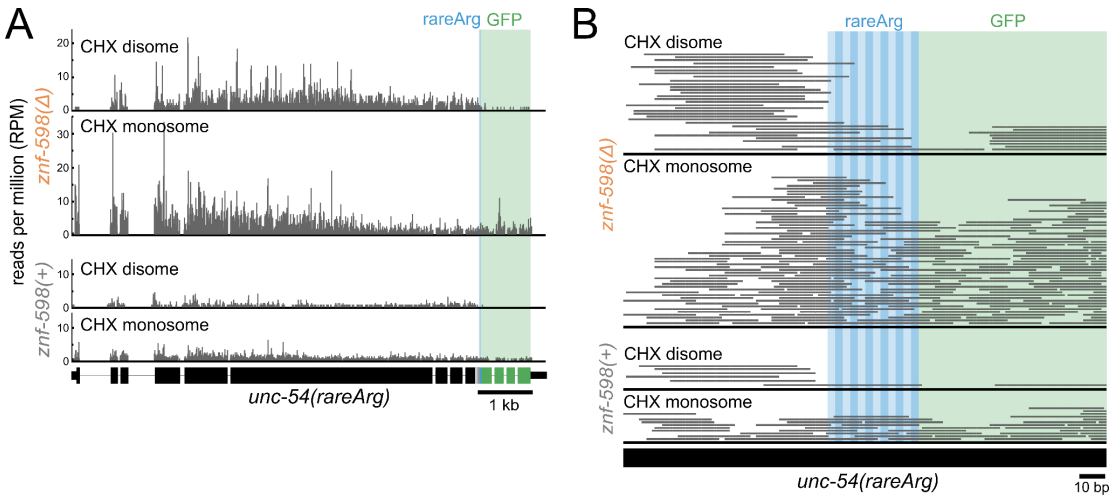

Figure 3.3: A low abundance of stalled ribosome footprints captured by CHX on a NGD substrate. (A) Gene plot showing CHX disome (50-62nt) and monosome (28-30nt) Ribo-seq RPM on *unc-54(rareArg)* in the indicated backgrounds. Reads are aligned by their 5' ends. Locations of 12 rare arginine codons (blue) and GFP (green) are annotated. **(B)** Read diagrams of CHX disome (50-62nt) and monosome (28-30nt) Ribo-seq reads around rareArg in the indicated backgrounds. Each arginine codon is represented by a vertical blue stripe. Each bar represents one read. Monosome datasets and disome datasets are subsampled to equal depth across the two backgrounds.

In an effort to identify a stall-decoding species, we performed 18-30nt monosome Ribo-seq and 40-60nt disome Ribo-seq with anisomycin (ANS) rather than cycloheximide (CHX) (Fig S3.6A, Methods). CHX inhibits translocation by binding the E-site and preventing deacylated tRNAs from exiting the P-site. Thus, CHX stabilizes ribosomes in a hybrid, pre-translocation state (Fig 3.4A). ANS is thought to inhibit peptide-bond formation by binding

the A-site and competing with aminoacyl-tRNAs for the peptidyl transferase center (reviewed in Dmitriev et al., 2020). Previous studies have used ANS to stabilize ribosomes with short 21nt footprints (Lareau et al., 2014; Wu et al., 2019). These ribosomes are thought to be in a classical state with either an empty A-site (pre-accomodation) or a free tRNA in their A-site (pre-peptidyl transfer) (Fig 3.4A). Given the expectation for slow accommodation at rare codons, we investigated whether ANS could be used to recover stall-decoding ribosomes.

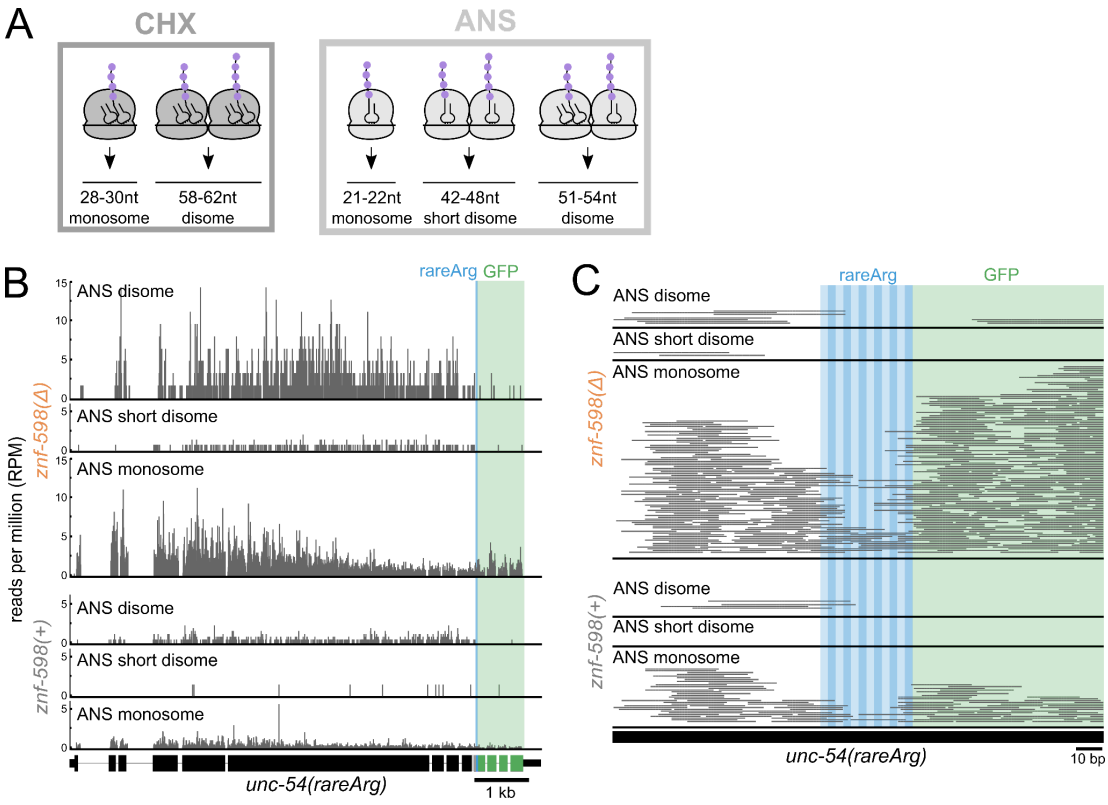

Figure 3.4: A conspicuous absence of ribosome accumulations within a poly-arginine stall. (A) Cartoon of ribosome conformations and footprint sizes with cycloheximide (CHX) vs. anisomycin (ANS). **(B)** Gene plot showing ANS disome (50-62nt), ANS short disome (40-49nt), and monosome (18-30nt) Ribo-seq RPM on *unc-54(rareArg)* in the indicated backgrounds. Reads are counted by their 5' ends. Locations of 12 rare arginine codons (blue) and GFP (green) are annotated. **(C)** Read diagrams of ANS disome (50-62nt), ANS short disome (40-49nt), and monosome (18-30nt) Ribo-seq reads around rareArg in the indicated backgrounds. Each arginine codon is represented by a vertical blue stripe. Each bar represents one read. Monosome datasets and disome datasets are subsampled to equal depth across the two backgrounds.

Surprisingly, we captured both 21nt and 28nt monosome footprints via ANS (Fig S3.6A). This result is in contrast to ANS work done in yeast which captured very few 28nt footprints (Lareau et al., 2014) and further work in yeast which required a cocktail of translation inhibitors to capture both size ranges (Wu et al., 2019). We utilized this feature to probe the positions of several ribosome species on our reporter. Given the rarity of their cognate tRNAs, we expected the rare arginine stretch to stall ribosomes with empty A-sites. However, we observed few ANS-stabilized monosome footprints (21nt or 28nt) within the stall. Despite a slight drop in ribosomes at the stall, we observed a robust number of footprints immediately following the stall (Fig 3.4B, Fig 3.4C). Thus, similar to CHX-stalled ribosomes, ANS-stalled ribosomes do not accumulate in the vicinity of a stall-inducing feature.

We also considered the possibility that arginine-decoding ribosomes exist as disomes rather than monosomes. To this end, we captured a wide range of disome species using ANS: 42-48nt, 51nt-54nt, and 58-62nt (Fig S3.6B, S3.6C). We expected that the two smaller species lacking from CHX disome libraries represent events when both ribosomes are in the classical state (42-48nt), or one ribosome is in the classical state with the other in the hybrid state (51-54nt). We observed reasonable triplet periodicity for such disome species, suggesting that the libraries were indeed derived from a translational species *in vivo*. Despite our capture of additional species via ANS, monosomes remained a general predictor of disome counts, and we failed to detect accumulations of disomes species at and around the poly-arginine stall.

DISCUSSION

Taken together, we propose that standard monosome and disome Ribo-seq protocols are unable to capture metazoan ribosomes at strong stalls. Surprisingly, we observed a lack of a notable stalled ribosome peak in either monosomes or disomes at the site on *unc-54(rareArg)*. Instead, we observed a depletion of footprints at the stall. While this result

was contrary to the arginine-stalled ribosomal peaks seen in yeast (Meydan et al., 2020; D'Orazio et al., 2019; Zhao et al. 2021), our re-analysis of Ribo-seq data from worms, zebrafish, mice, and humans revealed a subdued ribosomal presence at arginine stretches (Stadler and Fire, 2011; Glover et al., 2020; Han et al., 2020; Arpat et al., 2020). Moreover, our genome-wide analysis presented here, in both wildtype and *znf-598* animals, exhibited a similar depletion at arginine stretches, suggesting that the effect is not peculiar to *unc-54(rareArg) per se*.

This result might be interpreted as faster decoding within arginine stretches; however, multiple lines of evidence argue against this model:

(1) Ribosomes stalled on our reporter are faced with two of the rarest codons in *C. elegans*. These codons additionally require decoding by very lowly expressed tRNAs. These factors point towards delayed aminoacyl-tRNA accommodation and therefore slow decoding.

(2) On the *unc-54(rareArg)* reporter and genome-wide, poly-basic stretches are expected to trigger slower translocation due to interactions between the positively-charged nascent peptide and the peptide exit tunnel (Lu and Deutsch, 2008; Chandrasekaran et al., 2019). We expect these interactions to produce increased ribosomal density within the poly-basic-encoding codons and immediately downstream.

(3) Ribosomes entering a strong stall could conceivably experience faster or discontinuous elongation via a yet-unknown mechanism, akin to "shunting" observed during translation of some viruses (Ryabova and Hohn, 2000). This model would be consistent with lower density at the stall, but would also result in increased density after the stall due to a return to normal elongation. We did not observe an accumulation of ribosomes post-stall on our reporter or genome-wide, thus we do not have support for a faster elongation model. Furthermore, on our reporter, "shunted" ribosomes would have to first produce at least some polyArg peptide to generate the NLS::GFP as observed (Monem et al., 2023). Thus we do not favor this model.

Given the lack of support for faster elongation through arginines we propose several non-mutually exclusive explanations for a missing stalled ribosomal species:

(1) Ribosomes stalled within the arginine stretch on *unc-54(rareArg)* may experience preferential disassembly by a factor such as the ASCC complex (Juszkiewicz et al., 2020). While such a model could explain the reduced ribosomal density at stall sites on *unc-54(rareArg),* this model would predict a reduced ribosome density downstream of stalls. This was not observed. Furthermore, it remains unclear why mutations in ASCC factors were not identified in our screens. In order to reconcile these observations, one could invoke a model in which ASCC actively disassembles the stalled ribosome species in lysates like those used to prepare ribosome footprinting libraries (Aleksashin et al., 2023).

(2) Ribosomes decoding strong stall sites may be present as a rare, higher-order structure. This structure could consist of trisomes, tetrasomes, pentasomes, etc. which are inefficiently visualized and captured. Alternatively, this structure could be a ribosome (monosome or higher-order) with a tightly-bound accessory factor giving rise to a unique footprint size. We considered a broad range of footprint sizes in this work and did not observe this species associated with either monosomes or disomes, but it remains a possibility that in the course of performing sucrose gradients we may have selected against a relevant higher-order ribosome:mRNA species.

(3) NGD may occur in a subcellular compartment which is not captured in standard cellular lysis conditions. Given evidence of specialized subcellular compartments for translation and mRNA decay (such as stress granules and P-bodies) (reviewed in Das et al., 2021), some proportion of NGD could feasibly occur in a compartment which is lost during lysis. Similarly, recent work has reported on a subclass of ribosomes sedimenting differently in sucrose gradients due to their active engagement with membranes (Ferguson et al., 2023). Altered lysis conditions may be required to extract such ribosomes from animals (Mandelboum et al., 2023).

(4) Stalled ribosomes that elicit NGD may be unstable in lysates. Ribo-seq is known to preferentially capture elongating ribosomes. If the stalled ribosome species was not easily trapped by translation elongation inhibitors (such as CHX and ANS), the stalled species may escape detection by this method. These stalled ribosomes may instead require the use of translation inhibitors targeting alternate conformations. Further, NGD-eliciting ribosomes may be especially vulnerable to RNase I treatment during preparation in lysates. Consistent with this, recent work observed unique ribosome species stabilized by modified digestion conditions (Ferguson et al., 2023). The instability of stalled ribosomes could conceivably be exacerbated by cellular quality control factors which may remain active in lysates, *e.g.*, ASCC (see first point).

In light of many recent disome studies, we propose a model where not all stalled ribosomes are captured in standard Ribo-seq preparations, and that existing metazoan disome data represent ribosomes in the PPG-like paused state. Our work with a validated NGD reporter provides evidence that the PPG-like state is distinct from that which occurs during NGD. In order to study endogenous targets of NGD in metazoans, future work will need to elucidate the unique features of stalled ribosomes to optimize their capture. Identification of this species would therefore provide new molecular insights into decay-inducing ribosomal stalling vs. programmed or transient ribosomal pausing.

SUPPLEMENTAL FIGURES

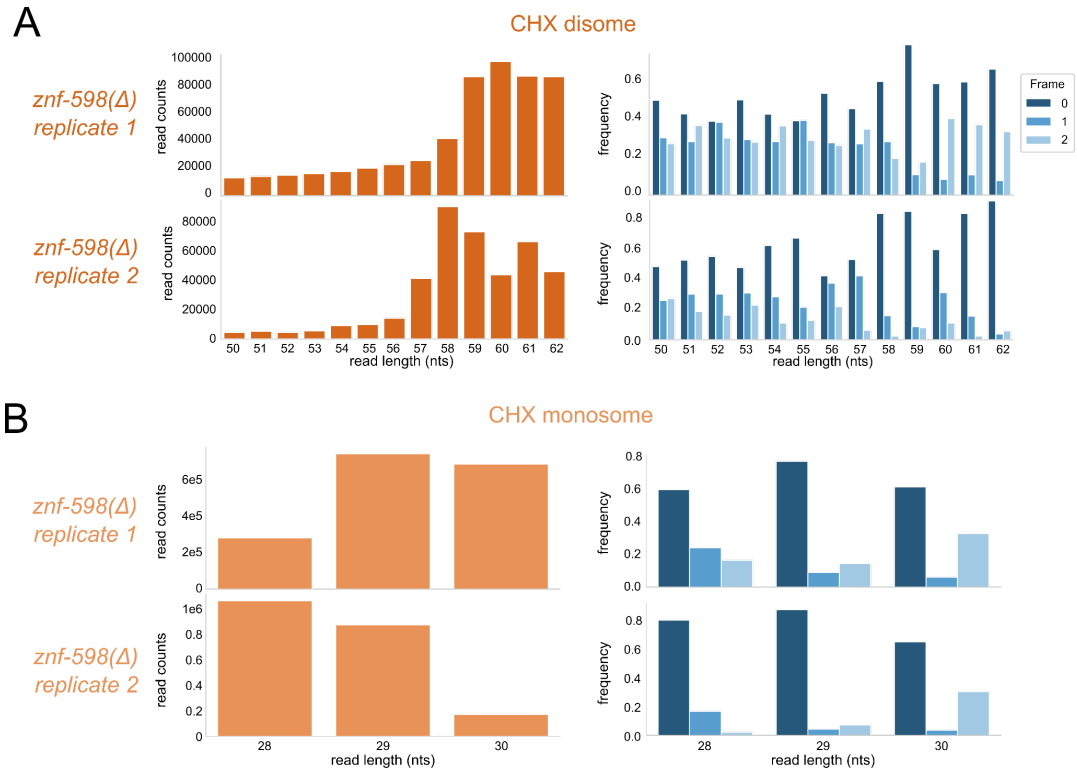

Figure S3.1: Footprint size and frame distributions in CHX Ribo-seq. (A) Size and frame distributions of CHX disome footprints from two biological replicates of *znf-598(Δ)* libraries. Frame 0 is shown in dark blue, frame 1 in medium blue, and frame 2 in light blue. Similar results were obtained in wildtype libraries. **(B)** As in (A), showing CHX monosome footprints. Similar results were obtained in wildtype libraries.

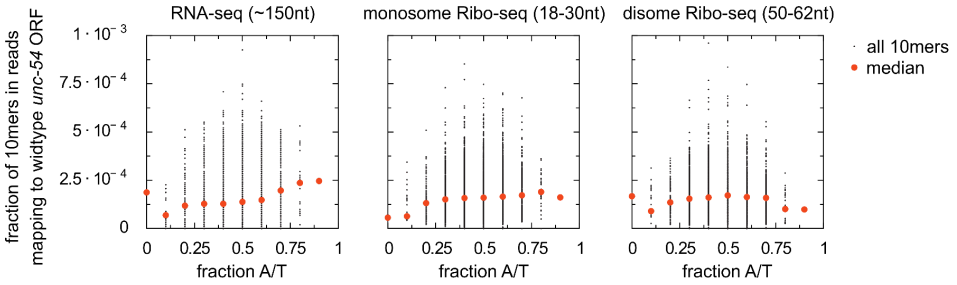

Figure S3.2: Distribution of nucleotide content in deep sequencing libraries. Scatter plots showing read coverage of 10nt sequences mapping to the wildtype *unc-54* ORF from RNA-seq, monosome Ribo-seq, and disome Ribo-seq libraries. An unbiased RNA fragment capture protocol would produce approximately uniform coverage of all 10nt sequences across mRNAs. Sequential Arg (CGN or AGR), Lys (AAR), Pro (CCN), and Gly (GGN) codons could create stretches of GC-rich and GC-poor sequence. Similar results were obtained from other replicates, genetic backgrounds, genes, and kmer sizes.

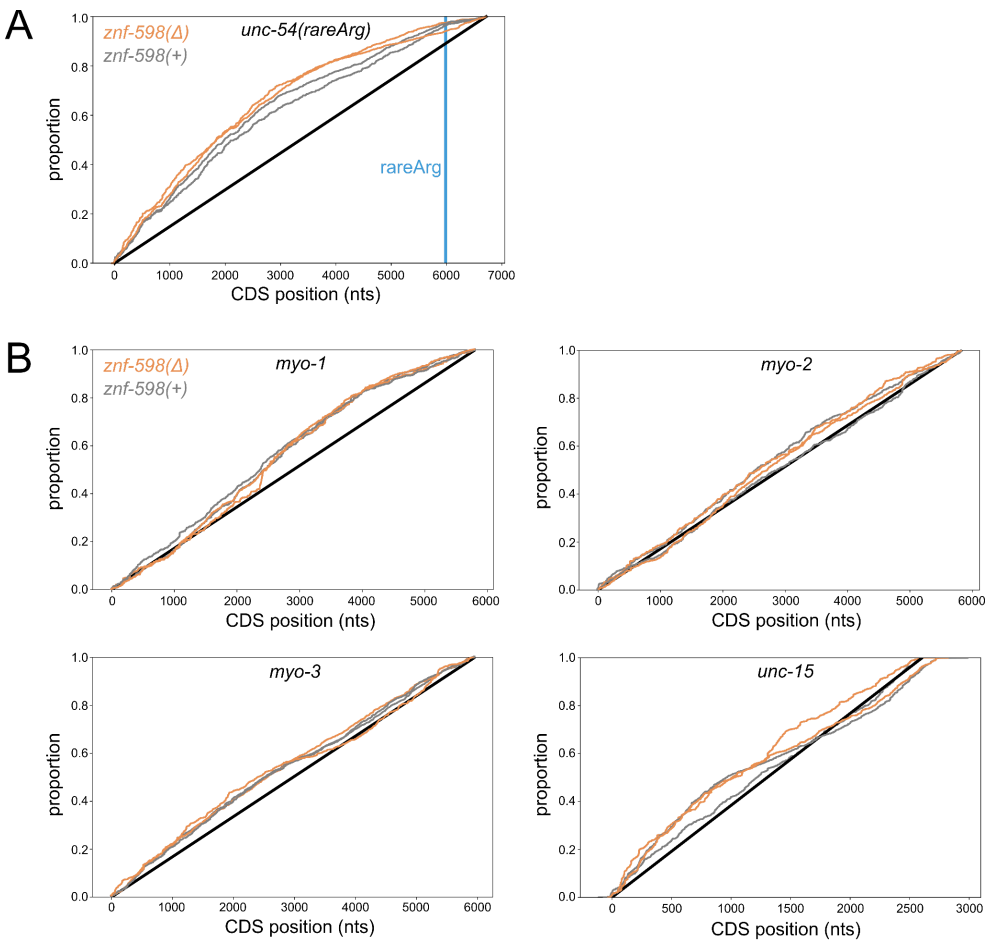

Figure S3.3: 5' bias of ribosomes on *unc-54(rareArg)* exceeds that seen on other myosins. (A) Cumulative distribution function (CDF) showing proportion of CHX monosome Ribo-seq reads along CDS positions on unc-54(rareArg) from two biological replicates. *znf-598(Δ)* is shown in orange and *znf-598(+)* is shown in grey. Black line indicates expected CDF from a uniform distribution of ribosomes throughout the ORF. **(B)** As in (A), showing the proportion of monosome reads along *myo-1, myo-2, myo-3,* and *unc-15*.

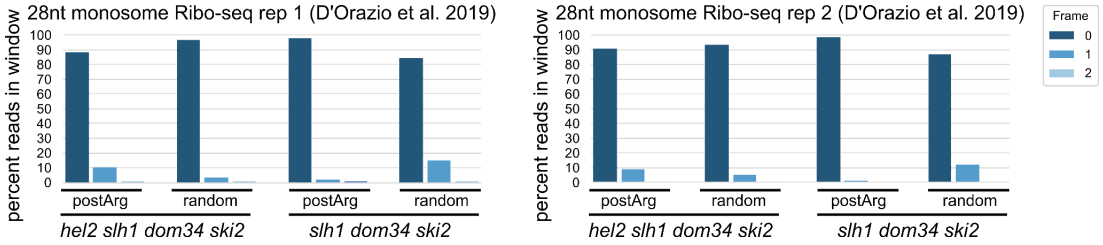

Figure S3.4: Post-stall ribosomes remain in frame on a yeast NGD substrate. Frame analysis as in Figure 2B, done on *S. cer* 28nt monosome Ribo-seq reads on a NGD reporter with and without mutation of the *S. cer* ZNF-598 homolog *hel2* (D'Orazio et al., 2019).

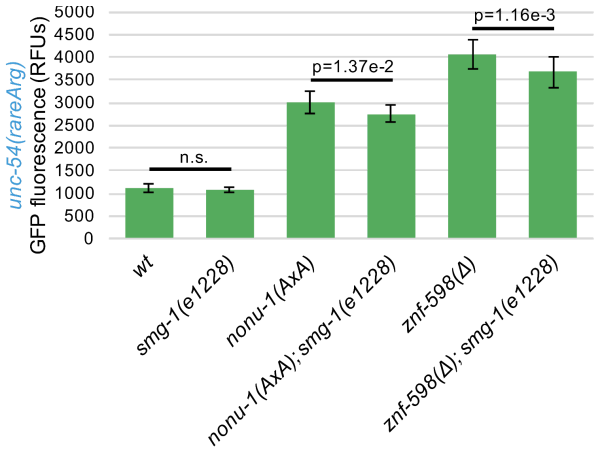

Figure S3.5: Compromised NGD does not lead to NMD activation on a NGD substrate. Mean RFUs (relative fluorescence units) of indicated strains (n≥15 animals/strain) in the *unc-54(rareArg)* background. One standard deviation shown as error bars. p values from Welch's t-test.

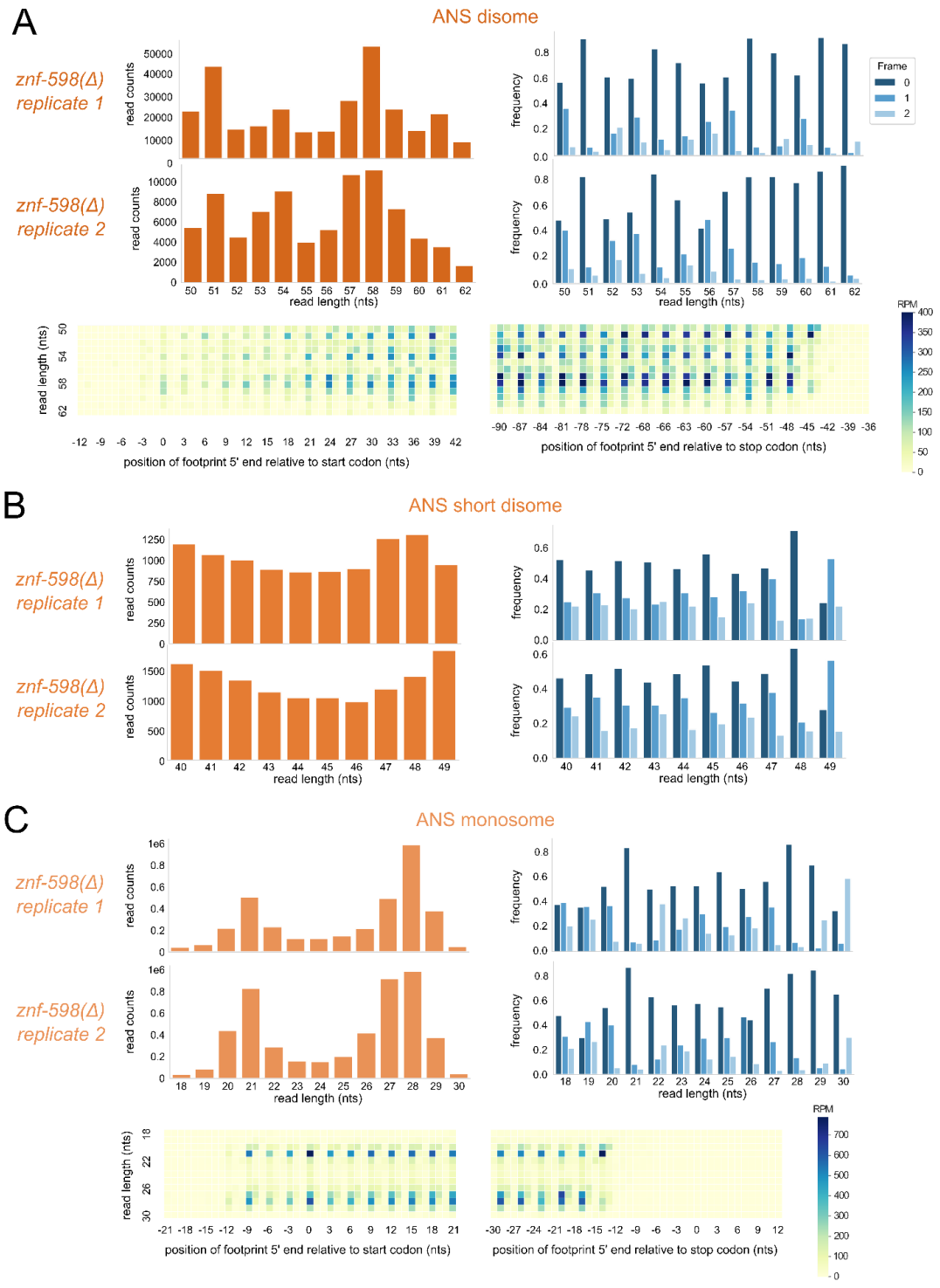

Figure S3.6: Footprint size and frame distributions in ANS Ribo-seq. (A) Size and frame distributions of ANS disome footprints from two biological replicates of *znf-598(Δ)*. Frame 0 is shown in dark blue, frame 1 in medium blue, and frame 2 in light blue. Bottom heat map shows footprint 5' end positions relative to start and stop codons of all genes. Similar results were obtained in wildtype. **(B)** As in (A), showing ANS short disome footprints. **(C)** As in (A), showing ANS monosome footprints.

METHODS

C. elegans strain construction and propagation

C. elegans strains were derived from the VC2010 strain (N2) (Thompson et al., 2013). Animals were grown at 16C or 20C on NGM plates seeded with OP50 as a food source (Brenner, 1974). Some strains were obtained from the Caenorhabditis Genetic Center (CGC), which is funded by NIH Office of Research Infrastructure Programs (P40 OD010440). CRISPR/Cas9 was performed to introduce genomic edits as previously described (Arribere et al., 2014). Multiple independent isolates of each mutation were recovered and observed to have identical phenotypes. Mutant combinations were generated by crossing. A full list of strains, sequences of mutant alleles, PCR primers, and sources is available in Table S1.

RNA-seq

Animals were synchronized by hypochlorite treatment, propagated on NGM plates with OP50 at 16C, and harvested at the L4/young adult stage. Animals were washed off with N50, passed through a 5% sucrose cushion in N50 to remove *E. coli,* and snap frozen in liquid nitrogen. Animals were lysed by grinding in a mortar and pestle cooled in liquid nitrogen in the presence of frozen PLB (20mM Tris pH8.0, 140mM KCl, 1.5mM MgCl2, 1% Triton) and 100ug/mL cycloheximide. Ground animals were stored as frozen powder at -70C.

Total RNA was extracted with trizol, resuspended in TE pH7.4, and quantified by Qubit. Ribosomal RNA was depleted using custom *C. elegans*-specific rRNA hybridization oligos, similar to a planarian protocol as described (Kim et al., 2019). Oligos for this protocol are included in Table S1. Libraries were prepared using an NEBNext Ultra II Directional RNA Library Prep Kit for Illumina sequencing. Libraries were sequenced at Novogene Corporation Inc. UC Davis Sequencing Center on a NovaSeq 6000.

Ribo-seq

For cycloheximide experiments, ground animals as described in RNA-seq were thoroughly mixed with ice cold PLB and 100ug/mL cycloheximide. For anisomycin experiments, animals were ground in frozen PLB and 100ug/mL anisomycin, then mixed with ice cold PLB and 100ug/mL anisomycin. Ribosome::mRNA complexes were obtained via a 10 min clarifying spin at 10,000 rcf at 4C and quantified via Nanodrop A260 measurement. Total OD units were calculated and RNaseI (Ambion) was added as per the following equation: total OD units × 0.3 = ul RNaseI. RNA was digested for 30 min at 23C and immediately loaded onto a chilled 10%-50% sucrose gradient containing 100ug/mL cycloheximide or 100ug/mL anisomycin.

Gradients were spun in an SW41 Ti rotor in an ultracentrifuge at 35,000 rpm for 4.5hrs at 4C. Monosomes and disomes were collected on a fractionator (Brandel) and digested with proteinase K. Monosome and disome RNA was cleaned up by acid phenol chloroform extraction, precipitated, and stored in TE pH7.4. 2ug of purified monosome and disome RNA were run on 15% polyacrylamide gels and size-selected. For cycloheximide experiments, 28-30nt (monosome) and 50-62nt (disome) footprints were excised. For anisomycin experiments, 18-30nt (monosome), 40-49nt (short disome), and 50-62nt (disome) footprints were excised.

Gel-purified RNA was treated with T4 PNK (NEB) to remove 3′phosphates. RNA was then extracted with phenol chloroform, precipitated, and resuspended in TE pH7.4. Pre-adenylated adaptor containing 8nt UMI sequences (JA-AF-34.5) was ligated onto RNA 3′ends with T4 RNA Ligase 2 truncated KQ (NEB). Adaptor-ligated RNA was run on a 15% polyacrylamide gel, and the ligated species was excised, eluted, and precipitated. Reverse transcription was performed using JA-AF-126 and superscript II RT (Thermo Fisher). cDNA was gel-purified and precipitated from a 15% polyacrylamide gel and circularized with CircLigase (Lucigen). Circularized DNA was amplified by PCR (10-14 cycles) using primers

containing Illumina-compatible adaptors. Libraries were sequenced at Novogene Corporation Inc. UC Davis Sequencing Center on a NovaSeq 6000.

RNA- and Ribo-seq analyses

RNA- and Ribo-seq reads were trimmed using cutadapt v2.9 (Martin, 2011) and PCR duplicates (identified by the 8nt UMI on AF-JA-34.5) were collapsed using custom scripts. We generated a custom *C. elegans* genome (Ensembl, WBCel235) containing *unc-54(rareArg)* as a separate chromosome and a masked endogenous *unc-54* locus. Reads were mapped to this genome including annotated splice junctions using STAR v2.5.4b (Dobin and Gingeras, 2015) allowing for zero mismatches. All downstream analyses were restricted to uniquely mapping reads.

Analyses were performed in python3 and plotted using matplotlib or PyX v0.15 using custom scripts. In rocket plots, read counts were median-normalized using DESeq (Anders and Huber, 2010).

Percent readthrough was calculated via the average footprints post-rareArg divided by the average footprints pre-rareArg, normalized to length. This was done omitting 100nts upstream of the 5' end of a ribosome with the first arginine codon in its P-site and 100nts downstream of the 5' end of a ribosome with the last arginine in its P-site. We note that this metric will include effects such as 5' bias into the readthrough calculation; similar calculations with smaller window sizes centered about the stall revealed similar results.

Meta-codon plots of footprint density around motifs were created similarly to that done previously (Meydan et al., 2020). Briefly, we generated a list of every occurrence of amino acid triplets in the *C. elegans* transcriptome. Average normalized monosome and disome density were plotted by their 3' ends 50nt upstream and downstream of the first nucleotide of the first amino acid in the motif. Dotted lines were drawn at locations indicating the footprint 3' end position when the third codon of each motif is in each ribosomal site.

Fluorescence microscopy and image analysis

All animals were maintained at 20C. L4 animals were selected and anesthetized in 3uL EN50 with 1mM levamisole in a microscope well slide with a 0.15mm coverslip. A Zeiss AxioZoom microscope was used with a 1.0x objective to acquire images for GFP quantification experiments. The following parameters were used for all images: exposure time of 250ms., shift of 50%, and zoom of 80%. 15-25 representative animals were imaged for each strain. All comparisons shown are between images obtained during the same imaging session. We used FIJI to define the area of the animal, subtract the background, and determine mean pixel intensity for the area of each animal.

CHAPTER 4: CONCLUSIONS AND FUTURE DIRECTIONS

Functional roles for ribosomal ubiquitination

A large body of work established ribosomal ubiquitination as an integral part of No-Go mRNA Decay (NGD), yet how this ubiquitination changes gene expression has remained unclear (Juszkiewicz & Hegde, 2017; Sundaramoorthy et al., 2017). Our work here (Chapter 2) revealed several key details in the function of ribosomal ubiquitination, providing its first clear contributions in NGD.

In light of the recent discovery of the first known NGD endonuclease, NONU-1/Cue2/YPL199C (Glover et al., 2020; D'Orazio et al., 2019), we posit a model connecting NONU-1 to ribosomal ubiquitination through ubiquitin-binding. Additionally, we elucidate an unexpected step in NONU-1 recruitment by reporting its requirement for ribosome rescue prior to mRNA cleavage. This finding provides a long-awaited explanation for surprising results seen almost two decades ago showing a requirement for the rescue factor HBS-1 in mRNA decay (Doma & Parker 2006). These novel results allow for the investigation of outstanding questions concerning NONU-1 recruitment and function, as described below.

Where does NONU-1 bind stalled ribosomes?

Our work reports a ubiquitin-based recruitment mechanism for NONU-1; however, it is unclear which ubiquitins on the ribosome and which CUE domains in NONU-1 participate in recruitment.

We anticipate that structural studies of NONU-1 on stalled ribosomes will prove insightful for understanding its binding site(s) on ribosomes. It may be most straightforward to seek NONU-1 bound to stalled, collided disomes as accepted by the field as the substrate for NGD (Simms et al., 2017; Juszkiewicz et al., 2018; Ikeuchi et al., 2019). However, we

hypothesize that NONU-1 may instead act on a peculiar post-rescue 40S:80S collision species, as indicated by our genetic requirement for ribosome rescue prior to NONU-1 mRNA cleavage. Credibility for this hypothesis also comes from recent ribosome profiling work detecting a potential post-rescue 40S:80S complex (Ferguson et al., 2023). We therefore expect stabilization of this species to be a key prerequisite for solving the structure of NONU-1 bound to stalled ribosomes.

Where does NONU-1 cleave mRNA relative to stalled ribosomes?

To understand the effects of NONU-1:ribosome binding, it will also be important to visualize NONU-1's precise cleavage site at stalls. Hints emerged through prior ribosome profiling data: cleavages are in the vicinity of stalled ribosomes, suggesting that NONU-1/CUE2 cleaves mRNA near the trailing ribosome (Glover et al., 2020; D'Orazio et al., 2019). However, interpretations are limited due to the diffuse stall site on arginine reporters and the technical complications of profiling NGD ribosomes in animals.

We propose the expression of an exogenous tRNase to knockdown tRNAs decoding three codons (Glu GAA, Lys AAA, Gln CAA) (Lentini et al., 2018), thus inducing global stalls at these codons. This method can solve the issue of a diffuse stall, allowing us to map the precise NONU-1 cleavage site relative to the known stalled, leading ribosome. Furthermore, recent knowledge of the ribosome substrate for NONU-1 (described above) and optimizations of ribosome footprint profiling (Ferguson et al., 2023) will enable a clear understanding of NONU-1 cleavage sites in NGD.

Endogenous targets of stalling-induced decay

A major outstanding question in the field is how cells utilize NGD. Most NGD studies use artificial reporters with synthetic stall sequences that do not resemble endogenous sequences. To-date, studies have only identified a handful of genes whose mRNAs experience NGD in yeast (*SDD1*, *RNA14*, *YAP1*) (Matsuo et al., 2020; D'Orazio et al., 2019).

Despite the evolutionary conservation of NGD factors and their relationships, no endogenous mRNA targets of these factors are known in animals. It therefore remains unclear to what extent NGD operates as (1) a housekeeping quality control mechanism called into action when ribosomes stochastically collide, (2) a service for a select few transcripts prone to collisions during times of high ribosome load, (3) a solution when errors are introduced during mRNA transcription and/or processing, and/or (4) a way to combat stall-inducing mutations during disease states.

In an effort to identify endogenous NGD targets, many recent studies emerged mapping closely-translating disomes genome-wide (Meydan et al., 2020; Han et al., 2020; Arpat et al., 2020; Zhao et al., 2021). However, no clear connection has been made between these disomes and NGD. Our work (Chapter 3) highlighted this limitation in current literature through our use of a thoroughly validated NGD reporter. We are currently working to fill this gap of knowledge through our collection of NGD factor mutants, our reporter, and novel ribosome capture methods.

We expect that the identification of endogenous targets will vastly expand the field of NGD, both in the study of molecular mechanism and in human health. Intriguingly, prior work reported neurodegeneration as a result of ribosome stalling via dysfunctional tRNAs (Ishimura et al., 2014). Additionally, our NGD screen (Chapter 2) identified a novel factor required for NGD (*catp-6*) whose human homolog (ATP13A2) is implicated in Parkinson's Disease. We therefore hypothesize that NGD mitigates the harmful effects of an unknown class of mRNAs, and that loss of the pathway is detrimental to neuronal health and function. Discovery of endogenous NGD mRNAs will thus enable a greater understanding of translational control during disease states.

Uncharacterized signaling events on the ribosome

Recent studies provided a glimpse into the complicated nature of ribosomal ubiquitination during NGD (Garshott et al., 2020). Our work on the function of ribosomal

ubiquitination may inform future studies of signaling events on the ribosome. Namely, we showed that NGD could be prevented by ablation of only three ubiquitination sites.

In the course of analyzing ubiquitination sites (Chapter 1), we noticed that there are hundreds of such sites, suggesting widespread and diverse cellular signaling at the ribosome (Higgins et al., 2015; Koyuncu et al., 2021). Through experiments similar to those we used to study NGD, it may be possible to understand the functions of these ubiquitination sites. We expect that many of these sites participate in novel translational control pathways, with their discovery opening the door to intriguing new facets of the ribosome.

REFERENCES

1. Alam, S. L., Sun, J., Payne, M., Welch, B. D., Blake, B. K., Davis, D. R., Meyer, H. H., Emr, S. D., & Sundquist, W. I. (2004). Ubiquitin interactions of NZF zinc fingers. *EMBO Journal, 23*(7), 1411–1421.

2. Aleksashin, N. A., Tsai-Lan Chang, S., & D Cate, J. H. (2023). A highly efficient human cell-free translation system. *BioRxiv*, 2023.02.09.527910.

3. Allen, G. E., Panasenko, O. O., Villanyi, Z., Zagatti, M., Weiss, B., Pagliazzo, L., Huch, S., Polte, C., Zahoran, S., Hughes, C. S., Pelechano, V., Ignatova, Z., & Collart, M. A. (2021). Not4 and Not5 modulate translation elongation by Rps7A ubiquitination, Rli1 moonlighting, and condensates that exclude eIF5A. *Cell Reports*, 36(9), 109633.

4. Anders, S., & Huber, W. (2010). Differential expression analysis for sequence count data. Genome biology, 11(10), R106.

5. Anderson, P., & Brenner, S. (1984). A selection for myosin heavy chain mutants in the nematode Caenorhabditis elegans. *Proceedings of the National Academy of Sciences of the United States of America*, 81(14 I), 4470–4474.

6. Arpat, A., Liechti, A., De Matos, M., Dreos, R., Janich, P., & Gatfield, D. (2020). Transcriptome-wide sites of collided ribosomes reveal principles of translational pausing. *Genome Research,* 30(7), 985–999.

7. Arribere, J. A., Bell, R. T., Fu, B. X., Artiles, K. L., Hartman, P. S., & Fire, A. Z. (2014). Efficient marker-free recovery of custom genetic modifications with CRISPR/Cas9 in *Caenorhabditis elegans*. *Genetics, 198*(3), 837–846.

8. Arribere JA, Cenik ES, Jain N, Hess GT, Lee CH, Bassik MC, et al. Translation readthrough mitigation. Nature. 2016;534(7609):719-723.

9. Arribere, J. A., & Fire, A. Z. (2018). Nonsense mRNA suppression via nonstop decay. *eLife, 7*, 1–23.

10. Becker, T., Armache, J. P., Jarasch, A., Anger, A. M., Villa, E., Sieber, H., Motaal, B. A., Mielke, T., Berninghausen, O., & Beckmann, R. (2011). Structure of the no-go mRNA decay complex Dom34-Hbs1 bound to a stalled 80S ribosome. *Nature Structural and Molecular Biology, 18(6)*, 715–720.

11. Bejsovec, A., & Anderson, P. (1988). Myosin heavy-chain mutations that disrupt Caenorhabditis elegans thick filament assembly. Genes & Development, 2(10), 1307–1317.

12. Bengtson, M. H., & Joazeiro, C. A. P. (2010). Role of a ribosome-associated E3 ubiquitin ligase in protein quality control. *Nature, 467*(7314), 470–473.

13. Brandman, O., Stewart-Ornstein, J., Wong, D., Larson, A., Williams, C. C., Li, G. W., Zhou, S., King, D., Shen, P. S., Weibezahn, J., Dunn, J. G., Rouskin, S., Inada, T.,

Frost, A., & Weissman, J. S. (2012). A ribosome-bound quality control complex triggers degradation of nascent peptides and signals translation stress. *Cell, 151*(5), 1042–1054.

14. Brenner S. (1974). The genetics of *Caenorhabditis elegans*. *Genetics, 77(*1), 71–94.

15. Brickner, J. R., Soll, J. M., Lombardi, P. M., Vågbø, C. B., Mudge, M. C., Oyeniran, C., Rabe, R., Jackson, J., Sullender, M. E., Blazosky, E., Byrum, A. K., Zhao, Y., Corbett, mark A., Gécz, J., Field, M., Vindigni, A., Slupphaug, G., Wolberger, C., & Mosammaparast, N. (2017). A ubiquitin-dependent signalling axis specific for ALKBH-mediated DNA dealkylation repair. *Nature*, 551(7680), 389–393.

16. Buetow, L., & Huang, D. T. (2016). Structural insights into the catalysis and regulation of E3 ubiquitin ligases. *Nature Reviews Molecular Cell Biology*, 7(10), 626–642.

17. Buschauer, R., Matsuo, Y., Sugiyama, T., Chen, Y. H., Alhusaini, N., Sweet, T., Ikeuchi, K., Cheng, J., Matsuki, Y., Nobuta, R., Gilmozzi, A., Berninghausen, O., Tesina, P., Becker, T., Coller, J., Inada, T., & Beckmann, R. (2020). The Ccr4-Not complex monitors the translating ribosome for codon optimality. *Science*, 368(6488).

18. Bustos, D., Bakalarski, C. E., Yang, Y., Peng, J., & Kirkpatrick, D. S. (2012). Characterizing ubiquitination sites by peptide-based immunoaffinity enrichment. *Molecular and Cellular Proteomics*, 11(12), 1529–1540.

19. Cali, B. M., Kuchma, S. L., Latham, J., & Anderson, P. (1999). *smg-7* is required for mRNA surveillance in *Caenorhabditis elegans*. *Genetics, 151*(2), 605–616.

20. Cassar, P. A., Carpenedo, R. L., Samavarchi-Tehrani, P., Olsen, J. B., Park, C. J., Chang, W. Y., Chen, Z., Choey, C., Delaney, S., Guo, H., Guo, H., Tanner, R. M., Perkins, T. J., Tenenbaum, S. A., Emili, A., Wrana, J. L., Gibbings, D., & Stanford, W. L. (2015). Integrative genomics positions MKRN 1 as a novel ribonucleoprotein within the embryonic stem cell gene regulatory network. *EMBO Reports*, 16(10), 1334–1357.

21. Chandrasekaran, V., Juszkiewicz, S., Choi, J., Puglisi, J. D., Brown, A., Shao, S., Ramakrishnan, V., & Hegde, R. S. (2019). Mechanism of ribosome stalling during translation of a poly(A) tail. *Nature Structural and Molecular Biology, 26*(12), 1132–1140.

22. Clague, M. J., & Urbé, S. (2010). Ubiquitin: Same molecule, different degradation pathways. *Cell*, 143(5), 682–685.

23. Collart, M. A. (2016). The Ccr4-Not complex is a key regulator of eukaryotic gene expression. *Wiley Interdisciplinary Reviews: RNA*, 7(4), 438–454.

24. Davis, Z. H., Mediani, L., Antoniani, F., Vinet, J., Li, S., Alberti, S., Lu, B., Holehouse, A. S., Carra, S., & Brandman, O. (2021). Protein products of nonstop mRNA disrupt nucleolar homeostasis. Cell Stress & Chaperones, 26(3), 549–561.

25. Das, S., Vera, M., Gandin, V., Singer, R. H., & Tutucci, E. (2021). Intracellular mRNA transport and localized translation. Nature Reviews Molecular Cell Biology, 22(7), 483–504.

26. Dolan, J. W., & Fields, S. (1990). Overproduction of the yeast STE12 protein leads to constitutive transcriptional induction. *Genes & development*, 4(4), 492–502.

27. Deshaies, R. J., & Joazeiro, C. A. P. (2009). RING domain E3 ubiquitin ligases. *Annual Review of Biochemistry*, 78, 399–434.

28. Dey, G., & Meyer, T. (2015). Phylogenetic Profiling for Probing the Modular Architecture of the Human Genome. *Cell Systems, 1(*2), 106–115.

29. Dimitrova, L. N., Kuroha, K., Tatematsu, T., & Inada, T. (2009). Nascent peptide-dependent translation arrest leads to Not4p-mediated protein degradation by the proteasome. *Journal of Biological Chemistry*, 284(16), 10343–10352.

30. Dmitriev, S. E., Vladimirov, D. O., & Lashkevich, K. A. (2020). A Quick Guide to Small-Molecule Inhibitors of Eukaryotic Protein Synthesis. Biochemistry (Moscow), 85(11), 1389–1421.

31. Dobin, A., & Gingeras, T. R. (2015). Mapping RNA-seq Reads with STAR. *Current protocols in bioinformatics, 51*, 11.14.1–11.14.19.

32. Doitsidou, M., Poole, R. J., Sarin, S., Bigelow, H., & Hobert, O. (2010). C. elegans mutant identification with a one-step whole-genome-sequencing and SNP mapping strategy. *PloS one, 5*(11), e15435.

33. Doma, M. K., & Parker, R. (2006). Endonucleolytic cleavage of eukaryotic mRNAs with stalls in translation elongation. *Nature, 440*(7083), 561–564.

34. D'Orazio, K. N., Wu, C. C. C., Sinha, N., Loll-Krippleber, R., Brown, G. W., & Green, R. (2019). The endonuclease cue2 cleaves mRNAs at stalled ribosomes during no go decay. *eLife, 8.*

35. Edgar, R., Domrachev, M., & Lash, A. E. (2002). Gene Expression Omnibus: NCBI gene expression and hybridization array data repository. *Nucleic acids research, 30*(1), 207–210.

36. Ferguson, L., Upton, H. E., Pimentel, S. C., Mok, A., Lareau, L. F., Collins, K., & Ingolia, N. T. (2023). Streamlined and sensitive mono-and di-ribosome profiling in yeast and human cells. BioRxiv.

37. Frischmeyer, P. A., Hoof, A. van, O'Donnell, K., Guerrerio, A. L., Parker, R., & Dietz, H. C. (2002). An mRNA Surveillance Mechanism That Eliminates Transcripts Lacking Termination Codons. *Science, 295*(5563), 2258–2261.

38. Garshott, D. M., Sundaramoorthy, E., Leonard, M., & Bennett, E. J. (2020). Distinct regulatory ribosomal ubiquitylation events are reversible and hierarchically organized. *eLife*, 9, 1–22.

39. Garshott, D. M., An, H., Sundaramoorthy, E., Leonard, M., Vicary, A., Harper, J. W., & Bennett, E. J. (2021). iRQC, a surveillance pathway for 40S ribosomal quality control during mRNA translation initiation. *Cell Reports*, 36(9), 109642.

40. Garzia, A., Jafarnejad, S. M., Meyer, C., Chapat, C., Gogakos, T., Morozov, P., Amiri, M., Shapiro, M., Molina, H., Tuschl, T., & Sonenberg, N. (2017). The E3 ubiquitin ligase and RNA-binding protein ZNF598 orchestrates ribosome quality control of premature polyadenylated mRNAs. *Nature Communications, 8*.

41. Garzia, A., Meyer, C., & Tuschl, T. (2021). The E3 ubiquitin ligase RNF10 modifies 40S ribosomal subunits of ribosomes compromised in translation. *Cell Reports, 36(*5).

42. Glover, M. L., Burroughs, A. M., Monem, P. C., Egelhofer, T. A., Pule, M. N., Aravind, L., & Arribere, J. A. (2020). NONU-1 Encodes a Conserved Endonuclease Required for mRNA Translation Surveillance. *Cell Reports, 30(*13), 4321-4331.e4.

43. Gutierrez, E., Shin, B. S., Woolstenhulme, C. J., Kim, J. R., Saini, P., Buskirk, A. R., & Dever, T. E. (2013). eIF5A promotes translation of polyproline motifs. Molecular Cell, 51(1), 35–45.

44. Han, M., Aroian, R. V., & Sternberg, P. W. (1990). The let-60 locus controls the switch between vulval and nonvulval cell fates in Caenorhabditis elegans. *Genetics*, 126(4), 899–913.

45. Han, P., Shichino, Y., Schneider-Poetsch, T., Mito, M., Hashimoto, S., Udagawa, T., Kohno, K., Yoshida, M., Mishima, Y., Inada, T., & Iwasaki, S. (2020). Genome-wide Survey of Ribosome Collision. *Cell Reports*, 31(5), 107610.

46. Hickey, K. L., Dickson, K., Cogan, J. Z., Replogle, J. M., Schoof, M., D'Orazio, K. N., Sinha, N. K., Hussmann, J. A., Jost, M., Frost, A., Green, R., Weissman, J. S., & Kostova, K. K. (2020). GIGYF2 and 4EHP Inhibit Translation Initiation of Defective Messenger RNAs to Assist Ribosome-Associated Quality Control. *Molecular Cell, 79*(6), 950-962.e6.

47. Higgins, R., Gendron, J. M., Rising, L., Mak, R., Webb, K., Kaiser, S. E., Zuzow, N., Riviere, P., Yang, B., Fenech, E., Tang, X., Lindsay, S. A., Christianson, J. C., Hampton, R. Y., Wasserman, S. A., & Bennett, E. J. (2015). The Unfolded Protein Response Triggers Site-Specific Regulatory Ubiquitylation of 40S Ribosomal Proteins. *Molecular Cell*, 59(1), 35–49.

48. Hilal, T., Yamamoto, H., Loerke, J., Bürger, J., Mielke, T., & Spahn, C. M. T. (2016). Structural insights into ribosomal rescue by Dom34 and Hbs1 at near-atomic resolution. *Nature Communications, 7*, 1–8.

49. Hildebrandt, A., Brüggemann, M., Rücklé, C., Boerner, S., Heidelberger, J. B., Busch, A., Hänel, H., Voigt, A., Möckel, M. M., Ebersberger, S., Scholz, A., Dold, A., Schmid, T., Ebersberger, I., Roignant, J. Y., Zarnack, K., König, J., & Beli, P. (2019). The RNA-binding ubiquitin ligase MKRN1 functions in ribosome-associated quality control of poly(A) translation. *Genome Biology*, 20(1), 1–20.

50. Husnjak, K., & Dikic, I. (2012). Ubiquitin-binding proteins: Decoders of ubiquitin-mediated cellular functions. *Annual Review of Biochemistry,* 81, 291–322.

51. Ikeuchi, K., Tesina, P., Matsuo, Y., Sugiyama, T., Cheng, J., Saeki, Y., Tanaka, K., Becker, T., Beckmann, R., & Inada, T. (2019). Collided ribosomes form a unique structural interface to induce Hel2-driven quality control pathways. *The EMBO Journal, 38*(5), 1–21.

52. Inada, T. (2020). Quality controls induced by aberrant translation. *Nucleic Acids Research*, 48(3), 1084–1096.

53. Ishimura, R., Nagy, G., Dotu, I., Zhou, H., Yang, X. L., Schimmel, P., Senju, S., Nishimura, Y., Chuang, J. H., & Ackerman, S. L. (2014). Ribosome stalling induced by mutation of a CNS-specific tRNA causes neurodegeneration. *Science, 345*(6195), 455–459.

54. Itzhak, D. N., Tyanova, S., Cox, J., & Borner, G. H. H. (2016). Global, quantitative and dynamic mapping of protein subcellular localization. *eLife*, 5, 1–36.

55. Jia, J., Absmeier, E., Holton, N., Pietrzyk-Brzezinska, A. J., Hackert, P., Bohnsack, K. E., Bohnsack, M. T., & Wahl, M. C. (2020). The interaction of DNA repair factors ASCC2 and ASCC3 is affected by somatic cancer mutations. *Nature Communications*, 11(1), 1–13.

56. Joazeiro, C. A. P. (2017). Ribosomal stalling during translation: Providing substrates for ribosome-associated protein quality control. *Annual Review of Cell and Developmental Biology*, 33, 343–368.

57. Jumper, J., Evans, R., Pritzel, A., Green, T., Figurnov, M., Ronneberger, O., Tunyasuvunakool, K., Bates, R., Žídek, A., Potapenko, A., Bridgland, A., Meyer, C., Kohl, S. A. A., Ballard, A. J., Cowie, A., Romera-Paredes, B., Nikolov, S., Jain, R., Adler, J., … Hassabis, D. (2021). Highly accurate protein structure prediction with AlphaFold. Nature, 596(7873), 583–589.

58. Juszkiewicz, S., & Hegde, R. S. (2017). Initiation of Quality Control during Poly(A) Translation Requires Site-Specific Ribosome Ubiquitination. *Molecular Cell, 65(*4), 743-750.e4.

59. Juszkiewicz, S., Chandrasekaran, V., Lin, Z., Kraatz, S., Ramakrishnan, V., & Hegde, R. S. (2018). ZNF598 Is a Quality Control Sensor of Collided Ribosomes. *Molecular Cell, 72*(3), 469-481.e7.

60. Juszkiewicz, S., Speldewinde, S. H., Wan, L., Svejstrup, J. Q., & Hegde, R. S. (2020). The ASC-1 Complex Disassembles Collided Ribosomes. *Molecular Cell*, 79(4), 603-614.e8.

61. Kang, R. S., Daniels, C. M., Francis, S. A., Shih, S. C., Salerno, W. J., Hicke, L., & Radhakrishnan, I. (2003). Solution structure of a CUE-ubiquitin complex reveals a conserved mode of ubiquitin binding. *Cell*, 113(5), 621–630.

62. Keeling, P. J., Burki, F., Wilcox, H. M., Allam, B., Allen, E. E., Amaral-Zettler, L. A., Armbrust, E. V., Archibald, J. M., Bharti, A. K., Bell, C. J., Beszteri, B., Bidle, K. D., Cameron, C. T., Campbell, L., Caron, D. A., Cattolico, R. A., Collier, J. L., Coyne, K., Davy, S. K., Deschamps, P., … Worden, A. Z. (2014). The Marine Microbial Eukaryote Transcriptome Sequencing Project (MMETSP): illuminating the functional diversity of eukaryotic life in the oceans through transcriptome sequencing. *PLoS biology, 12*(6), e1001889.

63. Kim, I. V., Ross, E. J., Dietrich, S., Döring, K., Sánchez Alvarado, A., & Kuhn, C. D. (2019). Efficient depletion of ribosomal RNA for RNA sequencing in planarians. *BMC genomics, 20*(1), 909.

64. Kim, J. H., Park, S. M., Kang, M. R., Oh, S. Y., Lee, T. H., Muller, M. T., & Chung, I. K. (2005). Ubiquitin ligase MKRN1 modulates telomere length homeostasis through a proteolysis of hTERT. *Genes and Development*, 19(7), 776–781.

65. Kim, W., Bennett, E. J., Huttlin, E. L., Guo, A., Li, J., Possemato, A., Sowa, M. E., Rad, R., Rush, J., Comb, M. J., Harper, J. W., & Gygi, S. P. (2011). Systematic and quantitative assessment of the ubiquitin-modified proteome. *Molecular Cell*, 44(2), 325–340.

66. Komander, D., & Rape, M. (2012). The Ubiquitin Code. *Annu. Rev. Biochem*., 81, 203–229.

67. Kostova, K. K., Hickey, K. L., Osuna, B. A., Hussmann, J. A., Frost, A., Weinberg, D. E., & Weissman, J. S. (2017). CAT-tailing as a fail-safe mechanism for efficient degradation of stalled nascent polypeptides. *Science, 357*(6349), 414–417.

68. Koyuncu, S., Loureiro, R., Lee, H. J., Wagle, P., Krueger, M., & Vilchez, D. (2021). Rewiring of the ubiquitinated proteome determines ageing in *C. elegans*. *Nature*, 596(7871), 285–290.

69. Kriachkov, V., Ormsby, A. R., Kusnadi, E. P., McWilliam, H. E. G., Mintern, J. D., Amarasinghe, S. L., Ritchie, M. E., Furic, L., & Hatters, D. M. (2023). Arginine-rich C9ORF72 ALS proteins stall ribosomes in a manner distinct from a canonical ribosome-associated quality control substrate. Journal of Biological Chemistry, 299(1).

70. Kulkarni, M., & Smith, H. E. (2008). E1 ubiquitin-activating enzyme UBA-1 plays multiple roles throughout C. elegans development. *PLoS Genetics, 4*(7), 1000131.

71. Lareau, L. F., Hite, D. H., Hogan, G. J., & Brown, P. O. (2014). Distinct stages of the translation elongation cycle revealed by sequencing ribosome-protected mRNA fragments. eLife, 3, e01257. 1–16.

72. Lentini, J. M., Ramos, J., & Fu, D. (2018). Monitoring the 5-methoxycarbonylmethyl-2-thiouridine (mcm5s2U) modification in eukaryotic tRNAs via the γ-toxin endonuclease. RNA, 24(5), 749–758.

73. Letzring, D. P., Wolf, A. S., Brule, C. E., & Grayhack, E. J. (2013). Translation of CGA codon repeats in yeast involves quality control components and ribosomal protein L1. *RNA*, 19(9), 1208–1217.

74. Lu, J., & Deutsch, C. (2008). Electrostatics in the Ribosomal Tunnel Modulate Chain Elongation Rates. *Journal of Molecular Biology, 384*(1), 73–86.

75. Lu, J., Wu, T., Zhang, B., Liu, S., Song, W., Qiao, J., & Ruan, H. (2021). Types of nuclear localization signals and mechanisms of protein import into the nucleus. *Cell communication and signaling, 19*(1), 60.

76. Mandelboum, S., Herrero, M., Atzmon, A., Ehrlich, M., & Elroy-Stein, O. (2013). Effective extraction of polyribosomes exposes gene expression strategies in primary astrocytes. Nucleic Acids Research, 1(1256879), 13–14.

77. Martínez-Férriz, A., Ferrando, A., Fathinajafabadi, A., & Farràs, R. (2021). Ubiquitin-mediated mechanisms of translational control. *Seminars in Cell & Developmental Biology*.

78. Martin, M. (2011). Cutadapt removes adapter sequences from high-throughput sequencing reads.

79. Matsuda, R., Ikeuchi, K., Nomura, S., & Inada, T. (2014). Protein quality control systems associated with no-go and nonstop mRNA surveillance in yeast. *Genes to Cells*, 19(1), 1–12.

80. Matsuo, Y., Ikeuchi, K., Saeki, Y., Iwasaki, S., Schmidt, C., Udagawa, T., Sato, F., Tsuchiya, H., Becker, T., Tanaka, K., Ingolia, N. T., Beckmann, R., & Inada, T. (2017). Ubiquitination of stalled ribosome triggers ribosome-associated quality control. *Nature Communications*, 8(1).

81. Matsuo, Y., Tesina, P., Nakajima, S., Mizuno, M., Endo, A., Buschauer, R., Cheng, J., Shounai, O., Ikeuchi, K., Saeki, Y., Becker, T., Beckmann, R., & Inada, T. (2020). RQT complex dissociates ribosomes collided on endogenous RQC substrate SDD1. *Nature Structural and Molecular Biology, 27*(4), 323–332.

82. Mayor, T., Lipford, J. R., Graumann, J., Smith, G. T., & Deshaies, R. J. (2005). Analysis of polyubiquitin conjugates reveals that the Rpn10 substrate receptor contributes to the turnover of multiple proteasome targets. *Molecular and Cellular Proteomics*, 4(6), 741–751.

83. Meydan, S., & Guydosh, N. R. (2020). Disome and Trisome Profiling Reveal Genome-wide Targets of Ribosome Quality Control. *Molecular Cell*, 79(4), 588-602.e6.

84. Meydan, S., & Guydosh, N. R. (2021). A cellular handbook for collided ribosomes: surveillance pathways and collision types. *Current Genetics*, 67(1), 19–26.

85. McKenna, A., Hanna, M., Banks, E., Sivachenko, A., Cibulskis, K., Kernytsky, A., Garimella, K., Altshuler, D., Gabriel, S., Daly, M., & DePristo, M. A. (2010). The Genome Analysis Toolkit: a MapReduce framework for analyzing next-generation DNA sequencing data. *Genome research, 20*(9), 1297–1303.

86. Mello, C. C., Kramer, J. M., Stinchcomb, D., & Ambros, V. (1991). Efficient gene transfer in C.elegans: Extrachromosomal maintenance and integration of transforming sequences. EMBO Journal, 10(12), 3959–3970.

87. Mi, H., Ebert, D., Muruganujan, A., Mills, C., Albou, L. P., Mushayamaha, T., & Thomas, P. D. (2021). PANTHER version 16: a revised family classification, tree-based classification tool, enhancer regions and extensive API. *Nucleic Acids Research, 49*(D1), D394–D403.

88. Moerman, D. G., Plurad, S., Waterston, R. H., & Baillie, D. L. (1982). Mutations in the unc-54 myosin heavy chain gene of caenorhabditis elegans that alter contractility but not muscle structure. *Cell*, 29(3), 773–781.

89. Monem, P. C., Vidyasagar, N., Piatt, A. L., Sehgal, E., & Arribere, J. A. (2023). Ubiquitination of stalled ribosomes enables mRNA decay via HBS-1 and NONU-1 in vivo. *PLoS Genetics*, 19(1): e1010577

90. Monem, P. C., & Arribere, J. A. (2023). A ubiquitin language communicates ribosomal distress. *Seminars in Cell & Developmental Biology*, S1084-9521(23)00072-1. Advance online publication.

91. Mishima, Y., Han, P., Ishibashi, K., Kimura, S., & Iwasaki, S. (2022). Ribosome slowdown triggers codon‐mediated mRNA decay independently of ribosome quality control. *The EMBO Journal*, 41(5), e109256.

92. Mueller, T. D., & Feigon, J. (2002). Solution Structures of UBA Domains Reveal a Conserved Hydrophobic Surface for Protein–Protein Interactions. *Journal of Molecular Biology, 319*(5), 1243–1255.

93. Panasenko, O. O., & Collart, M. A. (2012). Presence of Not5 and ubiquitinated Rps7A in polysome fractions depends upon the Not4 E3 ligase. *Molecular Microbiology*, 83(3), 640–653.

94. Panasenko, O. O. (2014). The role of the E3 ligase Not4 in cotranslational quality control. *Frontiers in Genetics*, 5.

95. Passos, D. O., Doma, M. K., Shoemaker, C. J., Muhlrad, D., Green, R., Weissman, J., Hollien, J., & Parker, R. (2009). Analysis of Dom34 and Its Function in No-Go Decay. *Molecular Biology of the Cell*, *20*, 3025–3032.

96. Peng, J., Schwartz, D., Elias, J. E., Thoreen, C. C., Cheng, D., Marsischky, G., Roelofs, J., Finley, D., & Gygi, S. P. (2003). A proteomics approach to understanding protein ubiquitination. *Nature Biotechnology*, 21(8), 921–926.

97. Pickart, C. M., & Eddins, M. J. (2004). Ubiquitin: Structures, functions, mechanisms. *Biochimica et Biophysica Acta - Molecular Cell Research*, 1695(1–3), 55–72.

98. Pisareva, V. P., Skabkin, M. A., Hellen, C. U. T., Pestova, T. V., & Pisarev, A. V. (2011). Dissociation by Pelota, Hbs1 and ABCE1 of mammalian vacant 80S ribosomes and stalled elongation complexes. *EMBO Journal, 30*(9), 1804–1817.

99. Prag, G., Misra, S., Jones, E. A., Ghirlando, R., Davies, B. A., Horazdovsky, B. F., & Hurley, J. H. (2003). Mechanism of ubiquitin recognition by the CUE domain of Vps9p. *Cell, 113*(5), 609–620.

100. Preissler, S., Reuther, J., Koch, M., Scior, A., Bruderek, M., Frickey, T., & Deuerling, E. (2015). Not4-dependent translational repression is important for cellular protein homeostasis in yeast. *The EMBO Journal*, 34(14), 1905–1924.

101. Radwan, M., Ang, C. S., Ormsby, A. R., Cox, D., Daly, J. C., Reid, G. E., & Hatters, D. M. (2020). Arginine in C9ORF72 dipolypeptides mediates promiscuous proteome binding and multiple modes of toxicity. Molecular and Cellular Proteomics, 19(4), 640–654.

102. Randles, L., & Walters, K. J. (2012). Ubiquitin and its binding domains. *Frontiers in Bioscience,* 17, 2140–2157.

103. Ryabova, L. A., & Hohn, T. (2000). Ribosome shunting in the cauliflower mosaic virus 35S RNA leader is a special case of reinitiation of translation functioning in plant and animal systems. Genes & development, 14(7), 817–829.

104. Saito, S., Hosoda, N., & Hoshino, S. I. (2013). The Hbs1-Dom34 protein complex functions in non-stop mRNA decay in mammalian cells. *Journal of Biological Chemistry, 288*(24), 17832–17843.

105. Saito, K., Horikawa, W., & Ito, K. (2015). Inhibiting K63 Polyubiquitination Abolishes No-Go Type Stalled Translation Surveillance in Saccharomyces cerevisiae. *PLoS Genetics*, 11(4), 1–18.

106. Sandler, H., Kreth, J., Timmers, H. T. M., & Stoecklin, G. (2011). Not1 mediates recruitment of the deadenylase Caf1 to mRNAs targeted for degradation by tristetraprolin. *Nucleic Acids Research*, 39(10), 4373–4386.

107. Schmidt, C., Becker, T., Heuer, A., Braunger, K., Shanmuganathan, V., Pech, M., Berninghausen, O., Wilson, D. N., & Beckmann, R. (2016). Structure of the

hypusinylated eukaryotic translation factor eIF-5A bound to the ribosome. Nucleic Acids Research, 44(4).

108. Schuller, A. P., Wu, C. C., Dever, T. E., Buskirk, A. R., & Green, R. (2017). eIF5A Functions Globally in Translation Elongation and Termination. Molecular Cell, 66(2), 194–205.e5.

109. Shaham, S., & Horvitz, H. R. (1996). Developing Caenorhabditis elegans neurons may contain both cell-death protective and killer activities. *Genes & development*, 10(5), 578–591.

110. Shao, S., Murray, J., Brown, A., Taunton, J., Ramakrishnan, V., & Hegde, R. S. (2016). Decoding Mammalian Ribosome-mRNA States by Translational GTPase Complexes. *Cell*, 167(5), 1229-1240.e15.

111. Shcherbik, N., & Pestov, D. G. (2010). Ubiquitin and ubiquitin-like proteins in the nucleolus: Multitasking tools for a ribosome factory. *Genes and Cancer*, 1(7), 681–689.

112. Shih, S. C., Katzmann, D. J., Schnell, J. D., Sutanto, M., Emr, S. D., & Hicke, L. (2002). Epsins and Vps27p/Hrs contain ubiquitin-binding domains that function in receptor endocytosis. Nature Cell Biology, 4(5), 389–393.

113. Shoemaker, C. J., Eyler, D. E., & Green, R. (2010). Dom34:Hbs1 Promotes Subunit Dissociation and Peptidyl-tRNA Drop-Off to Initiate No-Go Decay. *Science, 330*(6002), 369–372.

114. Shoemaker, C. J., & Green, R. (2012). Translation drives mRNA quality control. *Nature Structural and Molecular Biology*, 19(6), 594–601.

115. Simms, C. L., Yan, L. L., & Zaher, H. S. (2017). Ribosome Collision Is Critical for Quality Control during No-Go Decay. *Molecular Cell, 68*(2), 361-373.e5.

116. Simms, C. L., Yan, L. L., Qiu, J. K., & Zaher, H. S. (2019). Ribosome Collisions Result in +1 Frameshifting in the Absence of No-Go Decay. Cell Reports, 28(7), 1679–1689.e4.

117. Singh, R. K., Gonzalez, M., Kabbaj, M.-H. M., & Gunjan, A. (2012). Novel E3 Ubiquitin Ligases That Regulate Histone Protein Levels in the Budding Yeast Saccharomyces cerevisiae. *PLoS ONE,* 7(5), 36295.

118. Sitron, C. S., Park, J. H., & Brandman, O. (2017). Asc1, Hel2, and Slh1 couple translation arrest to nascent chain degradation. *RNA*, 23(5), 798–810.

119. Smith, H. E., & Mitchell, A. P. (1989). A transcriptional cascade governs entry into meiosis in Saccharomyces cerevisiae. *Molecular and cellular biology*, 9(5), 2142–2152.

120. Spence, J., Rayappa, R. G., Dittmar, G., Sherman, F., Karin, M., & Finley, D. (2000). Cell Cycle-Regulated Modification of the Ribosome by a Variant Multiubiquitin Chain. *Cell*, 102, 67–76.

121. Stadler, M., & Fire, A. Z. (2011). Wobble base-pairing slows in vivo translation elongation in metazoans. RNA, 17(12), 2063–2073.

122. Stein, K. C., Morales-Polanco, F., van der Lienden, J., Rainbolt, T. K., & Frydman, J. (2022). Ageing exacerbates ribosome pausing to disrupt cotranslational proteostasis. Nature, 601(7894), 637–642.

123. Stinchcomb, D. T., Shaw, J. E., Carr, S. H., & Hirsh, D. (1985). Extrachromosomal DNA transformation of Caenorhabditis elegans. Molecular and Cellular Biology, 5(12), 3484–3496.

124. Sugiyama, T., Li, S., Kato, M., Ikeuchi, K., & Ichimura, A. (2019). Sequential Ubiquitination of Ribosomal Protein uS3 Triggers the Degradation of Non-functional 18S rRNA. *Cell Reports*, 26, 3400–3415.

125. Sundaramoorthy, E., Leonard, M., Mak, R., Liao, J., Fulzele, A., & Bennett, E. J. (2017). ZNF598 and RACK1 Regulate Mammalian Ribosome-Associated Quality Control Function by Mediating Regulatory 40S Ribosomal Ubiquitylation. *Molecular Cell, 65*(4), 751-760.e4.

126. Takehara, Y., Yashiroda, H., Matsuo, Y., Zhao, X., Kamigaki, A., Matsuzaki, T., Kosako, H., Inada, T., & Murata, S. (2021). The ubiquitination-deubiquitination cycle on the ribosomal protein eS7A is crucial for efficient translation. IScience, 24(3), 102145.

127. Thompson, O., Edgley, M., Strasbourger, P., Flibotte, S., Ewing, B., Adair, R., Au, V., Chaudhry, I., Fernando, L., Hutter, H., Kieffer, A., Lau, J., Lee, N., Miller, A., Raymant, G., Shen, B., Shendure, J., Taylor, J., Turner, E. H., Hillier, L. W., … Waterston, R. H. (2013). The million mutation project: a new approach to genetics in *Caenorhabditis elegans*. *Genome research, 23*(10), 1749–1762.

128. Tomomatsu, S., Watanabe, A., Tesina, P., Hashimoto, S., Ikeuchi, K., Li, S., Matsuo, Y., Beckmann, R., & Inada, T. (2022). Two modes of Cue2-mediated mRNA cleavage with distinct substrate recognition initiate no-go decay. *Nucleic Acids Research*, 1–18.

129. Tucker, M., Valencia-Sanchez, M. A., Staples, R. R., Chen, J., Denis, C. L., & Parker, R. (2001). The transcription factor associated Ccr4 and Caf1 proteins are components of the major cytoplasmic mRNA deadenylase in Saccharomyces cerevisiae. *Cell*, 104(3), 377–386.

130. van den Elzen, A. M. G., Henri, J., Lazar, N., Gas, M. E., Durand, D., Lacroute, F., Nicaise, M., van Tilbeurgh, H., Séraphin, B., & Graille, M. (2010). Dissection of Dom34-Hbs1 reveals independent functions in two RNA quality control pathways. *Nature Structural & Molecular Biology*, *17*(12), 1446–1452.

131. Wang, J., Zhou, J., Yang, Q., & Grayhack, E. J. (2018). Multi-protein bridging factor 1(Mbf1), Rps3 and Asc1 prevent stalled ribosomes from frameshifting. eLife, 7, 1–26.

132. Wu, C. C. C., Zinshteyn, B., Wehner, K. A., & Green, R. (2019). High-Resolution Ribosome Profiling Defines Discrete Ribosome Elongation States and Translational Regulation during Cellular Stress. *Molecular Cell*, 73(5), 959-970.e5.

133. Wu, Z., Wang, Y., Lim, J., Liu, B., Li, Y., Vartak, R., Stankiewicz, T., Montgomery, S., & Lu, B. (2018). Ubiquitination of ABCE1 by NOT4 in Response to Mitochondrial Damage Links Co-translational Quality Control to PINK1-Directed Mitophagy. *Cell Metabolism*, 28(1), 130-144.e7.

134. Yan, L. L., Simms, C. L., McLoughlin, F., Vierstra, R. D., & Zaher, H. S. (2019). Oxidation and alkylation stresses activate ribosome-quality control. Nature Communications, 10(1).

135. Zhao, T., Chen, Y.-M., Li, Y., Wang, J., Chen, S., Gao, N., & Qian, W. (2021). Disome-seq reveals widespread ribosome collisions that promote cotranslational protein folding. *Genome Biology*, 22(1), 1–35.

136. Zheng, N., & Shabek, N. (2017). Ubiquitin ligases: Structure, function, and regulation. *Annual Review of Biochemistry*, 86, 129–157.